**Title**

EPIGENETIC AND TRANSCRIPTIONAL REGULATIONS IN PANCREATIC DUCTAL ADENOCARCINOMA



**Author**

Xu, Reno Jihao

**Publication Date**

2024

Peer reviewed|Thesis/dissertation

Epigenetic and Transcriptional Regulations in Pancreatic Ductal Adenocarcinoma

By

RENO JIAHO XU
DISSERTATION

Submitted in partial satisfaction of the requirements for the degree of

DOCTOR OF PHILOSOPHY

in

Biochemistry, Molecular, Cellular, and Developmental Biology

in the

OFFICE OF GRADUATE STUDIES

of the

UNIVERSITY OF CALIFORNIA

DAVIS

Approved:

_____

Chang-il Hwang, Chair

_____

Alexander Borowsky

_____

Paul Knoepfler

Committee in Charge

2024

**Abstract**

Pancreatic ductal adenocarcinoma (PDA) presents a significant challenge in oncology due to its aggressive nature and limited treatment options. Despite advancements in understanding the genomic landscape of PDA initiation and progression, the mechanisms driving metastasis remain elusive. This doctoral thesis explores the critical role of epigenetic mechanisms, specifically focusing on transcriptional regulation, histone modification, and molecular crowding in PDA metastasis. Through a multidisciplinary approach, encompassing genomic analyses, functional studies, and biophysical investigations, the thesis sheds light on the intricate interplay between genetic and epigenetic factors driving PDA progression. Chapters elucidate the aberrant expression of the homeodomain transcription factor EN1 in PDA, its impact on downstream signaling pathways, and its promotion of PDA transformation and metastasis. Furthermore, the thesis uncovers the influence of nucleoplasmic macromolecular crowding, particularly highlighting the role of nesprin-3, in regulating nuclear dynamics and metastatic potential in PDA. By integrating genetic, epigenetic, and biophysical perspectives, this work not only advances our understanding of PDA pathogenesis but also paves the way for the development of targeted therapeutic interventions. Additionally, the thesis underscores the significance of pancreatic cancer organoid models in recapitulating disease progression, elucidating molecular dynamics, and guiding precision medicine approaches. Overall, this research underscores the importance of a comprehensive approach in deciphering the complexities of PDA and offers valuable insights for future therapeutic strategies aimed at improving patient outcomes.

**Table of Contents**

**Acknowledgment**

As I begin to write the dissertation, I cannot help but feel overwhelmed by the immense support I have received throughout my academic journey. It has been a wild ride with emotions, stress, challenges, and growth. One thing that is certain: I could not have done it without the incredible people:

Luba Voloshko, Ph.D.

James Baxter, Ph.D.

Reen Wu, Ph.D.

Ching-Hsien Chen, Ph.D.

Celina Juliano, Ph.D.

Enoch Baldwin, Ph.D.

Jacqueline Barlow, Ph.D.

Daniel Starr, Ph.D.

G.W. Gant Luxton, Ph.D.

Keely Ji

Sarah Wang

Thesis Advisor:

Chang-il Hwang, D.V.M., Ph.D.

Dissertation Committee Members:

Alexander Borowsky, M.D. & Paul Knoepfler, Ph.D.

To my parents, 冀蓓红 and 徐忠, my husband Aaron Lawman, my in-laws Roberta and Larry Lawman, and my beloved dogs Bruno and Elsie Lawman: your unwavering love, tolerance, and belief in me are my greatest sources of strength throughout this journey.

To my friends, Cesar Mendez, Suyakarn Archasappawat, Duc Pham, Selin Gumusderelioglu, Natalie Sahabandu, Theresa Wechsler, Hannah Morris Little, Wenzhe Li, Ryan Hart, Jessica Bolivar, Aron Judd Mendiola, Nick DeCuzzi, Abhineet Ram, Osman Sharifi, Alyssa Parsons, and those who may not mentioned here but are no less significant, thank you. This dissertation is as much yours as it is mine.

## Chapter One – Epigenetic Alterations in Pancreatic Cancer Metastasis*

*This chapter is published in *Biomolecules* 2021, 11(8), 1082; https://doi.org/10.3390/biom11081082, under an open-access Creative Common CC BY license.

### Summary

Pancreatic cancer is the third leading cause of cancer-related deaths in the United States. Pancreatic ductal adenocarcinoma (PDA) is the most common (90%) and aggressive type of pancreatic cancer. Genomic analyses of PDA specimens have identified the recurrent genetic mutations that drive PDA initiation and progression. However, the underlying mechanisms that further drive PDA metastasis remain elusive. Despite many attempts, no recurrent genetic mutation driving PDA metastasis has been found, suggesting that epigenetic fluctuations rather than genetic factors drive PDA metastasis. Therefore, establishing epigenetic mechanisms of PDA metastasis would facilitate the development of successful therapeutic interventions. In this review, we provide a comprehensive overview of the role of epigenetic mechanisms in PDA as a critical contributor to PDA progression and metastasis. In particular, we explore the recent advancements elucidating the role of nucleosome remodeling, histone modification, and DNA methylation in the process of cancer metastasis.

## Introduction

Pancreatic cancer is the third leading cause of cancer-related deaths in the United States. These poor survival outcomes are primarily because pancreatic cancer is often asymptomatic in its early stages, making early diagnoses difficult. The five-year survival rate for pancreatic cancer is 10%, the lowest among common cancers, and pancreatic cancer is expected to surpass colorectal cancer as the second leading cause of cancer-related deaths by 2030 [1,2]. Of pancreatic cancer types, pancreatic ductal adenocarcinoma (PDA) is the most common and aggressive, comprising 90% of pancreatic cancer patients [3]. Despite the fact that recent advances in first-line chemotherapy, such as FOLFIRINOX or gemcitabine/nab-paclitaxel, survival benefits for PDA patients remain modest [4,5]. As a consequence, significant effort has been made to understand the progression of the disease.

Whole-genome sequencing technologies have undoubtedly revealed that PDA is a disease that arises from genetic aberrations. Notably, the initiating genetic event in over 90% of PDA cases is a gain-of-function mutation of *KRAS* in acinar or ductal cells, which results in the formation of pancreatic lesions called pancreatic intraepithelial neoplasia (PanIN). Subsequent loss-of-function mutations or deletions in tumor suppressor genes, such as *TP53, SMAD4*, and *CDKN2A*, cooperate with *KRAS* mutation to drive tumor formation and further exacerbate the disease progression (Figure 1) [6,7]. In addition to genetic aberrations, it has become increasingly clear over the last two decades that epigenetic alterations also promote the progression of almost every type of cancer [8–11]. Epigenetic mechanisms

regulate gene transcription, and the proper functioning of these mechanisms is essential for normal development and tissue differentiation. When these mechanisms are aberrantly altered in cancer cells, they can silence tumor suppressor genes or promote the expression of oncogenes to confer advantageous adaptations of the cancer cells, such as increased survival and proliferation, leading to aggressive cell phenotypes and metastasis.

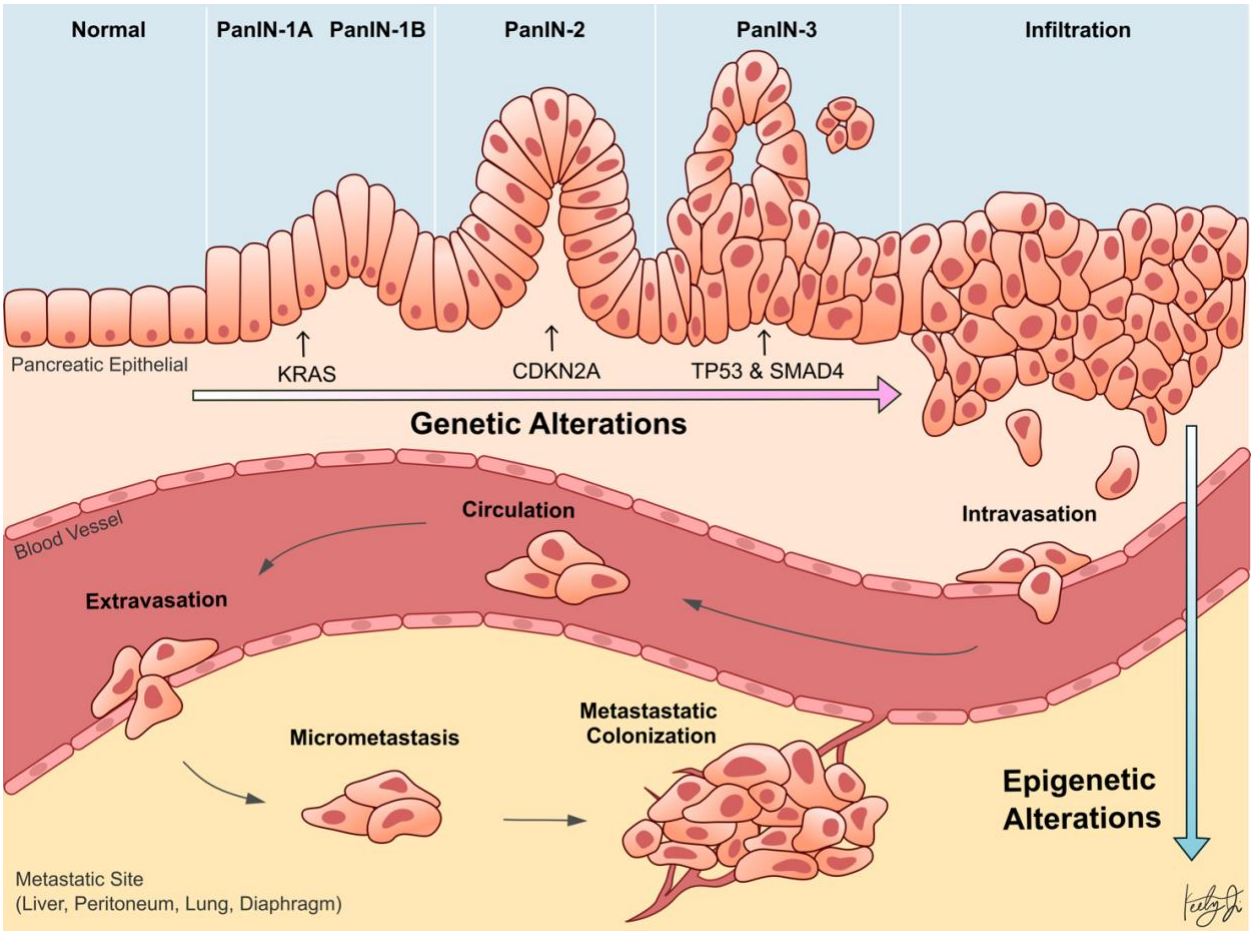


**Figure 1.** Schematic illustration showing pancreatic ductal adenocarcinoma (PDA) progression from the normal pancreas, pancreatic intraepithelial neoplasia (PanIN), and metastasis. Early pancreatic carcinogenesis is driven by genetic alterations in *KRAS*, *CDKN2A*, *TP53*, and *SMAD4* (**top**). During metastasis, PDA cells penetrate the blood vessel (intravasation), circulate through the bloodstream, invade into the

metastatic site (extravasation), and colonize to form a secondary malignant tumor. The process of pancreatic cancer metastasis is facilitated by epigenetic alterations (**bottom**).

This review seeks to comprehensively assess the current progress regarding the role of epigenetic alterations in PDA progression and metastasis. Specifically, recent studies investigating the role of alterations in epigenetic regulators, histone modifications, chromatin accessibilities, and DNA methylation in PDA are highlighted (Table 1).

**Table 1.** Summary of reviewed genes that are related to epigenetic alterations during PDA progression and metastasis in the categories of germline PTV mutation, somatic mutation, chromatin accessibility and nucleosome remodeling, histone modification, and DNA methylation. ↓ denotes decrease and ↑ denotes increase.

| Category | Gene | Molecular Function | Molecular Phenotype in PDA | Phenotype in PDA | Reference |
|---|---|---|---|---|---|
| Germline PTV Mutation in Epigenetic | TET2 | Dioxygenase of 5-methylcytosine, involved in demethylation of cytosines | loss of function in encoded protein | ↓ patient survival | [12] |
| | DNMT3a | DNA methyltransferase, involved in de novo DNA methylation | loss of function in encoded protein | ↓ patient survival | [12] |

| | | | | | |
|---|---|---|---|---|---|
| Regulators | ASXL1 | Polycomb group protein, involved in gene transcriptional regulation and chromatin architecture maintenance | loss of function in encoded protein | ↑ proliferation, ↓ patient survival | [12] |
| Somatic Mutation in Epigenetic Regulators | ARID1A | Chromatin remodeler, involved in chromatin remodeling and gene transcriptional regulation | loss of function in encoded protein | ↑ progression, ↓ survival | [6–8,13,14] |
| | KDM6A | Lysine-specific histone demethylase, involved in promoter and enhancer activities | loss of function in encoded protein | ↑ squamous identity, ↓ survival | [6,7,13,14] |
| Chromatin Accessibility | ZKSCAN1 | Transcription factor, involved in proliferation and differentiation | ↑ TF binding via open chromatin | ↑ metastasis | [15] |
| | HNF1B | Transcription factor, involved in beta cell development in the pancreas | ↓ TF binding via closed chromatin | ↑ metastasis | [15] |
| Transcription Factor-Mediated Histone Modification | FOXA1 | Transcription factor, involved in cell differentiation and chromatin remodeling | ↑ enhancer activation (H3K27ac) | ↑ cell growth, ↑ invasion, ↑ progression | [16] |
| | TP63 | Transcription factor, involved in cell proliferation, differentiation, and apoptosis | ↑ enhancer activation (H3K27ac) | ↑ squamous identity | [17] |
| DNA Methylation | TFPI-2 | Serine proteinase inhibitor, involved in negative regulation of pro-metastasis extracellular matrix degradation | ↓ expression via hypermethylation | ↑ progression, ↑ proliferation, ↑ migration | [18] |

| | | | | |
|---|---|---|---|---|
| RELN | Extracellular matrix serine protease, involved in neuronal migration | ↓ expression via hypermethylation | ↓ patient survival, ↑ migration, ↑ invasion, ↑ colony formation | [19] |
| MET | Receptor tyrosine kinase, involved in cell survival, migration, and invasion | ↑ expression via hypomethylation | ↓ patient survival | [20] |
| ITGA2 | Integrin, involved in adhesion of cells to the extracellular matrix | ↑ expression via hypomethylation | ↓ patient survival | [20] |

**Genetic Alterations in Epigenetic Regulators**

While *KRAS, TP53, SMAD4,* and *CDKN2A* driver mutations are core to early PDA progression, there is a vast genetic heterogeneity among PDA patients, harboring a range of less frequent genetic mutations that facilitate carcinogenesis [6,7]. For one, around 10% of PDA cases belong to familial pancreatic cancer and are commonly affected by germline pre-mature truncating variant (PTV) mutations in genes related to the DNA repair pathways (e.g., *BRCA1/2, ATM,* and *PALB2*), which have been predicted to inactivate the proteins [6,12]. Interestingly, a subset of these patients also have germline PTV mutations in epigenetic regulators (e.g., *TET2*, *DNMT3A,* and *ASXL1*) [12], suggesting that aberrant changes to the epigenome are important in predisposing individuals to PDA by altering the transcriptional profile of cells.

In addition to the germline mutations in PDA, whole exome and genome sequencing revealed that a significant percentage of patients with PDA have somatic mutations in epigenetic regulators and chromatin remodeling complexes (e.g., *ARID1A/B*, *PBRM1*, *MLL2/3/4*, *KDM6A*, *SMARCA2/4*) [6,7]. Furthermore, somatic mutations in SWI/SNF complex regulators (e.g., *ARID1A*) and inactivation of histone modification enzymes (e.g., *MLL3*, *MLL5*, *KDM6A*) frequently occurred in conjunction with oncogenic *KRAS* in sleeping beauty transposon insertional mutagenesis screens [13,14]. Indeed, Mann et al. found that 100% of the tumors in this screen harbored one or more mutations in genes coding for histone-modifying enzyme [13]. These mutations cooperated with oncogenic KRAS to promote PDA

progression, suggesting that alterations to the epigenome are important for driving PDA progression [13]. Together these findings highlight the significance of epigenetic regulation in pancreatic cancer progression.

Despite our firm understanding of the genetic alterations that underlie PDA progression, there is limited understanding of the genetic drivers of PDA metastasis. To this day, there is no known recurrent mutation that drives this metastatic process [21–24]. This suggests that epigenetic mechanisms, rather than genetic, are driving PDA metastasis (Figure 1). Perturbed epigenetic programs, including transcription factor (TF)-mediated histone modifications, chromatin remodeling, DNA methylation patterns, and subsequently altered transcriptional programs, are emerging mechanisms of PDA progression and metastasis [25].

**Chromatin Accessibility and Metastasis**

Chromatin is composed of nucleosomes, which are formed by DNA wrapped around canonical histone molecules, including H2A, H2B, H3, and H4 (Figure 2) [26]. There are two distinct chromatin states: open or euchromatin and closed or heterochromatin. In the heterochromatin state, nucleosomes are highly condensed, preventing TF binding and subsequent RNA polymerase recruitment [27]. Therefore, to initiate gene transcription, both *cis* (gene promoters and enhancers) and *trans* (TFs and RNA polymerases) regulatory elements interact in a spatial and temporal manner to establish the euchromatin architecture, allowing the recruitment of transcriptional machinery that favors transcription initiation. To achieve this, *trans* pioneer TFs first bind to nucleosomal DNA within the heterochromatin and recruit chromatin remodeling enzymes to remodel nucleosomes and expose the *cis* elements, such as enhancers [28]. Enhancers are distal elements independent of the distance and orientation of the targeted genes [29]. In addition, enhancers contain unique DNA sequence motifs to recruit specific TFs and co-activators or co-repressors, and the gene transcription activities are determined by the summation of all the co-regulators [30].

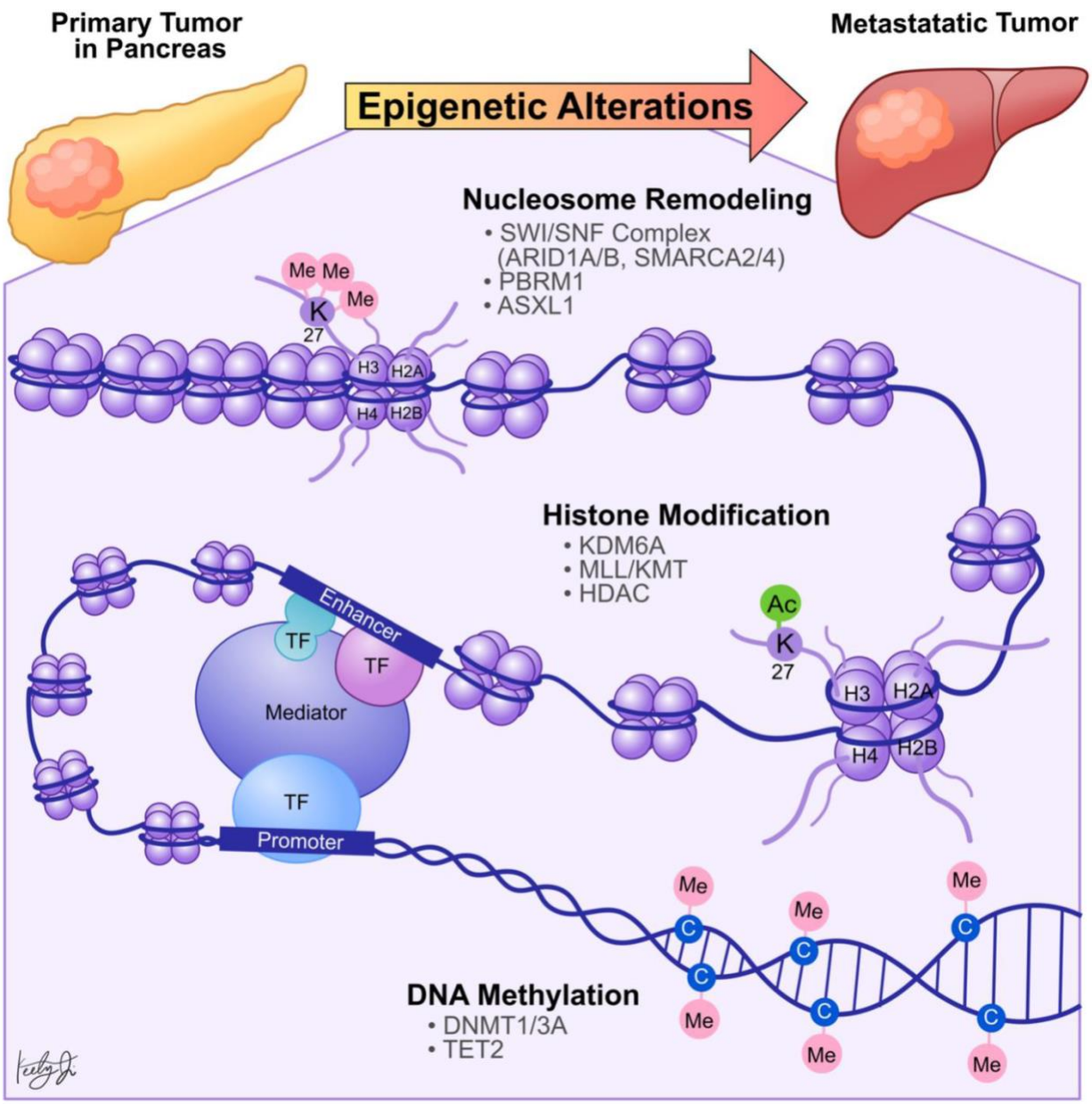


**Figure 2.** Summary of the epigenetic mechanisms behind PDA metastasis. Metastatic PDA tumors have aberrant epigenetic profiles that are different from PDA primary tumors. Nucleosome remodeling and histone modification (e.g., acetylation of histone 3 lysine 9) increase chromatin accessibility, allowing for transcription factor binding and gene transcription. On the other hand, DNA methylation of CpG islands leads to gene repression. These processes are mediated by epigenetic regulators, some of which are noted in the figure.

In the context of cancer metastasis, Denny et al. compared chromatin accessibility between primary and metastatic small cell lung cancer (SCLC) using Assay for Transposase-Accessible Chromatin followed by sequencing (ATAC-seq) [31]. The study showed that aggressive metastatic SCLC overexpresses embryonic developmental TF NF1 to remodel nucleosomes around the TF-binding enhancers and establish the euchromatin architecture. In turn, the open chromatin architecture allows the upregulation of transcription programs related to axon guidance, neuron development, cell-cell adhesion, migration, and differentiation. Together, evidenced by *in vitro* cell migration and colony formation assays and *in vivo* subcutaneous and intravenous transplantation assays, these programs promote the proliferation and migratory abilities of the cancer cell *in vitro* and metastasis *in vivo* [31]. In pancreatic cancer, Dhara et al. used ATAC-seq to analyze chromatin accessibility of surgically resected PDA between patients with disease-free survival (DSF) less than one year (cancer recurrent/metastases group) and patients with DSF greater than one year (cancer non-recurrent/non-metastases group) and found 1092 differentially accessible chromatin peaks between the PDA recurrent and non-recurrent patients [15]. Subsequent computational TF motif analysis identified 61 TFs with binding motifs within these chromatin regions. These TFs included tumor-promoting ZKSCAN1 from the open chromatin regions of metastase patients and tumor suppressor HNF1B from the open chromatin regions of non-metastase patients [15]. Together, these studies demonstrated that cancer cells, including PDA, can remodel chromatin landscape and accessibility to recruit or prevent TF binding as a mechanism to initiate tumor metastasis. Furthermore, detection of the disrupted

chromatin landscapes in tumor biopsy samples could potentially be used for PDA prognostic predictions in clinical settings.

**Transcription Factor-Mediated Histone Modification and Metastasis**

Several histone post-translational modifications (PTMs) co-occur during chromatin remodeling and gene transcription, which can be used as indicators of transcriptional activities. In general, active promoters are marked by dual H3K27 acetylation (H3K27ac) and H3K4 trimethylation (H3K4me3), while active enhancers are marked by dual H3K27ac and H3K4 monomethylation (H3K4me1) [32]. Conversely, histone H3K9 and H3K27 methylation are used to indicate repressive gene transcription [33]. These histone PTMs alter the biochemical properties of the chromatin, not only leading to the formation of euchromatin or heterochromatin but also the sequestering or docking of effector enzymes, such as histone acetylase, deacetylase, methyltransferase, and demethylase [34].

Dysregulation in histone PTMs, in conjunction with the recruitment of effector chromatin remodelers, modifies chromatin architecture, leading to aberrant gene activation or repression, which contributes to cancer metastasis (Figure 2). For example, by comparing primary PDA tumors to matched distant lung and proximal peritoneum metastases, McDonald et al. used chromatin immunoprecipitation followed by sequencing (ChIP-seq) to demonstrate that global alterations of H3K9me2/3 and H3K27ac may contribute to aggressive tumor phenotypes [35]. Specifically, ChIP-seq showed that H3K9 methylation levels are reduced at Large Organized Chromatin K9-modified (LOCK) heterochromatin regions in distant metastases compared to their matched primary tumors [35], suggesting that transcription activities of certain genes within these regions (LOCK genes) are

upregulated during PDA metastasis. Indeed, using RNA-seq and ChIP-seq analysis, the study showed that decreased H3K9me2 and H3K27me3 and increased H3K27ac occupancies at gene promoters in LOCK regions are positively correlated with the expression of the associated genes in distant metastases [35]. Furthermore, subsequent gene ontology analysis revealed that the reprogrammed LOCK regions contain genes related to cellular differentiation and morphogenesis, epithelial-to-mesenchymal transitions, cell adhesion, and migration [35]. This suggests that a histone modification-mediated epigenetic switch from heterochromatin to euchromatin state is associated with cellular transformation, which promotes aggressive tumor phenotypes and facilitates PDA tumor-to-metastasis transitions.

Histone modification-dependent epigenetic landscape reprogramming can be carried out by TFs through first targeting nucleosomal DNA and then recruiting histone and chromatin remodeling enzymes [28]. In the context of pancreatic cancer, we identified that the developmental Forkhead family TF FOXA1 drives enhancer landscape reprogramming during the PDA tumor-to-metastasis transition [16]. To dissect the molecular mechanisms of enhancer activation/inactivation during PDA metastasis, we developed a 3D organoid culture using PDA cells collected from the primary tumors and matched metastatic lesions derived from the *Kras*$^{+/LSL\text{-}G12D}$; *Trp53*$^{+/LSL\text{-}R172H}$; *Pdx1-Cre* (KPC) PDA mouse model [36]. The organoid culture model of PDA preserves the unique biological characteristics of normal, PanIN, tumor, and metastase lesions. In addition, this model can be used for direct biochemical comparisons during each stage of the disease progression [36]. H3K27ac ChIP-

seq analysis revealed 857 regions with increased H3K27ac occupancy (*GAIN* region) in the metastases organoids compared to the normal, PanIN, and tumor organoids [16], suggesting that the dysregulation of H3K27ac landscape within these enhancer regions could be responsible for PDA progression and metastasis. Combining RNA-seq and TF motif analysis, we then identified that FOXA1 activates *GAIN* region enhancers by increasing H3K27ac occupancy in the primary PDA. *In vitro*, overexpression of FOXA1 in primary PDA tumor cells activated foregut developmental genes that promoted anchorage-independent cell growth and invasion in sphere-formation and Matrigel invasion assays, respectively. *In vivo*, overexpression of FOXA1 contributed to overall PDA progression and metastasis in tail vein injection and organoid transplantation experiments [16]. This work demonstrated that PDA cells could repurpose FOXA1 to activate enhancers of developmental gene programs [37], promote anchorage-independent growth, and induce branching morphogenesis of the epithelial cells [38, 39]. Furthermore, upregulation of FOXA1 in PDA cells promotes aggressive cell phenotypes, such as proliferation, invasion, and migration, allowing cells to better withstand stressful conditions during metastasis. In support of our work, Kim et al. discovered that *FOXA1* gene transcription is enhanced by missense mutations of p53 ($p53^{R172H}$, $p53^{R245W}$, and $p53^{R270H}$) that directly bind to the *FOXA1* promoter and induce oncogenic KRAS activation of cyclic AMP responsive element binding protein 1 (CREB1) [40]. In turn, FOXA1 promotes β-catenin stabilization and subsequently activates canonical WNT transcriptional programs to promote anchorage-independent cell growth, proliferation, and metastasis [40, 41]. Together, these studies demonstrated that PDA cells could reprogram the epigenetic landscape and subsequent transcription programs through (1) recruiting TFs,

(2) altering chromatin architectures through histone modifications, and (3) recruiting transcription co-activators (i.e., mutant p53 and CREB1) to sustain their growth, differentiation, and metastasis (Figure 2).

**Transcription Factor-Mediated Enhancer Regulation in Aggressive PDA Molecular Subtype Differentiation**

PDA can be categorized into four subtypes based on the gene transcriptional programs identified by Bailey et al. They are the squamous, pancreatic progenitor, immunogenic, and aberrantly differentiated endocrine exocrine (ADEX) subtype [42]. The two most common are the squamous and the progenitor subtype [42–44]. The progenitor subtype of PDA expresses pancreatic endoderm lineage-specific TFs, including PDX1, GATA6, FOXA2/3, HNF1A/B, and HNF4A/G [42, 43]. In contrast, the squamous subtype of PDA represses the endoderm lineage-specific TFs through DNA hypermethylation at the gene promoters [42]. In addition, the squamous subtype upregulates TF p63 expression and is often associated with poor PDA patient prognosis [42, 44]. Somerville et al. demonstrated that aberrant expression of p63 reprograms the enhancer landscape of PDA, leading to the upregulation of squamous transcriptional programs to promote tumor growth and metastatic potential, which is evident by primary tumor size and number of metastatic lesions in the xenograft transplantation model [17]. Similar to FOXA1-dependent enhancer reprogramming, this study found that p63 increases H3K27ac occupancy at the enhancers of squamous lineage genes, resulting in increased transcriptions of genes including *KRT5/6*, *TRIM29*, and *PTHLH*. Together, the squamous transcriptional program governed by epigenetic mechanisms promotes aggressive PDA phenotypes *in vivo* [17].

Mutations in epigenetic modulators, including histone H3K27me2/3-specific lysine demethylase 6A (KDM6A) [42, 45], are commonly found in PDA squamous subtypes. Therefore, the cancer cell could potentially utilize or silence these epigenetic modulators to acquire metastatic traits. For example, given that at least 18% of PDA patients carry KDM6A mutations [7], which are associated with the squamous molecular subtype, Andricovich et al. found that loss of KDM6A in PDA can directly induce the squamous identity by upregulating the expressions of specific TF encoding genes, including *p63*, *ZEB1*, *RUNX3*, and *MYC* [45]. Mechanistically, loss of KDM6A allowed histone type 2 lysine methyltransferases (KMT2) to occupy and activate enhancers of squamous differentiation-promoting genes (squamous elements), which is evident by increased H3K4me1 and KMT2D occupancies at the squamous elements [45]. KMT2 enzyme families are histone H3K4-specific methyltransferases that mark active gene enhancers with H3K4me1 [32, 46]. Interestingly, KDM6A has been shown to partner with KMT2 to form the COMPASS (complex of proteins associated with Set1)-like complex [47], suggesting that PDA utilizes the loss of KDM6A to relieve enhancer repressions through COMPASS-like complex-dependent histone H3K4 modifications. In turn, the activated enhancers facilitate the expression of the squamous lineage genes to gain metastatic potential. Together, these studies showed that PDA cells could remodel the epigenetic landscape by repressing key epigenetic modulators to upregulate TFs that drive squamous PDA transcriptional programs. These programs favor cellular adaptations that promote an aggressive PDA phenotype and metastasis.

**DNA Methylation and Metastasis**

Another epigenetic mechanism that is likely contributing to PDA metastasis is DNA methylation (Figure 2). DNA methylation is the process by which a methyl group is added to the 5' carbon of cytosines, primarily at CpG sites where the cytosine is followed by guanine [48]. This methylation is catalyzed by DNA methyltransferases (DNMTs) and removed by ten-eleven translocase (TET) enzymes or inhibition of the maintenance methylase, DNMT1 [49, 50]. At promoters and enhancers, DNA methylation is negatively correlated with gene expression as the methylation can inhibit the binding of transcription factors, promote the binding of transcriptional repressor complexes, and encourage a closed, heterochromatin state [51–53]. In intergenic regions, DNA methylation is positively correlated with gene expression, but the role and regulations of this methylation are still poorly understood [54, 55]. Numerous studies have shown that DNA methylation is dysregulated in virtually every cancer, with cancer cells exhibiting extensive differential methylation compared to normal cells [56–58].

In PDA, aberrant DNA methylation has been widely documented. Early on, these studies involved methylated CpG island amplification (MCA) followed by microarray sequencing. More recently, bisulfite treatment paired with large microarray platforms or next-generation sequencing, such as reduced-representative bisulfite sequencing (RRBS) or whole-genome bisulfite sequencing (WGBS), have been used to assess the DNA methylome at base-pair resolution. Using these methods, DNA methylation in PDA has been correlated with several

disease outcomes and histopathological phenotypes. For example, Thompson et al. identified 17,251 CpG sites that are negatively associated with survival outcomes and 3256 sites that are positively associated with survival outcomes in a comparison of RRBS data from a small cohort of PDA patient tissues and adjacent normal pancreas tissues [59]. Similarly, Mishra et al. identified 406 promoter methylation loci associated with survival in an analysis of 450K array methylation data from the 154 PDA samples in The Cancer Genome Atlas pancreatic cancer patient database (TCGA-PAAD) [60]. Unsupervised clustering of TCGA-PAAD samples based on the differentially methylated CpG sites resulted in three distinct clusters of patient samples [61]. These clusters were each enriched with a different tumor grade, indicating that DNA methylation can be used to estimate the histopathological stage of PDA tumors [61]. In an analysis of both TCGA-PAAD transcriptome and DNA methylome data, unsupervised subtyping of TCGA-PAAD samples based on genes whose expression was significantly correlated with methylation expression patterns was performed [62]. Interestingly, this analysis identified five subtypes, four of which correspond to the molecular subtypes identified by Bailey et al. (i.e., squamous, pancreatic progenitor, immunogenic, and aberrantly differentiated endocrine exocrine [ADEX]), and the last unique subtype was enriched for tumor microenvironment related genes [42, 62]. Together, these data suggest that aberrant DNA methylation is associated with aggressive PDA phenotypes.

To identify pathways that may be involved in DNA methylation-mediated PDA aggressiveness, gene ontology and/or pathway analysis is often performed on differentially methylated genes in PDA. In the Thompson et al. study, CpG sites with a negative correlation between

methylation and survival rate were associated with pancreas-specific development genes [59]. Normally, pancreas-specific development genes are only active in early embryonic stages, but reactivation of these genes during PDA is common [63, 64]. Differential methylation of pancreas development genes has also been noted in the TCGA-PAAD dataset, suggesting that reactivation of the embryonic pancreas development program in PDA is epigenetically regulated [61]. Other differentially methylated genes found in the TCGA-PAAD dataset were enriched for cancer-related pathways, including MAPK, Rap1, and calcium signaling [60, 61]. In addition, core signaling pathways that are commonly altered in PDA, such as Wnt/Notch signaling, apoptosis, cell-cycle regulation, and cell adhesion, were enriched in aberrantly methylated genes found in the analysis of TCGA-PAAD database as well as a separate bisulfite microarray study of 167 PDA and 29 adjacent normal pancreata conducted by Nones et al. [20, 61, 65]. Interestingly, Nones et al. also observed that stellate cell activation genes were often hypomethylated and therefore, likely downregulated in PDA [20]. In support of this, Espinet et al. discovered that stellate cells exposed to conditioned media derived from high-interferon (IFN) signature patient tissues showed increased stellate cell growth *in vitro* and tumor formation *in vivo* [66]. Because the IFN pathway is involved in anti-viral defense and activated stellate cells are involved in ECM remodeling, this pathway may be activating and reprogramming stellate cells to produce a pro-inflammatory stroma that facilitates tumor growth. Hypermethylation of homeobox genes, which encode key transcription factors of embryonic development, was also commonly detected in several PDA methylome studies [53, 61, 66, 67]. This provides additional evidence that PDA tumors reactivate developmental pathways via epigenetic mechanisms to promote metastatic

characteristics. Overall, these studies suggest that processes commonly implicated in cancer aggressiveness and metastasis, such as apoptosis, cell-cycle regulation, and development pathways, are heavily influenced by aberrant DNA methylation in PDA.

Aberrant methylation of several individual genes and their association with worse survival outcomes have also been documented. Most of these genes have been reported to have hypermethylated promoters. For example, Sato et al. showed that the low expression of *TFPI-2*, which encodes a negative regulator of pro-metastasis extracellular matrix degradation, is frequently seen in both PDA cell lines and primary tumors and is associated with hypermethylation of the *TFPI-2* promoter [18]. Restoration of TFPI-2 in the PDA cell lines reduced proliferation and migratory potential [18]. Likewise, *RELN*, which encodes a critical regulator of neuronal migration, is commonly hypermethylated and silenced in pancreatic cancer [19]. Furthermore, low expression of *RELN* was significantly associated with worse survival outcomes, and siRNA knockdown of RELN in RELN-expressing pancreatic cancer cells enhanced cell motility, invasion, and colony formation [19]. Nevertheless, promoter hypomethylation of certain genes has also been implicated in a worse prognosis. For example, hypomethylation of *MET*, whose aberrant expression promotes metastasis, and *ITGA2*, which is involved in cell adhesion, correlated with increased mRNA expression and associated with poor survival in PDA by Nones et al. [20]. Thus, aberrant promoter methylation likely contributes to the aggressive nature of PDA by altering the expression of genes such as *TFPI-2*, *RELN*, *MET*, and *ITGA2*.

While the above studies provide a strong indication that aberrant DNA methylation in PDA likely contributes to metastasis, it is important to note that many of these studies are largely association-based and, therefore, do not functionally implicate genes or pathways in the process. Studies with functional experiments have shown that altering the expression of aberrantly methylated genes with loss-of-function or gain-of-function approaches affects metastatic potential *in vitro*, but analogous experiments *in vivo* are lacking. Furthermore, no study has directly shown the consequences of altered DNA methylation on the metastatic characters in PDA. Mechanistic studies linking aberrant DNA methylation to the aggressive behavior of PDA in both *in vitro* and *in vivo* contexts are necessary to better elucidate the role of DNA methylation in PDA metastasis.

**Therapeutic Implications of Epigenetic Regulators**

Currently, there is a lack of effective chemotherapies and targeted therapies for late-stage PDA patients, who make up most of the PDA patient population. The inability to identify a recurrent genetic mutation driving PDA metastasis suggests that epigenetic alterations are especially important for the tumor-to-metastasis transition and that targeting epigenetic regulators may be an effective strategy for treating late-stage patients. Fortunately, many small-molecule inhibitors of epigenetic regulators, such as histone methyltransferases, histone deacetylases (HDACs), and bromodomain and extra-terminal (BET) acetylation readers, have already been developed and have seen success as a treatment for several diseases [68]. In PDA clinical trials, these inhibitors were largely disappointing as monotherapies and have since been investigated in combination therapies with chemotherapeutic agents or other targeted therapies [69]. Unfortunately, combination therapies involving inhibitors of epigenetic regulators have shown mixed results in PDA clinical trials, highlighting a need to better understand the molecular mechanisms and synthetic lethal interactions that enable their effectiveness in preclinical studies [69].

In addition to being a potential therapeutic avenue for treating aggressive and late-stage PDA, epigenetic modifications can also be used as prognostic and/or predictive biomarkers for PDA. DNA methylation is especially promising for this purpose as circulating tumor cell-free DNA (cfDNA) in the bloodstream can be used to non-invasively identify abnormal DNA methylation patterns in tumors of PDA patients [70]. In fact, a method to detect pancreatic

cancer by assessing five DNA methylation markers in cfDNA along with *KRAS* mutation status had 68% sensitivity and 86% specificity when tested on cfDNA samples from 47 pancreatic cancer patients and 14 normal volunteers [71]. Furthermore, patients who were successfully identified with this screen were more likely to have larger tumors and liver metastases, suggesting that this method could be especially useful for identifying late-stage PDA patients [71]. Methylation of individual gene promoters has also been shown to have prognostic value. For example, in methylation of *SPARC* differentiated early-stage PDA from pancreatitis patients, high methylation of *SPARC* and *NPTX2* is associated with late-stage or metastatic patients and worse survival outcomes [72]. Similarly, promoter methylation of *CDO1* was found to be specific to PDA tumors, positively correlated with PDA progression, and identifiable in pancreatic juice and small needle biopsy samples [73]. In addition, low cellular levels of H3K4me2, H3K9me2, and H3K18ac in PDA patient tumor cells were all independent and significant predictors of poor survival in a 140-patient clinical trial comparing fluorouracil to gemcitabine treatment [74], suggesting that histone modifications may have predictive value in PDA. Identification of other epigenetic biomarkers is an area of research that is actively being pursued.

## Conclusions

PDA has long been thought of as a disease arising and progressing from genetic mutations. More recently, it has become clear that epigenetic alterations are also important contributors to PDA progression and metastasis. While no single epigenetic regulator is commonly mutated in PDA, a growing body of evidence indicated that metastatic tissues exhibit distinct epigenetic status compared to primary tumor tissues, which might be exploited for cancer therapeutics and diagnostics. Studies have shown that aberrant expression of histone modification in the PDA epigenome induces chromatin remodeling that alters the recruitment of TFs and co-regulators, resulting in transcriptional changes that promote PDA aggressiveness *in vitro* and *in vivo* [15–17, 35]. Similarly, aberrant DNA methylation has been shown to affect the transcriptome in a way that promotes the acquisition of metastatic characteristics. However, the specific transcriptional programs that most significantly affect PDA metastasis and the mechanisms by which they do so are still largely unknown and are active areas of investigation.

Overall, alterations to the epigenome clearly play an important role in PDA progression and metastasis, but the mechanisms by which they do so are not well understood. An improved understanding of these mechanisms will better inform the development of combination therapies targeting epigenetic regulators and prognostic biomarkers for the improved treatment of PDA patients, especially those in the late stages.

**References**


1. Rahib L, Smith BD, Aizenberg R, et al (2014) Projecting cancer incidence and deaths to 2030: The unexpected burden of thyroid, liver, and pancreas cancers in the united states. Cancer Res. 74:2913–2921
2. Siegel RL, Miller KD, Fuchs HE, Jemal A (2021) Cancer Statistics, 2021. CA Cancer J Clin 71:7–33. https://doi.org/10.3322/caac.21654
3. Ying H, Dey P, Yao W, et al (2016) Genetics and biology of pancreatic ductal adenocarcinoma. Genes Dev. 30:355–385
4. Conroy T, Desseigne F, Ychou M, et al (2011) FOLFIRINOX versus Gemcitabine for Metastatic Pancreatic Cancer. N Engl J Med 364:1817–1825. https://doi.org/10.1056/nejmoa1011923
5. Von Hoff DD, Ervin T, Arena FP, et al (2013) Increased Survival in Pancreatic Cancer with nab-Paclitaxel plus Gemcitabine. N Engl J Med 369:1691–1703. https://doi.org/10.1056/nejmoa1304369
6. Raphael BJ, Hruban RH, Aguirre AJ, et al (2017) Integrated Genomic Characterization of Pancreatic Ductal Adenocarcinoma. Cancer Cell 32:185-203.e13. https://doi.org/10.1016/j.ccell.2017.07.007
7. Waddell N, Pajic M, Patch AM, et al (2015) Whole genomes redefine the mutational landscape of pancreatic cancer. Nature 518:495–501. https://doi.org/10.1038/nature14169
8. Baylin SB, Jones PA (2016) Epigenetic determinants of cancer. Cold Spring Harb Perspect Biol 8:a019505. https://doi.org/10.1101/cshperspect.a019505

9. Baylin SB, Jones PA (2011) A decade of exploring the cancer epigenome-biological and translational implications. Nat. Rev. Cancer 11:726–734

10. Feinberg AP, Ohlsson R, Henikoff S (2006) The epigenetic progenitor origin of human cancer. Nat. Rev. Genet. 7:21–33

11. Ting AH, McGarvey KM, Baylin SB (2006) The cancer epigenome - Components and functional correlates. Genes Dev. 20:3215–3231

12. Roberts NJ, Norris AL, Petersen GM, et al (2016) Whole genome sequencing defines the genetic heterogeneity of familial pancreatic cancer. Cancer Discov 6:166–175. https://doi.org/10.1158/2159-8290.CD-15-0402

13. Mann KM, Ward JM, Yew CCK, et al (2012) Sleeping Beauty mutagenesis reveals cooperating mutations and pathways in pancreatic adenocarcinoma. Proc Natl Acad Sci U S A 109:. https://doi.org/10.1073/pnas.1202490109

14. Pérez-Mancera PA, Rust AG, Van Der Weyden L, et al (2012) The deubiquitinase USP9X suppresses pancreatic ductal adenocarcinoma. Nature 486:. https://doi.org/10.1038/nature11114

15. Dhara S, Chhangawala S, Chintalapudi H, et al (2021) Pancreatic cancer prognosis is predicted by an ATAC-array technology for assessing chromatin accessibility. Nat Commun 12:3044. https://doi.org/10.1038/s41467-021-23237-2

16. Roe JS, Hwang C Il, Somerville TDD, et al (2017) Enhancer Reprogramming Promotes Pancreatic Cancer Metastasis. Cell 170:875-888.e20. https://doi.org/10.1016/j.cell.2017.07.007

17. Somerville TDD, Xu Y, Miyabayashi K, et al (2018) TP63-Mediated Enhancer

Reprogramming Drives the Squamous Subtype of Pancreatic Ductal Adenocarcinoma. Cell Rep 25:1741-1755.e7. https://doi.org/10.1016/j.celrep.2018.10.051

18. Sato N, Parker AR, Fukushima N, et al (2005) Epigenetic inactivation of TFPI-2 as a common mechanism associated with growth and invasion of pancreatic ductal adenocarcinoma. Oncogene 24:850–858. https://doi.org/10.1038/sj.onc.1208050
19. Sato N, Fukushima N, Chang R, et al (2006) Differential and epigenetic gene expression profiling identifies frequent disruption of the RELN pathway in pancreatic cancers. Gastroenterology 130:548–565. https://doi.org/10.1053/j.gastro.2005.11.008
20. Nones K, Waddell N, Song S, et al (2014) Genome-wide DNA methylation patterns in pancreatic ductal adenocarcinoma reveal epigenetic deregulation of SLIT-ROBO, ITGA2 and MET signaling. Int J Cancer 135:1110–1118. https://doi.org/10.1002/ijc.28765
21. Campbell PJ, Yachida S, Mudie LJ, et al (2010) The patterns and dynamics of genomic instability in metastatic pancreatic cancer. Nature 467:1109–1113. https://doi.org/10.1038/nature09460
22. Connor AA, Denroche RE, Jang GH, et al (2019) Integration of Genomic and Transcriptional Features in Pancreatic Cancer Reveals Increased Cell Cycle Progression in Metastases. Cancer Cell 35:267-282.e7. https://doi.org/10.1016/j.ccell.2018.12.010
23. Makohon-Moore AP, Zhang M, Reiter JG, et al (2017) Limited heterogeneity of known

driver gene mutations among the metastases of individual patients with pancreatic cancer. Nat Genet 49:358–366. https://doi.org/10.1038/ng.3764

24. Priestley P, Baber J, Lolkema MP, et al (2019) Pan-cancer whole-genome analyses of metastatic solid tumours. Nature 575:. https://doi.org/10.1038/s41586-019-1689-y

25. Embuscado EE, Laheru D, Ricci F, et al (2005) Immortalizing the complexity of cancer metastasis: Genetic features of lethal metastatic pancreatic cancer obtained from rapid autopsy. Cancer Biol Ther 4:548–554. https://doi.org/10.4161/cbt.4.5.1663

26. McGinty RK, Tan S (2015) Nucleosome structure and function. Chem. Rev. 115:2255–2273

27. Tamaru H (2010) Confining euchromatin/heterochromatin territory: Jumonji crosses the line. Genes Dev. 24:1465–1478

28. Mayran A, Drouin J (2018) Pioneer transcription factors shape the epigenetic landscape. J. Biol. Chem. 293:13795–13804

29. Maston GA, Evans SK, Green MR (2006) Transcriptional regulatory elements in the human genome. Annu. Rev. Genomics Hum. Genet. 7:29–59

30. Shlyueva D, Stampfel G, Stark A (2014) Transcriptional enhancers: From properties to genome-wide predictions. Nat. Rev. Genet. 15:272–286

31. Denny SK, Yang D, Chuang CH, et al (2016) Nfib Promotes Metastasis through a Widespread Increase in Chromatin Accessibility. Cell 166:328–342. https://doi.org/10.1016/j.cell.2016.05.052

32. Hyun K, Jeon J, Park K, Kim J (2017) Writing, erasing and reading histone lysine methylations. Exp Mol Med 49:324. https://doi.org/10.1038/emm.2017.11

33. Wong CM, Wong CCL, Ng YL, et al (2011) Transcriptional repressive H3K9 and H3K27 methylations contribute to DNMT1-mediated DNA methylation recovery. PLoS One 6:. https://doi.org/10.1371/journal.pone.0016702

34. Berger SL, Kouzarides T, Shiekhattar R, Shilatifard A (2009) An operational definition of epigenetics. Genes Dev 23:781–783. https://doi.org/10.1101/gad.1787609

35. McDonald OG, Li X, Saunders T, et al (2017) Epigenomic reprogramming during pancreatic cancer progression links anabolic glucose metabolism to distant metastasis. Nat Genet 49:367–376. https://doi.org/10.1038/ng.3753

36. Boj SF, Hwang C Il, Baker LA, et al (2015) Organoid models of human and mouse ductal pancreatic cancer. Cell 160:324–338. https://doi.org/10.1016/j.cell.2014.12.021

37. Gao N, LeLay J, Vatamaniuk MZ, et al (2008) Dynamic regulation of Pdx1 enhancers by Foxa1 and Foxa2 is essential for pancreas development. Genes Dev 22:3435–3448. https://doi.org/10.1101/gad.1752608

38. Vigil D, Martin TD, Williams F, et al (2010) Aberrant overexpression of the Rgl2 Ral small GTPase-specific guanine nucleotide exchange factor promotes pancreatic cancer growth through Ral-dependent and Ral-independent mechanisms. J Biol Chem 285:34729–34740. https://doi.org/10.1074/jbc.M110.116756

39. Larsen HL, Grapin-Botton A (2017) The molecular and morphogenetic basis of pancreas organogenesis. Semin. Cell Dev. Biol. 66:51–68

40. Kim MP, Li X, Deng J, et al (2021) Oncogenic KRAS recruits an expansive transcriptional network through mutant p53 to drive pancreatic cancer metastasis.

Cancer Discov candisc.1228.2020. https://doi.org/10.1158/2159-8290.cd-20-1228

41. Zhan T, Rindtorff N, Boutros M (2017) Wnt signaling in cancer. Oncogene 36:1461–1473

42. Bailey P, Chang DK, Nones K, et al (2016) Genomic analyses identify molecular subtypes of pancreatic cancer. Nature 531:47–52. https://doi.org/10.1038/nature16965

43. Moffitt RA, Marayati R, Flate EL, et al (2015) Virtual microdissection identifies distinct tumor- and stroma-specific subtypes of pancreatic ductal adenocarcinoma. Nat Genet 47:1168–1178. https://doi.org/10.1038/ng.3398

44. Collisson EA, Sadanandam A, Olson P, et al (2011) Subtypes of pancreatic ductal adenocarcinoma and their differing responses to therapy. Nat Med 17:500–503. https://doi.org/10.1038/nm.2344

45. Andricovich J, Perkail S, Kai Y, et al (2018) Loss of KDM6A Activates Super-Enhancers to Induce Gender-Specific Squamous-like Pancreatic Cancer and Confers Sensitivity to BET Inhibitors. Cancer Cell 33:512-526.e8. https://doi.org/10.1016/j.ccell.2018.02.003

46. Lavery WJ, Barski A, Wiley S, et al (2020) KMT2C/D COMPASS complex-associated diseases [KCDCOM-ADs]: An emerging class of congenital regulopathies. Clin. Epigenetics 12:1–20

47. Piunti A, Shilatifard A (2016) Epigenetic balance of gene expression by polycomb and compass families. Science (80-. ). 352

48. Li E, Zhang Y (2014) DNA methylation in mammals. Cold Spring Harb Perspect Biol

6:. https://doi.org/10.1101/cshperspect.a019133

49. Wu SC, Zhang Y (2010) Active DNA demethylation: Many roads lead to Rome. Nat. Rev. Mol. Cell Biol. 11:607–620

50. Valinluck V, Sowers LC (2007) Endogenous cytosine damage products alter the site selectivity of human DNA maintenance methyltransferase DNMT1. Cancer Res 67:946–950. https://doi.org/10.1158/0008-5472.CAN-06-3123

51. Brenet F, Moh M, Funk P, et al (2011) DNA Methylation of the First Exon Is Tightly Linked to Transcriptional Silencing. PLoS One 6:e14524. https://doi.org/10.1371/journal.pone.0014524

52. Angeloni A, Bogdanovic O (2019) Enhancer DNA methylation: Implications for gene regulation. Essays Biochem. 63:707–715

53. Vincent A, Omura N, Hong SM, et al (2011) Genome-wide analysis of promoter methylation associated with gene expression profile in pancreatic adenocarcinoma. Clin Cancer Res 17:4341–4354. https://doi.org/10.1158/1078-0432.CCR-10-3431

54. Ball MP, Li JB, Gao Y, et al (2009) Targeted and genome-scale strategies reveal gene-body methylation signatures in human cells. Nat Biotechnol 27:361–368. https://doi.org/10.1038/nbt.1533

55. Aran D, Toperoff G, Rosenberg M, Hellman A (2011) Replication timing-related and gene body-specific methylation of active human genes. Hum Mol Genet 20:670–680. https://doi.org/10.1093/hmg/ddq513

56. Paz MF, Fraga MF, Avila S, et al (2003) A systematic profile of DNA methylation in human cancer cell lines. Cancer Res 63:1114–1121

57. Saghafinia S, Mina M, Riggi N, et al (2018) Pan-Cancer Landscape of Aberrant DNA Methylation across Human Tumors. Cell Rep 25:1066-1080.e8. https://doi.org/10.1016/j.celrep.2018.09.082

58. Salhab A, Nordström K, Gasparoni G, et al (2018) A comprehensive analysis of 195 DNA methylomes reveals shared and cell-specific features of partially methylated domains. Genome Biol 19:. https://doi.org/10.1186/s13059-018-1510-5

59. Thompson MJ, Rubbi L, Dawson DW, et al (2015) Pancreatic Cancer Patient Survival Correlates with DNA Methylation of Pancreas Development Genes. PLoS One 10:e0128814. https://doi.org/10.1371/journal.pone.0128814

60. Mishra NK, Southekal S, Guda C (2019) Survival analysis of multi-omics data identifies potential prognostic markers of pancreatic ductal adenocarcinoma. Front. Genet. 10

61. Mishra NK, Guda C (2017) Genome-wide DNA methylation analysis reveals molecular subtypes of pancreatic cancer. Oncotarget 8:28990–29012. https://doi.org/10.18632/oncotarget.15993

62. Roy S, Singh AP, Gupta D (2021) Unsupervised subtyping and methylation landscape of pancreatic ductal adenocarcinoma. Heliyon 7:. https://doi.org/10.1016/j.heliyon.2021.e06000

63. Hezel AF, Kimmelman AC, Stanger BZ, et al (2006) Genetics and biology of pancreatic ductal adenocarcinoma. Genes Dev. 20:1218–1249

64. Koizumi M, Doi R, Toyoda E, et al (2003) Increased PDX-1 expression is associated with outcome in patients with pancreatic cancer. Surgery 134:260–266.

https://doi.org/10.1067/msy.2003.231

65. Jones S, Zhang X, Parsons DW, et al (2008) Core signaling pathways in human pancreatic cancers revealed by global genomic analyses. Science (80- ) 321:1801–1806. https://doi.org/10.1126/science.1164368

66. Espinet E, Gu Z, Imbusch CD, et al (2020) Aggressive PDACs show hypomethylation of repetitive elements and the execution of an intrinsic IFN program linked to a ductal cell-of-origin. Cancer Discov CD-20-1202. https://doi.org/10.1158/2159-8290.CD-20-1202

67. Tan AC, Jimeno A, Lin SH, et al (2009) Characterizing DNA methylation patterns in pancreatic cancer genome. Mol Oncol 3:425–438. https://doi.org/10.1016/j.molonc.2009.03.004

68. Kelly TK, De Carvalho DD, Jones PA (2010) Epigenetic modifications as therapeutic targets. Nat. Biotechnol. 28:1069–1078

69. Hessmann E, Johnsen SA, Siveke JT, Ellenrieder V (2017) Epigenetic treatment of pancreatic cancer: Is there a therapeutic perspective on the horizon? Gut 66:168–179. https://doi.org/10.1136/gutjnl-2016-312539

70. Brancaccio M, Natale F, Falco G, Angrisano T (2019) Cell-Free DNA Methylation: The New Frontiers of Pancreatic Cancer Biomarkers' Discovery. Genes (Basel) 11:14. https://doi.org/10.3390/genes11010014

71. Shinjo K, Hara K, Nagae G, et al (2020) A novel sensitive detection method for DNA methylation in circulating free DNA of pancreatic cancer. PLoS One 15:1–18. https://doi.org/10.1371/journal.pone.0233782

72. Singh N, Rashid S, Rashid S, et al (2020) Clinical significance of promoter methylation status of tumor suppressor genes in circulating DNA of pancreatic cancer patients. J Cancer Res Clin Oncol 146:897–907. https://doi.org/10.1007/s00432-020-03169-y

73. Nishizawa N, Harada H, Kumamoto Y, et al (2019) Diagnostic potential of hypermethylation of the cysteine dioxygenase 1 gene ( CDO 1 ) promoter DNA in pancreatic cancer. Cancer Sci 110:2846–2855. https://doi.org/10.1111/cas.14134

74. Manuyakorn A, Paulus R, Farrell J, et al (2010) Cellular histone modification patterns predict prognosis and treatment response in resectable pancreatic adenocarcinoma: Results from RTOG 9704. J Clin Oncol 28:1358–1365. https://doi.org/10.1200/JCO.2009.24.5639

## Chapter Two – *Engrailed-1* Promotes Pancreatic Cancer Metastasis

*This chapter is published in *Advanced Science*. 2024, 11, 2308537. https://doi.org/10.1002/advs.202308537, under an open-access Creative Common CC BY license.

### Summary

*Engrailed-1* (*EN1*) is a critical homeodomain transcription factor (TF) required for neuronal survival, and EN1 expression has been shown to promote aggressive forms of triple negative breast cancer. Here, we report that *EN1* is aberrantly expressed in a subset of pancreatic ductal adenocarcinoma (PDA) patients with poor outcomes. EN1 predominantly repressed its target genes through direct binding to gene enhancers and promoters, implicating roles in the activation of MAPK pathways and the acquisition of mesenchymal cell properties. Gain- and loss-of-function experiments demonstrated that *EN1* promoted PDA transformation and metastasis *in vitro* and *in vivo*. Our findings nominate the targeting of *EN1* and downstream pathways in aggressive PDA.

## Introduction

Pancreatic cancer is the third leading cause of cancer-related deaths in the United States, with a 12% 5-year relative survival rate, the lowest among all common cancers[1]. Pancreatic ductal adenocarcinoma (PDA) is the most common and challenging form of pancreatic cancer due to its highly metastatic nature, lack of screening, and resistance to current chemotherapeutic regimens. In PDA, carcinogenesis begins with a gain-of-function mutation of *KRAS* in the pancreatic ductal epithelial cells, leading to the formation of pancreatic intraepithelial neoplasia (PanIN) lesions. The activating mutation in *KRAS* then cooperates with the loss-of-function mutations of tumor suppressor genes, including *TP53*, *SMAD4*, and *CDKN2A*, to further promote PDA progression[2]. In contrast, recurrent genetic alterations driving PDA metastasis remain elusive. Instead, metastatic lesions harbor a similar pattern of driver mutations as seen throughout the primary PDA[3], suggesting that PDA metastasis may be driven by nongenetic alterations, such as fluctuations in signal transduction and transcriptional programs. However, the molecular mechanisms driving such fluctuations are understudied; therefore, there is an urgent need to understand the driving force behind PDA progression to develop new therapeutic strategies to counter disease progression and improve patients' survival.

Aberrant expressions of transcription factors (TFs) and the subsequent alterations in epigenetic landscapes may be responsible for the fluctuations of transcriptional programs during cancer progression[4]. For example, through modulating enhancer activities, TF TP63 is

capable of activating the transcriptional programs of the squamous PDA subtype, leading to an aggressive cancer phenotype[5]. Until recently, studying the dynamic changes of transcriptional programs as cancer progresses has been difficult due to the lack of *in vitro* PDA progression models for different stages of PDA. To address this, we previously established an *in vitro* organoid model derived from *Kras*$^{+/LSL\text{-}G12D}$*; Trp53*$^{+/LSL\text{-}R172H}$*; Pdx1-Cre* (KPC) mouse[6]. The KPC mouse model is considered the standard model to study PDA initiation and progression, which faithfully recapitulates many aspects of human disease[7]. The organoid models derived from the KPC PDA tissues allowed a direct comparison of the tumor (mT)- and paired metastasis (mM)-derived organoids. Previously, we showed that TF FOXA1 is capable of activating the transcriptional programs of endoderm lineage through enhancer reprogramming to promote PDA metastasis[8]. Likewise, it is possible that other TFs are also aberrantly regulated in PDA progression and confer aggressive characters through such epigenetic reprogramming, which warrants further investigation.

During development, the required cellular processes (e.g., differentiation and death) are tightly regulated by interactions between epigenomes and TF-mediated lineage-specific gene programs[9]. Interestingly, the genes involved in neurodevelopmental programs, such as axon guidance pathways, are frequently altered in many cancers, including PDA, leading to disease progression[10; 11]. It is, therefore, probable that cancer cells hijack TFs that govern these developmental pathways to confer a survival benefit. Homeobox TFs are evolutionarily conserved master regulators that are essential for embryonic development. Among the homeobox TFs, Engrailed-1 (EN1) is essential in the development of the central nervous

system and implicated in the control of cell differentiation, growth, survival, and axon guidance at the cellular level[12-16]. In addition, several studies have reported aberrantly expressed EN1 and its association with poor prognosis in human malignancies, including glioblastoma, salivary gland adenoid cystic carcinoma, and breast-related cancers[17-23]. However, the detailed molecular mechanisms by which EN1 promotes PDA progression remain unknown.

In this study, we first identified aberrant expression of EN1 from mM-derived PDA organoids. We then showed that EN1 promotes metastatic properties in PDA through direct bindings to promoter and enhancer of the genes involved in several cellular pathways, including cell death and mitogen-activated protein kinase (MAPK) pathways. As a result, aberrant expression of EN1 accelerates PDA progression *in vivo*. Therefore, targeting EN1 and its downstream pathways can be an effective therapeutic strategy for EN1-high PDA patients.

## Material and Methods

### Mouse models

All experiments were performed in accordance with the Institutional Animal Care and Use Committee (IACUC) of the University of California Davis and the NIH policies of the laboratory animal use. The behaviors and characterization of KPC (*Kras*$^{+/LSL\text{-}G12D}$*; Trp53*$^{+/LSL\text{-}R172H}$*; Pdx1-Cre*) alleles with the C57BL/6J strain have been described previously[8; 65]. 129S6/SvEvTac mouse harboring *En1*$^{tm8.1Alj}$ allele[66] were purchased from the Jackson Laboratory (JAX stock #007918) and the allele were introduced into KPC mice through a series backcrosses to generate KPEC (*Kras*$^{+/LSL\text{-}G12D}$*; Trp53*$^{+/LSL\text{-}R172H}$*; En1*$^{loxP/loxP}$*; Pdx1-Cre)* mice. For histological analysis, KPC and KPEC mice were sacrificed at 120 days of age. All animals were housed in the specific pathogen-free conditions and were regularly monitored by the veterinarians.

### Human specimens

Human tissue microarrays from 39 patients were obtained from the Rapid Autopsy Program at the University of Nebraska Medical Center. Written informed consent was obtained prior to tissue acquisition from all patients. Human pancreatic, metastatic, and unaffected specimens from decedents who have previously been diagnosed with pancreatic ductal adenocarcinoma were obtained from the University of Nebraska Medical Center's Tissue Bank through the Rapid Autopsy Program (RAP) in compliance with IRB 091-01. Non-cancer tissues are collected in a manner similar to RAP specimens through the UNMC Normal

Organ Recovery (NORs) Program. To ensure specimen quality, organs were harvested within three hours post-mortem, and the specimens flash-frozen in liquid nitrogen or were placed in formalin for immediate fixation. Sections are cut from paraffin blocks of formalin-fixed tissue into 4-micron thick sections and mounted on charged slides. Samples were assessed to be tumor and metastasis based on pathologist analysis.

**Tissue culture conditions**

Murine pancreatic primary tumor organoids (mT3, mT6, mT19, and mT23), metastatic organoids (mM1, mM3, mM6, and mM10), and tumor 2D cell lines (mT3-2D, mT4-2D, mT5-2D, and mT8-2D) from the tumor-bearing KPC mice were established and characterized previously[6; 8; 67]. Murine pancreatic organoid culture media contains Advanced DMEM/F-12 (Thermo Fisher 12634028), 10mM HEPES (Thermo Fisher 15630080), 1% Penicillin-Streptomycin (Thermo Fisher 15140122), 1% GlutaMAX Supplement (Thermo Fisher 35050061), 0.5μM A 83-01 (Fisher Scientific 29-391-0), 0.05μg/mL mEGF (Fisher Scientific PMG8043), 0.1mg/mL hFGF-10 (Pepro Tech 100-26), 0.01mM hGastrin I (Fisher Scientific 30-061), 0.1μg/mL mNoggin (Pepro Tech 250-38), 1.25mM *N*-Acetyl-L-cysteine (Millipore Sigma A9165), 10μM Nicotinamide (Millipore Sigma N0636), 1X B-27 Supplement (Fisher Scientific 17-504-044), and 1x RSPO1-conditioned medium. Murine 2D culture media contains DMEM (Corning 10-013-CV), 10% FBS (Gen Clone 25-550H), and 1% Penicillin-Streptomycin. Human PDA cell lines SUIT2 (Glow Biologics GBTC-1088B), CFPAC1 (ATCC CRL-1918), BxPC3 (ATCC CRL-1687), and PATU 8988s (Glow Biologics GBTC-0209H) were cultured with RPMI 1640 (Corning 10-040-CV), 10% FBS, and 1% Penicillin-Streptomycin.

## Next-generation sequencing

### Cleavage under targets & release using nuclease (CUT&RUN) assay

CUT&RUN assay was performed according to the manufacturer's instructions (Cell Signaling Technology CST 86652). Briefly, cells were trypsinized (Fisher Scientific 25-300-062) into single cells and counted using 0.4% Trypan Blue Stain (Thermo Fisher T10282) and Countess 3 FL Automated Cell Counter (Thermo Fisher). 250,000 cells were used for each reaction and input sample. CST CUT&RUN Protocol Section I.A. "Live Cell Preparation" was followed to precipitate histone marks, and the Section I.B. "Fixed Cell Preparation" was followed to precipitate FLAG-tagged EN1. 1μL of anti-acetyl-Histone H3 (Lys27) antibody (CST 8173), 1μL of anti-tri-Methyl-Histone H3 (Lys4) antibody (CST 9751), or 1μL of anti-FLAG® M2 antibody (Thomas Scientific C986X12) was added to each reaction. Antibody incubation was carried at 4°C for 16 hours. 50 pg sample normalization spike-in DNA was added into each reaction during DNA digestion and diffusion. Fragmented DNA was purified using ChIP DNA Clean & Concentrator (ZYMO Research D5205). Bioruptor (Diagenode) was used to sonicate the input samples for 13 cycles (30 sec on/30 sec off at high amplitude). For data analysis, pair-end raw data was aligned to mm9 reference genome using Bowtie2[68] and filtered using SAMtools[69]. bamCoverage[70] was used to generate UCSC BigWig file. Peak calling was performed using MACS2 callpeak[71; 72]. Data was annotated using ChIPseeker[73].

### RNA preparation for sequencing

For 2D cells, 70% confluent cells were trypsinized into single cells to yield $2x10^6$ cells. For organoids, 70% of confluent organoids were trypsinized into single cells to yield $5x10^5$ cells.

Cells were lysed with TRIzol reagent (Fisher Scientific 15-596-026), and RNA was collected per the manufacturer's instructions. Isolated RNA was treated with PureLink on-column DNase set (Thermo Fisher 12185010) and purified using PureLink RNA mini kit (Thermo Fisher 12183018A). For data analysis, pair-end raw data was aligned to the mm9 reference genome for murine samples and the hg19 reference genome for human samples using HISAT2[74]. Sequencing reads were counted and normalized using featureCounts[75]. DESeq2[76] was then used to identify differentially expressed genes.

**Library preparation and sequencing**

Library preparation and sequencing for CUT&RUN and RNA were performed by Novogene Co., LTD (Beijing, China). Briefly, for CUT&RUN, sample quality control was performed prior to library construction. Then, the DNA fragments were end-repaired, A-tailed, and ligated with Illumina adapters. Following this, the DNA library was filtered by size selection and PCR amplification. Quantified DNA libraries were pooled and sequenced using NovaSeq6000 PE150. Quality controls, including sequencing quality distribution, sequencing error rate distribution, ATCG base distribution, and adapter filtering, were performed before raw data delivery. For RNA, sample quality control was performed prior to library construction. Then, mRNA was purified from the total RNA using polyT-oligo beads. After fragmentation, the first strand of cDNA was synthesized using random hexamers, and the second strand of cDNA was synthesized using dTTP. Following, the cDNA was end-repaired, A-tailed, ligated with Illumina adapters, size selection, amplification, and purification. Quantified libraries were pooled and sequenced using NovaSeq6000, and paired-end reads were generated. Quality

controls, including removing adapter, poly-N, and low quality reads, and Q20, Q30, and GC content calculations, were performed before raw data delivery.

**Gene Ontology Analysis**

GO for the RNA-seq datasets was analyzed using GSEA[77; 78] C5: ontology gene sets derived from the GO Biologal Process ontology. GREAT analysis[79] was used to perform GO for the EN1 genomic targets generated from the CUT&RUN-seq experiment. After data annotation of the EN1 genomic targets by ChIPseeker, DAVID[80; 81] was used to perform GO for the EN1 target genes.

**Protein and DNA-related experiments**

**Cloning**

FLAG-tagged *En1* cDNA (Neo-FLAG-En1) was subcloned into MSCV-PGK-Neo-IRES-GFP (Neo-Empty) plasmid (Addgene 105505). FLAG-tagged *EN1* expression plasmid (MSCV-FLAG-EN1) was obtained from VectorBuilder (Vector ID: VB220501-1183hep) and the negative control plasmid (MSCV-Empty) was generated using restriction enzymes AvrII (NEB R0174S) and EcoRI-HF (NEB R3101S), and blunting & ligation kit (NEB E0542S) to remove FLAG-EN1 sequence. *En1* and *EN1* shRNAs were obtained from the TRC shRNA library available at the Broad Institute (sh*En1* #1 TRCN0000082149, sh*En1* #2 TRCN0000414478, sh*EN1* #1 TRCN0000013899, sh*EN1* #2 TRCN0000013968) in pLKO.1 puro construct. *Dusp1* promoter was generated using AmpliTaq Gold 360 Master Mix (Thermo Fisher 4398881) and cloned into a pLS-mP-Luc plasmid (Addgene 106253) using restriction enzymes Xbal (NEB

R0145S) and SbfI-HF (NEB R3642S). The primer pair used for *Dusp1* promoter PCR or EN1 gRNA cloning are listed in Table 2.

**Reverse transcription and quantitative PCR**

Total RNA was extracted using TRIzol reagents per the manufacturer's instructions as described in the RNA preparation for sequencing. RNA concentration was measured using NanoDrop 1000 (Thermo Fisher). 1500 ng of RNA was used for cDNA synthesis with a high-capacity cDNA reverse transcription kit (Thermo Fisher 4368814). 1 μL of the cDNA or CUT&RUN DNA was used for qPCR with *Power* SYBR green PCR master mix (Thermo Fisher 4368702) on LightCycler 480 instrument II (Roche Diagnostics). The qPCR results were quantified using the 2^(delta)(delta)Ct method with housekeeping gene *GAPDH*, *Gapdh*, or *ACTB*, *Actb* for data normalization. qPCR primer sequences used in the manuscript are listed in Table 2.

**Western blot analysis**

70% confluent cells were harvested and lysed with protein extraction buffer (50 mM Tris pH 7.4, 1 mM EDTA, 150 mM NaCl, 1% NP-40, and 1x Halt protease inhibitor cocktail (Thermo Fisher 78437)) on ice for 30 minutes, centrifuged at 20,000 RCF 4°C for 20 minutes, and collected the supernatant. Protein was measured for concentration with a protein assay kit (Bio-Rad 5000111) and denatured with a sample reducing agent (Thermo Fisher NP0009). 10 μg protein lysate was loaded into 4 to 12% Bis-Tris 1.0 cm gels (Thermo Fisher NP0321BOX or NP0322BOX) and electrophoresis was carried using mini gel tank (Thermo Fisher A25977)

at 120 V. Protein transfer to PVDF membrane (Millipore Sigma IPVH00010) was carried using transfer cell (Bio-rad 1703930) at 400 mA for 2 hours at 4°C. The membrane was blocked with 5% Non-fat milk dissolved in PBS with 1% Tween-20 (PBST) at room temperature for 1 hour, washed with PBST four times for 5 minutes each, and incubated with diluted primary antibody at 4°C for 16 hours. The membrane was washed with PBST four times 5 minutes each and incubated with diluted secondary antibody at room temperature for 1 hour, followed by PBST wash four times 5 minutes each. Luminol signals were developed using pico chemiluminescent substrate (Thermo Fisher 34577) and detected using Amersham Imager 600 (GE Healthcare Life Sciences). Antibodies used in the manuscript are listed in Table 3. For data analysis, phospho-ERK data normalization = (phospho-ERK bands intensities)/(ERK bands intensities). HIF-1a and c-MYC data normalization = HIF-1a or c-MYC bands intensities/Vinculin bands intensities. Secondary normalization was analyzed by comparing the *En1* knockdown groups with the scramble control.

**Nuclear co-immunoprecipitation and mass spectrometry**

A nuclear complex co-immunoprecipitation assay was performed according to the manufacturer's instructions (Active Motif 54001) using the high stringency buffer. Protein complex was captured using DynaGreen Protein A/G Magnetic beads (Thermo Fisher 80104G) and 5 μg of antibody per reaction. The antibodies used in this experiment are listed in Table 3. LC-MS/MS and data analysis were performed by the UC Davis Genome Center Proteomics Core Facility. The significantly enriched protein was identified based on log2 fold

change >2 in the peptide abundance between the experiment vs. the control, as determined from two independent biological samples.

**Genotyping**

Mice toes were clipped at day 10.5, and the genomic DNA was isolated using 30mL TaqAN buffer (10mM Tris-HCl, 50mM KCl, 2.5 mM $MgCl_2$, 0.45% NP-40, 0.45% Tween-20, and 3μL/mL of Proteinase K (NEB P8107S)) at 56°C for 1 hour followed by denaturation at 96°C for 10 minutes. *Taq* DNA polymerase (NEB M0273E) was used to PCR *Trp53* and *Cre*. Platinum hot start PCR master mix (Thermo Fisher 13000012) was used to PCR *Kras* and *En1*. PCR conditions for *Trp53, Trp53* het/homo, and *Cre* was 94°C 3 min, 40 cycles of 94°C 1 min / 60°C 1 min / 72°C 1 min, and 72°C 3 min. PCR conditions for *Kras* were 94°C 3 min, 35 cycles of 94°C 1 min / 69°C 2 min / 72°C 1 min, and 72°C 3 min. PCR conditions for *En1* were 94°C 2 min, 40 cycles of 94°C 30 sec / 60°C 30 sec / 72°C 30 sec, and 72°C 2 min. AmpliTaq Gold 360 master mix (Thermo Fisher 4398876) was used to PCR 1 loxP *En1*, and the PCR condition was 95°C 5 min, 40 cycles of 95°C 30 sec / 61°C 30 sec / 72°C 30 sec, and 72°C 5 min. PCR primer sequences used in the manuscript are listed in Table 2.

**Retrovirus production and infection**

Retrovirus was produced in either Phoenix-AMPHO (ATCC CRL-3213) or Phoenix-ECO (ATCC CRL-3214), and lentivirus was produced in HEK293T (ATCC CRL-3216) via X-tremeGENE9 (Millipore Sigma 6365809001) transfection. Cells were first grown to 70% confluence in a 10-cm tissue culture plate (Genesee Scientific 25-202). Before transfection, culture media was

replaced with DMEM supplemented with 10% FBS. For retrovirus, 10μg transfer plasmid and 15μL X-tremeGENE9 reagent were mixed well in 400μL DMEM. For lentivirus, 5μg transfer plasmid, 2.25μg psPAX2 (Addgene 12260), and 0.75μg pMD2.G (Addgene 12259) was mixed well in 400mL DMEM. The mixture was incubated at room temperature for 20 minutes then added to the cell culture dropwise. The condition media was collected after 48-72 hours and filtered through a 0.2mm filter (PALL 4612). Organoid infection procedures were described previously[8]. For infecting 2D cells, filtered conditional media was added to host cells grown at 50% confluence with 10mg/mL polybrene (Thomas Scientific C788D57 (EA/1)). Three days after infection, the cells were selected by 2μg/mL puromycin (Fisher Scientific 53-79-2), 1mg/mL Geneticin G418, or fluorescence-activated cell sorting (Sony SH800S).

**Luciferase reporter assay**

Pierce Firefly Luciferase Glow Assay Kit (Thermo Fisher 16176) was used to perform the luciferase reporter assay per the manufacturer's instructions. 30,000 cells were collected and lysed with 100 μL lysis buffer. 20 μL of the cell lysate was then mixed with 50 μL of the luciferase mix. After 10 minutes of incubation, avoiding light, the luciferase activity was detected by SpectraMax iD5 microplate reader (Molecular Devices).

**Histology**

**Immunohistochemistry staining**

Paraffin-embedded tissue sections were first placed in an oven at 60°C for 30 minutes. The slides were placed in Histo-Clear (National Diagnostics HS-200) for two changes 10 minutes

each, 100% EtOH two changes 2 minutes each, 95% EtOH two changes 2 minutes each, 85% EtOH two changes 2 minutes each, 75% EtOH two changes 2 minutes each, deionized distilled water ($ddH_2O$) one change for 1 minute, and PBS one change for 1 minute. To retrieve antigens, the slides were placed in Citrate-EDTA buffer (Abcam ab93678), boiled using an electric pressure cooker (Cuisinart) for 10 minutes at low pressure, and slowly cooled at room temperature for 1 hour. Incubate the sections with PBS, two changes 5 minutes each. The sections were then incubated with BLOXALL (Vector Lab SP-6000-100) for 10 minutes and 2.5% horse serum (Vector Lab S-2012-50) for 30 minutes. The sections were incubated with the horse serum diluted primary antibody for 16 hours at 4°C. Then, the slides were washed with PBST one change for 3 minutes and PBS one change for 3 minutes. Hereafter, the sections were processed using VECTASTAIN Universal ABC-HRP kit (Vector Lab PK-7200), DAB substrate kit (Vector Lab SK-4100), hematoxylin counterstain (Vector Lab H-3401), and mount with VectaMount (Vector Lab H-5000-60) per manufacturer's instructions. Antibodies used in the manuscript are listed in Table 3. For hematoxylin and eosin (H&E) staining, paraffin-embedded tissue sections were first placed in Histo-clear for three charges, 3 minutes each. A Hematoxylin and Eosin stain kit (Vector Lab H-3502) was then used to stain for H&E per the manufacturer's instructions.

**Immunofluorescence staining**

Paraffin-embedded tissue sections were first placed in an oven at 60°C for 30 minutes. The slides were placed in Histo-Clear (National Diagnostics HS-200) for two changes 10 minutes each, 100% EtOH two changes 2 minutes each, 95% EtOH two changes 2 minutes each,

85% EtOH two changes 2 minutes each, 75% EtOH two changes 2 minutes each, deionized distilled water ($ddH_2O$) one change for 1 minute, and PBS one change for 1 minute. To retrieve antigens, the slides were placed in Citrate-EDTA buffer (Abcam ab93678), boiled using an electric pressure cooker (Cuisinart) for 10 minutes at low pressure, and slowly cooled at room temperature for 1 hour. Incubate the sections with PBS, two changes 5 minutes each. The sections were then incubated with BLOXALL (Vector Lab SP-6000-100) for 10 minutes and 2.5% horse serum (Vector Lab S-2012-50) for 30 minutes. The sections were incubated with the blocking serum diluted antibody for 16 hours at 4°C. Then, the slides were washed with PBST with two changes for 5 minutes and PBS with one change for 5 minutes. The sections were incubated with the blocking serum diluted secondary antibody for 1 hour at room temperature. Then, the slides were washed with PBST with two changes for 5 minutes and PBS with one change for 5 minutes. Hereafter, the slides were mounted with a DAPI mounting medium (Thermo Fisher 00-4959-52). Antibodies used in the manuscript are listed in Table 3.

### *In vitro* assays

#### Colony formation assay

All cell lines were trypsinized to generate single cell suspensions and counted three times to average the cell counts. KPC-2D cell lines (1,000 cells) were resuspended in DMEM supplemented with 10% FBS and 1% Penicillin-Streptomycin and plated in 6-well tissue culture plates (Celltreat 229105) for 5 days. CFPAC1 (500 cells) and PaTu8988S (1000 cells) were resuspended in RPMI 1640 supplemented with 10% FBS and 1% Penicillin-

Streptomycin and plated in 6-well tissue culture plates for 7 and 14 days respectively. SUIT2 (500 cells) and BxPC3 (1000 cells) were resuspended in RPMI 1640 supplemented with 10% FBS and 1% Penicillin-Streptomycin and plated in 24-well tissue culture plates (Corning 3527) for 5 and 14 days respectively. Colonies were stained at room temperature for 1 hour with 2% crystal violet (Thomas Scientific 30430001-1) diluted in 100% methanol to reach the 0.5% final concentration, followed by tap water wash three times and running water wash for five minutes. The plates were imaged with a printer scanner (HP LaserJet Pro), and clonogenic growth was analyzed using the ImageJ (NIH) plugin ColonyArea[82].

**Tumor spheroid formation assay**

All cell lines were trypsinized to generate single cell suspensions and counted three times to average the cell counts. 500 cells of CFPAC1 or SUIT2, 1000 cells of PaTu8988S or BxPC3, and 25,000 cells of KPC-2D cells were resuspended in 3D Tumorsphere Medium XF (PromoCell C-28075) and plated in ultra-low attachment 24-well plates (Millipore Sigma CLS3473-24EA) for 7 days. Culture suspensions were mixed well prior to imaging using the EVOS M5000 imaging system (Fisher Scientific) under a 4x bright field. Spheroids were analyzed by the ImageJ plugin Cell Colony Edge[83].

**Wound-healing assay**

Cells were grown to 90% in 6-well tissue culture plates and wounded linearly using a 200 μL tip followed by three washes of PBS. 24 hours after, cell migration was imaged under 4x bright field. Percentage of migration was determined by ImageJ plugin MRI Wound Healing Tool[84].

**Boyden chamber invasion assay**

Matrigel (Corning 356231) was first diluted in DMEM at 1:3 dilution. 100 μL diluted Matrigel was then placed in a transwell insert (Neta Scientific SIAL-CLS3464) and incubated in the tissue culture incubator for 3 hours. 600 μL of DMEM supplemented with 10% FBS was added to the lower chamber. 50,000 per 200 μL of cells were then added on top of the solidified Matrigel and incubated for 24 hours. After, the transwell was removed and gently scrubbed with a cotton swab and washed twice with PBS. Cells were then stained with SYTO 13 GFP nucleic acid stain (Life Technologies S7575) per manufacturer's instructions and imaged under 4x GFP channel for cell count.

**Organoid survival assay**

Pancreatic organoids were maintained in the complete organoid media prior to single cell dissociation as previously described[8]. 5,000 cells were resuspended in 50 μL Matrigel and plated into a 24-well tissue culture plate for 4 or 5 days. Organoids were cultured either in the organoid complete media and the reduced media (DMEM supplemented with 10% FBS and 1% Penicillin-Streptomycin). Organoids were imaged under a 4x bright field and quantified by ImageJ.

**Organotypic tumor-on-a-chip assay**

Detailed protocols to micro-fabricate tumor-blood vessels have been described previously[33; 85]. Briefly, the organotypic PDA on-a-chip was made with polydimethysiloxane gaskets and

coated with 0.1 mg/mL poly-L-lysine (Millipore Sigma 4707), 1% glutaraldehyde (Electron Microscopy Sciences 16310), and 2.5 mg/mL rat tail collagen I (Corning 354236). Mouse KPC mT3-2D empty and En1 cells were grown in DMEM (Corning 10-013-CV) and human umbilical vein endothelial cells in EGM-2 (Lonza CC-3162). PDA cells were seeded on day 1, and endothelial cells were seeded on day 2. Media in the PDA channel and biomimetic blood vessel was refreshed and monitored daily throughout the experiment.

***In vivo* assays**

Female 6- to 8-week-old syngeneic C57BL/6J or athymic immune-compromised (NU/NU) nude mice were purchased from the Jackson Laboratory (000664) and Charles River Laboratory (088), respectively. All animal procedures were conducted in accordance with the IACUC at Cold Spring Harbor Laboratory. For subcutaneous transplantation, mice were first anesthetized by isoflurane. 500,000 cells resuspended with 50mL Matrigel were injected into the left flank of the subcutaneous space. For orthotopic transplantation, mice were first anesthetized by isoflurane. Iodine solution was applied to the incision site. Then, a small incision (~1 cm) was made at the upper left quadrant of the abdomen. Following, 500,000 cells resuspended with 50mL Matrigel were injected into the pancreas parenchyma. For tail vein transplantation, restrained mice were injected with 50,000 cells resuspended in 50mL PBS intravenously through the tail vein.

**Data Availability**

The sequencing data that support the findings of this study are openly available in NCBI Gene Expression Omnibus database: GSE228805.

Table 2 Oligonucleotide list.

| Primer Name | Sequence | PCR final concentration | Function |
|---|---|---|---|
| *EN1_F* | CTTCTTCAGCTTCCTGGTGC | 1 mM | RT-qPCR |
| *EN1_R* | GTGGTCAAAACTGACTCGCA | 1 mM | RT-qPCR |
| *En1_F* | TCCGAATAGCGTGTGCAGTA | 1 mM | RT-qPCR |
| *En1_R* | CCTACTCATGGGTTCGGCTA | 1 mM | RT-qPCR |
| *GAPDH_F* | CCAAGGAGTAAGACCCCTGG | 1 mM | RT-qPCR |
| *GAPDH_R* | AGGGGAGATTCAGTGTGGTG | 1 mM | RT-qPCR |
| *Gapdh_F* | AGGTCGGTGTGAACGGATTTG | 1 mM | RT-qPCR |
| *Gapdh_R* | TGTAGACCATGTAGTTGAGGTCA | 1 mM | RT-qPCR |
| *ACTB_F* | CACCAACTGGGACGACAT | 0.1 mM | RT-qPCR |
| *ACTB_R* | ACAGCCTGGATAGCAACG | 0.1 mM | RT-qPCR |
| *Actb_F* | GTGACGTTGACATCCGTAAAGA | 0.1 mM | RT-qPCR |
| *Actb_R* | GCCGGACTCATCGTACTCC | 0.1 mM | RT-qPCR |
| *FLAG-EN1_F* | GAGCTGTCTCTGAACGAATCC | 1 mM | RT-qPCR |
| *FLAG-EN1_R* | GGGCCAGCCCATTCTTTAT | 1 mM | RT-qPCR |

| | | | |
|---|---|---|---|
| *Dusp1 promoter 1F* | GGGGAGTGGGTAGTGAGAGA | 1 mM | CUT&RUN-qPCR |
| *Dusp1 promoter 1R* | ACTCTCGCCATTTGTCCTCG | 1 mM | CUT&RUN-qPCR |
| *Dusp1 promoter 2F* | CTGCGGTTCTCCAGAAAAAG | 1 mM | CUT&RUN-qPCR |
| *Dusp1 promoter 2R* | CGGTGAAGCCAGATTAGGAG | 1 mM | CUT&RUN-qPCR |
| *Dusp1 promoter 3F* | GGGAAAGGGGAGTGGGTAGT | 1 mM | CUT&RUN-qPCR |
| *Dusp1 promoter 3R* | CTCGCCATTTGTCCTCGGTA | 1 mM | CUT&RUN-qPCR |
| *Dusp1 intergenic F* | ACCCTGATGGATTGGCAAGG | 1 mM | CUT&RUN-qPCR |
| *Dusp1 intergenic R* | GCTGGTACCACACTGACTCC | 1 mM | CUT&RUN-qPCR |
| *En1_F* | CTAGCCAAACTGCTTTCGACCG | 0.2 mM | Genotyping |
| *En1_R* | GGTAGAGAAGAGGCGAGG | 0.2 mM | Genotyping |

| | | | |
|---|---|---|---|
| *Kras_1* | GTCGACAAGCTCATGCGGGTG | 0.2 mM | Genotyping |
| *Kras_2* | CCTTTACAAGCGCACGCAGACTGTAGA | 0.2 mM | Genotyping |
| *Kras_3* | AGCTAGCCACCATGGCTTGAGTAAGTCTGCA | 0.2 mM | Genotyping |
| *Trp53_1* | AGCTAGCCACCATGGCTTGAGTAAGTCTGCA | 0.2 mM | Genotyping |
| *Trp53_2* | CTTGGAGACATAGCCACACTG | 0.2 mM | Genotyping |
| *Trp53_3* | TTACACATCCAGCCTCTGTGG | 0.2 mM | Genotyping |
| *Trp53_loxp_F* | AGCCTGCCTAGCTTCCTCAGG | 0.2 mM | Genotyping |
| *Trp53_loxp_R* | CTTGGAGACATAGCCACACTG | 0.2 mM | Genotyping |
| *Cre Internal_F* | CTGTCCCTGTATGCCTCTGG | 0.2 mM | Genotyping |
| *Cre Internal_R* | AGATGGAGAAAGGACTAGGCTACA | 0.2 mM | Genotyping |

| | | | |
|---|---|---|---|
| *Cre_F* | CCTGGACTACATCTTGAGTTGC | 0.2 mM | Genotyping |
| *Cre_R* | AGGCAAATTTTGGTGTACGG | 0.2 mM | Genotyping |
| 1 loxP *En1*_F | GGACTCCAAGAACTCACTGTATCTT | 0.2 mM | Genotyping |
| 1 loxP *En1*_R | TGGGTGGGTAGAGAAGAGGC | 0.2 mM | Genotyping |
| *Dusp1* promoter F | CCTGCAGGACAGAAGCGGGGG | 1 mM | Cloning |
| *Dusp1* promoter R | CCTGCAGGTCAGCGTAAAACTTTTAAAGTGACATTC | 1 mM | Cloning |
| EN1 gRNA F | CACCGGCACCAAATACCCGGAGCA | 1 mM | Cloning |
| EN1 gRNA R | AAACTGCTCCGGGTATTTGGTGCC | 1 mM | Cloning |

Table 3. Antibody list.

| **Antibody Name** | **Manufacturer** | **Catalog** | **Experiment** | **Dilution** |
|---|---|---|---|---|
| EN1 | Biorbyt | orb37720 | IHC | 1 to 200 |

| | | | | |
|---|---|---|---|---|
| EN1 | Novus Biologicals | NBP2-57757 | IHC | 1 to 100 |
| EN1 | Developmental studies hybridoma bank | 4G11 | IHC | 1 to 200 |
| FLAG | Thomas Scientific | C986X12 (EA/1) | WB | 1 to 1000 |
| GAPDH | Santa Cruz Biotechnology | sc-32233 | WB | 1 to 2000 |
| Vinculin | Cell Signaling Technology | 13901 | WB | 1 to 2000 |
| Phospho-ERK1/2 | Cell Signaling Technology | 4370S | WB | 1 to 1000 |
| ERK1/2 | Cell Signaling Technology | 4695S | WB | 1 to 1000 |
| HIF-1alpha | Cell Signaling Technology | 36169S | WB | 1 to 1000 |
| c-MYC | Abcam | ab32072 | WB | 1 to 1000 |
| FLAG | Thomas Scientific | C986X12 (EA/1) | CUT&RUN | 1 mL/reaction |
| H3K27Ac | Cell Signaling Technology | 8137 | CUT&RUN | 1 mL/reaction |
| H3K4me3 | Cell Signaling Technology | 9751 | CUT&RUN | 1 mL/reaction |

| | | | | |
|---|---|---|---|---|
| Anti-mouse IgG | Fisher Scientific | NC9832458 | WB | 1 to 20,000 |
| Anti-rabbit IgG | Fisher Scientific | NC9736726 | WB | 1 to 20,000 |
| Vimentin | Abcam | ab92547 | IF | 1 to 300 |
| CK19 | Developmental studies hybridoma bank | TROMA-III | IF | 1 to 500 |
| Anti-human/rabbit IgG | Proteintech | srbAF488-1 | IF | 1 to 800 |
| Anti-rat IgG H&L | Abcam | ab150166 | IF | 1 to 200 |
| DUSP1 | Novus Biologicals | JJ0930 | WB | 1 to 1000 |
| DUSP1 | Novus Biologicals | JJ0930 | IF | 1 to 100 |
| FLAG | Thomas Scientific | C986X12 (EA/1) | IP | 5 mg/reaction |
| Anti-mouse IgG | Fisher Scientific | NC9832458 | IP | 5 mg/reaction |
| Ku80 | Fisher Scientific | PA5-17454 | WB | 1 to 1000 |
| Histone H3 | Novus Biologicals | NB500-171 | WB | 1 to 1000 |
| gH2A.X | Cell Signaling Technology | 9718 | WB | 1 to 1000 |

| | | | | |
|---|---|---|---|---|
| cleaved<br><br>Caspase3 | Cell Signaling Technology | 9664 | WB | 1 to 1000 |

## Results

### EN1 expression is associated with PDA progression and patient poor prognosis

To identify pro-survival factors contributing to PDA progression, we first developed an organoid survival assay where single cell-dissociated pancreatic organoids were grown in DMEM supplemented with 10% FBS without additional growth factors and Wnt ligands (hereafter referred to as the reduced media). In the reduced media, only mM organoid-derived cells survived, formed organoids, and could be passaged continuously, while mT organoid-derived cells failed to grow (Figure 3).

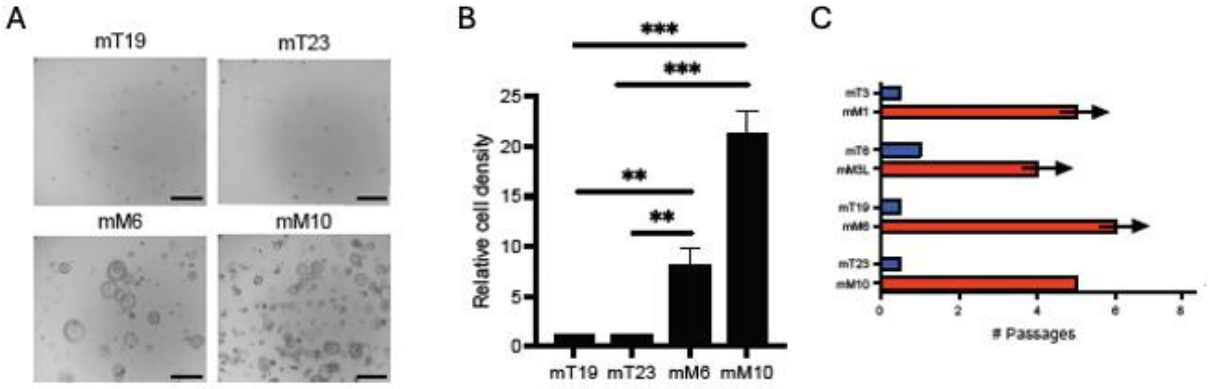


**Figure 3.** (A) Organoid survival assay of KPC tumor (mT)- and metastasis (mM)-derived organoids. Organoids were dissociated into single cells, plated, and grown in 10% FBS DMEM (reduced media) for 5 days. Scale bars, 1 mm. (B) Image-based quantification of mT and paired mM organoid survival in the reduced media 4 days post-cell seeding. n=3, mean ± SEM. (C) Bar plot representing the number of passages the organoids underwent. Arrow indicating the organoids can be passaged continuously in the reduced media. *p*-values were determined by unpaired student's *t* test (two-tail) and *, **, ***, **** indicate *p*-val < 0.05, < 0.01, <0.001, <0.0001, respectively.

Consistent with the known functions of wild-type p53 in cell death[24], the inactivation of p53 in mT organoids resulted in increased organoid formation in the organoid survival assay and promoted PDA progression in vivo (Figure 4), suggesting that organoid survival phenotype can serve as a translatable readout for the *in vivo* context.

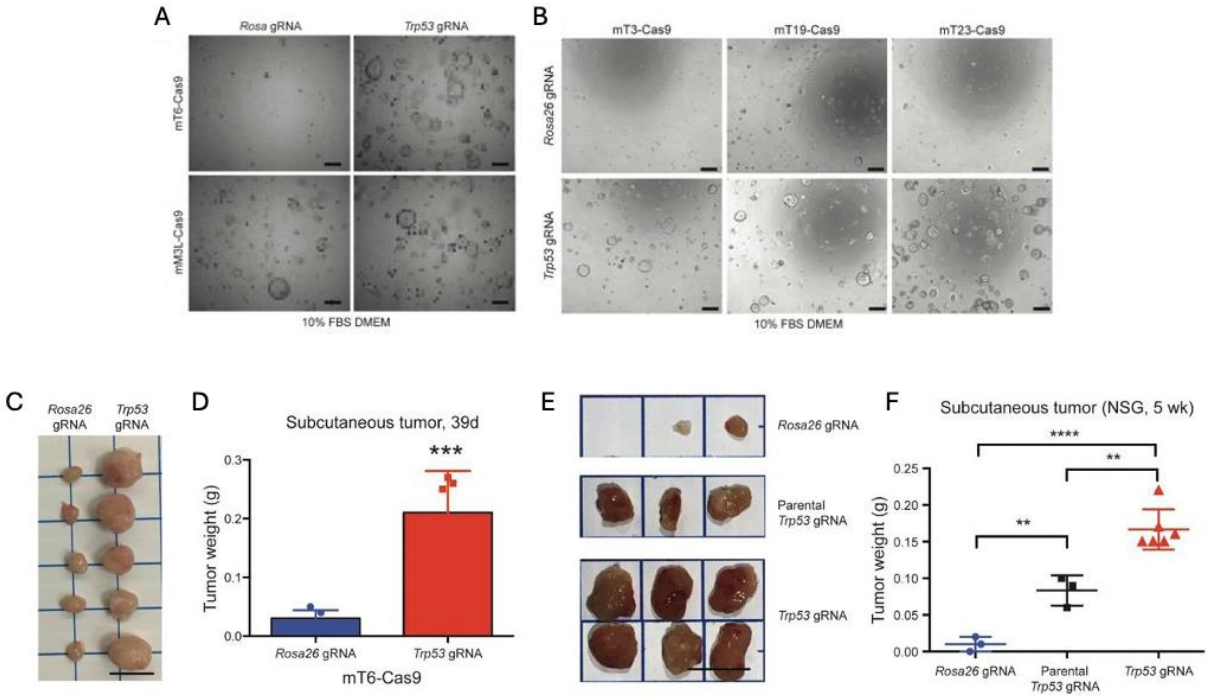


**Figure 4.** (A-B) Image representation of the development of organoid survival assay in the indicated mT and mM organoid pairs with *Trp53* knockout and *Rosa26* knockout control in the reduced media. Scale bar, 1mm. (C-D) Subcutaneous transplantation of mT6 organoids with *Trp53* knockout using CRISPR/Cas9. gRNA against the *Rosa26* locus was used as a control. The tumors were imaged (E) and quantified for tumor weight (F) at 39 days post-injection. n=5 per group, mean ± SD. Scale bar, 10mm. *p*-values were determined by unpaired student's *t* test (two-tail) and *, **, ***, **** indicate *p*-val < 0.05, < 0.01, <0.001, <0.0001, respectively.

Through transcriptome and epigenome profiling on the paired mT and mM organoids, we previously identified that aberrant expression of several developmental TFs led to enhancer

reprogramming and endowed aggressive characteristics seen in PDA metastasis[8; 25]. The TFs, including *Batf2*, *Foxa1*, *Gata5*, *Prrx2*, *Pax9*, *Trerf1*, and *En1*, were highly expressed in mM organoids compared to their paired mT organoids (Figure 5).

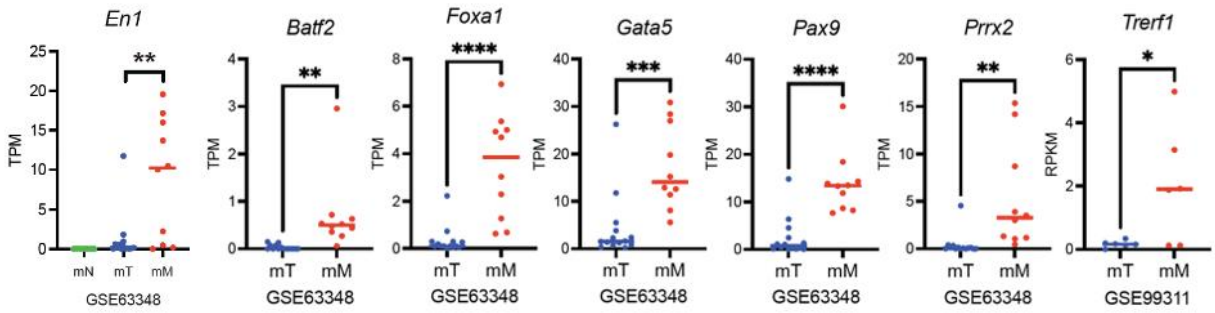


**Figure 5**. RNA-seq-based *En1, Batf2*, *Foxa1*, *Gata5*, *Prrx2*, *Pax9*, and *Trerf1* mRNA expression in organoids from Oni et al. (GSE66348) and Roe et al. (GSE99311). Each dot represents an organoid line. *p*-values were determined by unpaired student's *t* test (two-tail) and *, **, ***, **** indicate *p*-val < 0.05, < 0.01, <0.001, <0.0001, respectively.

To identify functionally important TF(s), we performed the organoid survival assay with mT organoids and the 7 TFs. The retroviral introduction of the 7 TFs enabled mT organoids to survive and propagate in the reduced media (Figure 6A). The withdrawal of an individual TF revealed that mT organoids failed to survive and form organoids without EN1 (Figure 6A-B). Likewise, the introduction of *En1* cDNA in mT organoids increased organoid survival, suggesting that EN1 is a critical pro-survival factor in PDA (Figure 6C-D).

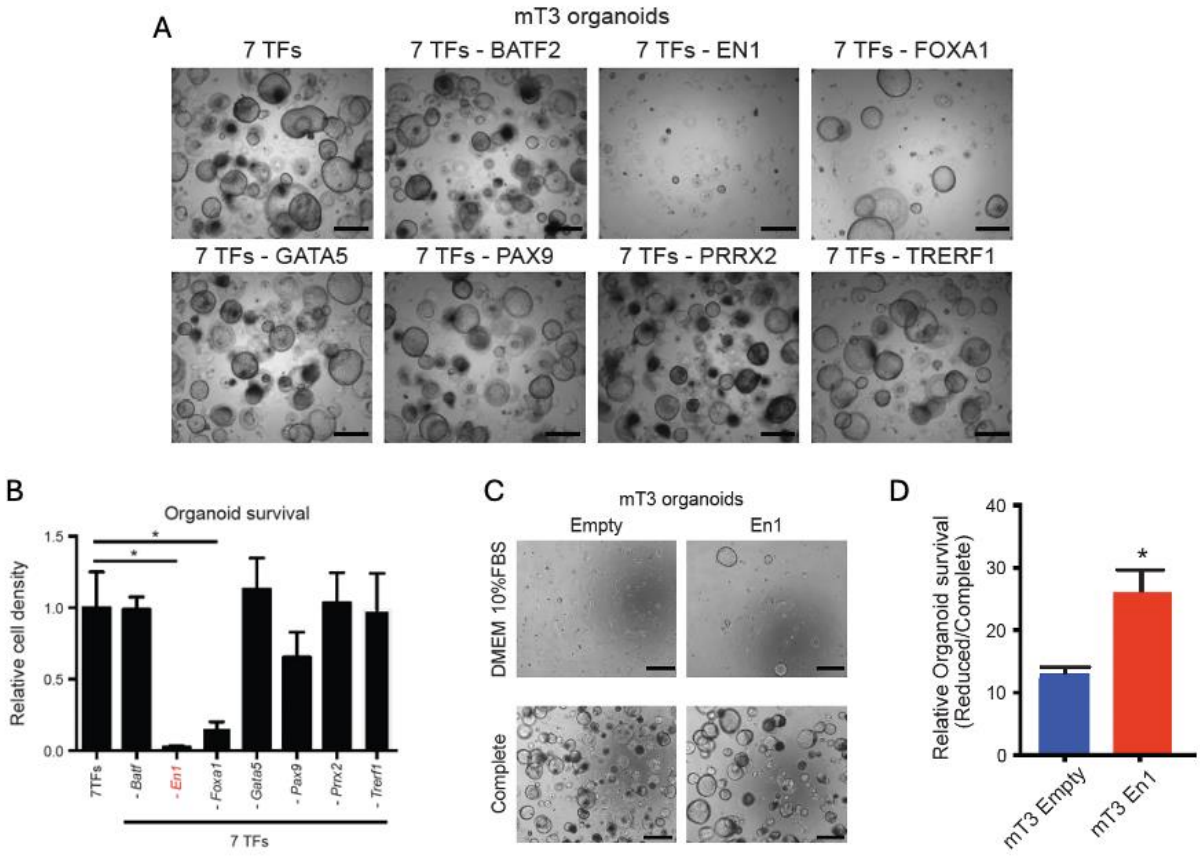


**Figure 6.** (A) 7 TFs (BATF, EN1, FOXA1, GATA5, PAX9, PRRX2, TRERF1) were introduced in mT3 organoids and subjected to organoid survival assay. Each TF was withdrawn from the 7 TFs combination. Scale bars, 1 mm. (B) Relative cell density in the organoid survival assay of Figure 6A was quantified. Mean ± SEM is shown. (C) mT3 organoids with En1 cDNA were subjected to organoid survival assay either in the reduced media or in the complete media for 5 days. (D) Relative cell density in the organoid survival assay of Figure 6C was quantified. Mean ± SEM is shown. *p*-values were determined by unpaired student's *t* test (two-tail) and *, **, ***, **** indicate *p*-val < 0.05, < 0.01, <0.001, <0.0001, respectively.

In concordance with our previous finding[8], when FOXA1 was removed from the 7 TF combination, the organoid survival was also impeded, although to a lesser degree than the EN1 withdrawal. To determine if the advanced stage of PDA expressed EN1 proteins, we performed EN1 IHC using the KPC mice tissue sections and the orthotopic transplantation

sections of the mT organoids. Indeed, we confirmed that EN1 expression was elevated in the late stage of PDA (Figure 7).

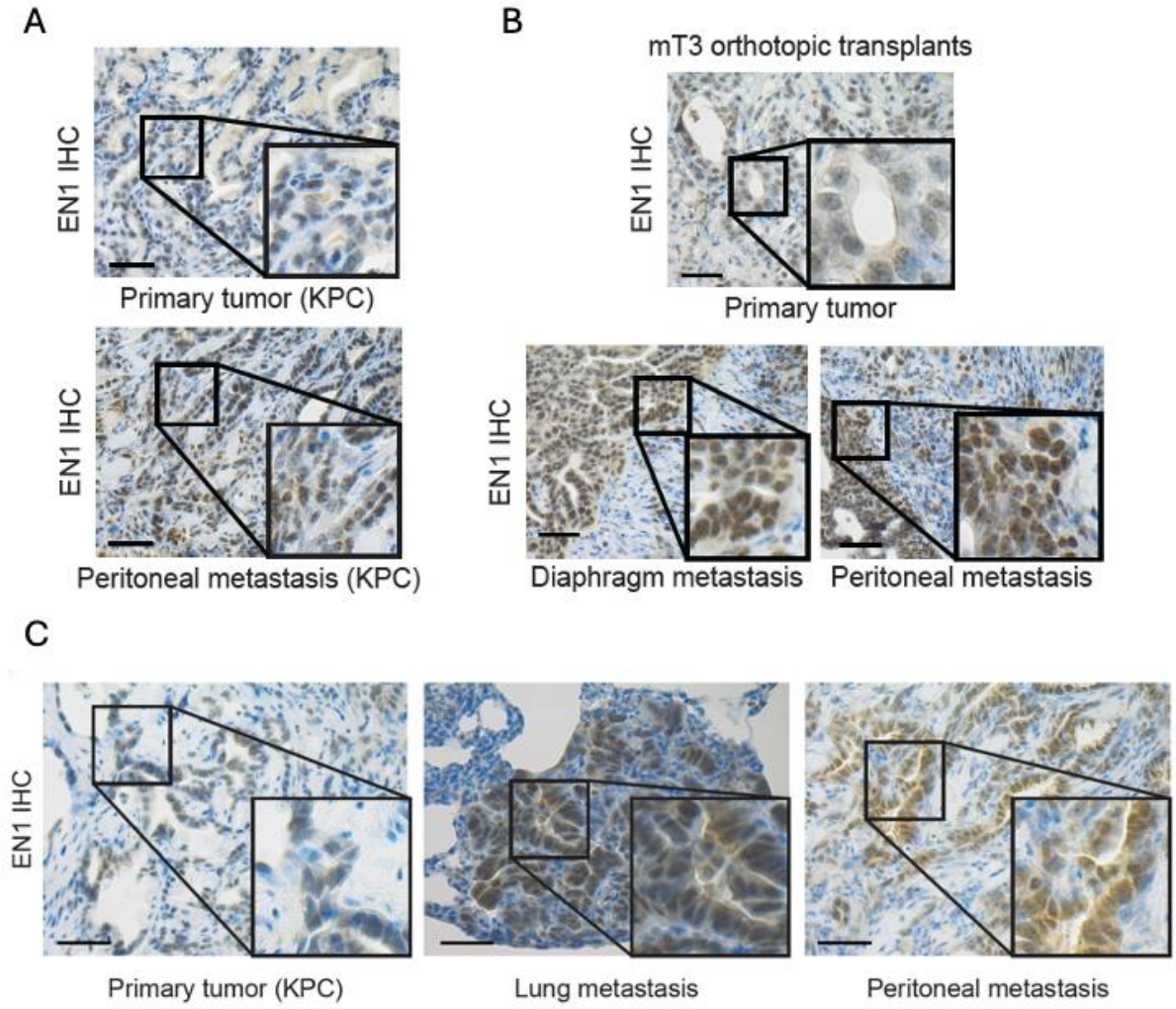


**Figure 7.** (A-B) EN1 IHC of the indicated tissue sections, including primary tumor and peritoneal metastatic lesions from KPC mice (A) and mT3 organoids orthotopic injection models (B). Scale bars, 100 mm. (C) EN1 IHC of the pancreatic primary tumor, lung, and peritoneal metastases from a KPC mouse. Scale bar, 100 μm.

We then analyzed the publicly available RNA-seq datasets of human PDA patients[26; 27]. Consistent with murine models of PDA, we found that *EN1* expression was elevated in the advanced stage of PDA (Figure 8A-B). In addition, analyses of the transcriptomic profile of PDA PDOs and the scRNA-seq dataset[28; 29] revealed that a subset of PDA patients showed EN1 expression (Figure 8C-D).

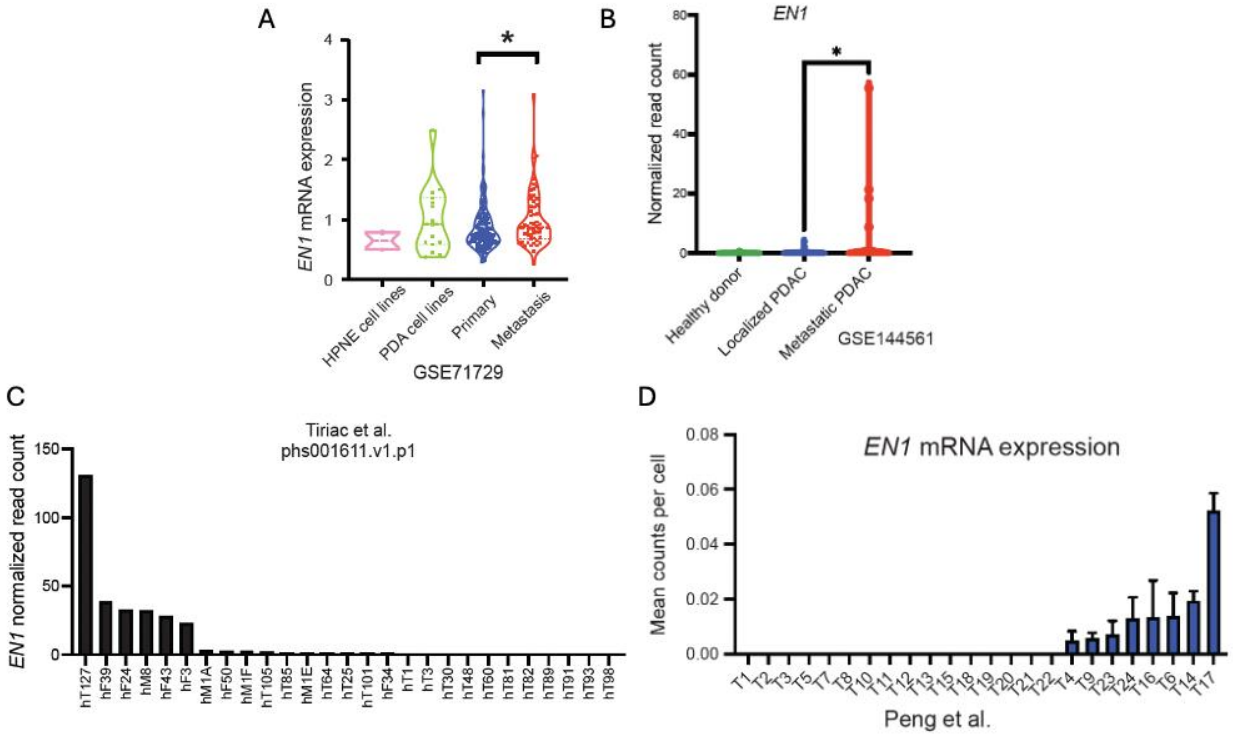


**Figure 8.** (A) Microarray-based *EN1* mRNA expression in cell lines and human PDA tissues from Moffitt et al. (GSE71729). (B) *EN1* normalized read count of primary purified circulating tumor cells from pancreatic cancer patients (localized and metastatic) and healthy donors from Franses et al. (GSE144561). (C) *EN1* mRNA normalized read count from PDA patient-derived organoids (PDOs) in Tiriac et al. (phs001611.v1.p1). (D) *EN1* mRNA mean counts per cell of 24 pancreatic patients from Peng et al. scRNA-seq (CRA001160). Mean ± SD is shown. *p*-values were determined by unpaired student's *t* test (two-tail) and *, **, ***, **** indicate *p*-val < 0.05, < 0.01, <0.001, <0.0001, respectively.

Moreover, we found that the increased expression of *EN1* was associated with poor prognosis in the TCGA dataset (Figure 9A). Gene Set Enrichment Analysis (GSEA) of the publicly available expression datasets[26; 29-32] further revealed that *EN1* expression was closely associated with the molecular signatures implicated in the aggressiveness of PDA, including epithelial-mesenchymal transition (EMT) and squamous/basal-like molecular subtype (Figure 1B-F). Therefore, EN1 is tightly associated with the aggressive features of PDA, and aberrant expression of EN1 could provide pro-survival cues and contribute to the aggressiveness of PDA cells.

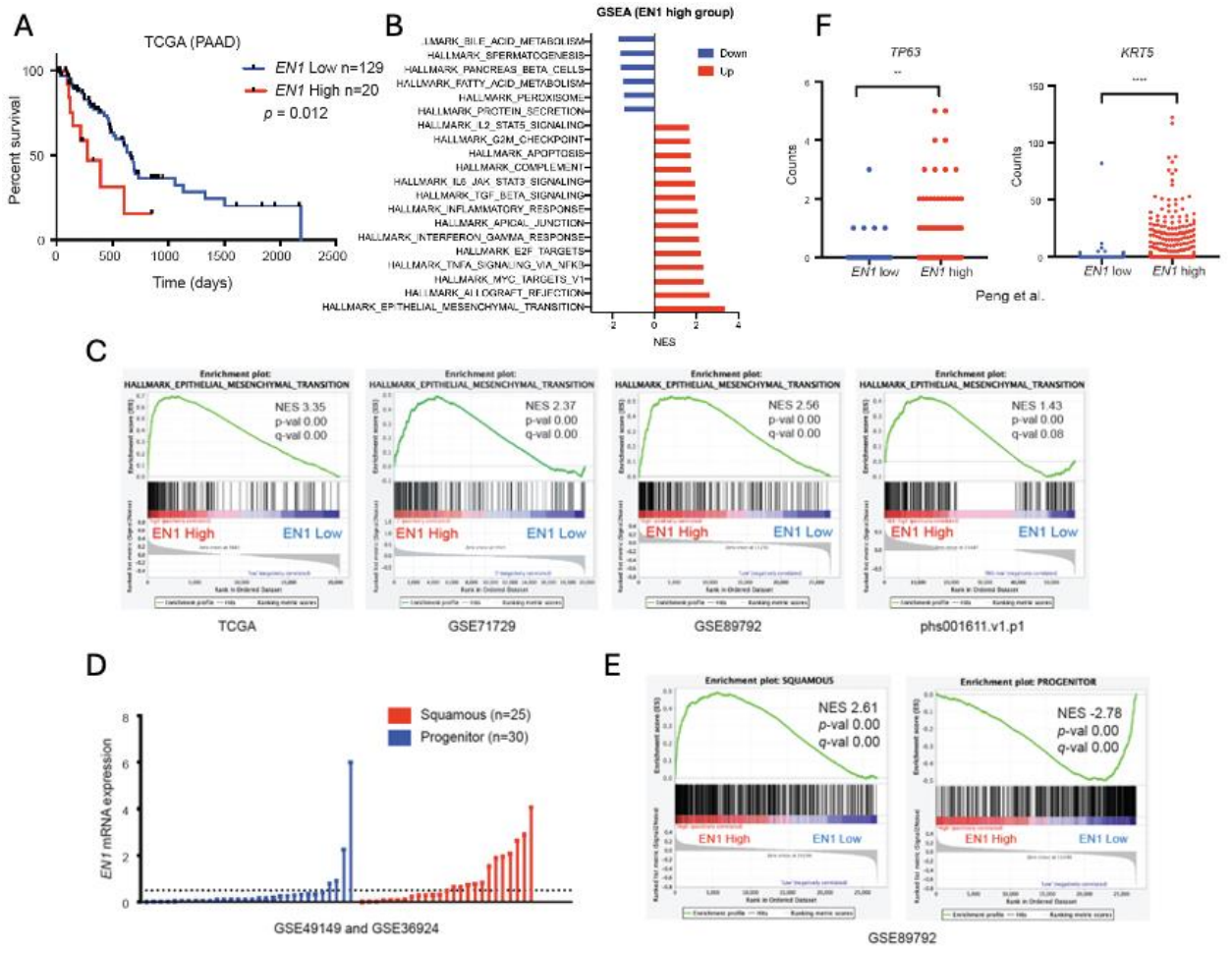

**Figure 9.** (A) EN1 is associated with patient poor prognosis. Pancreatic cancer patients (TCGA-PAAD) were stratified based on *EN1* expression (*EN1*-high n=20 vs. -low n=129). *p*-value was determined by logrank (Mantel-Cox) test. (B) Top 20 significantly enriched hallmarks of GSEA in *EN1*-high vs. -low patients from TCGA-PAAD. Normalized enrichment score (NES) is shown. (C) GSEA of epithelial-to-mesenchymal transition signatures in *EN1*-high vs. -low pancreatic cancer patients or cell lines from TCGA-PAAD, Moffitt et al. (GSE71729), Bian et al. (GSE89792), and Tiriac et al. (phs001611.v1.p1) NES, *p*-value, and FDR *q*-value were determined by GSEA. (D) Normalized *EN1* gene counts in progenitor and squamous PDA subtypes from Bailey et al. (GSE49149 and GSE36924). A dotted line indicates a cutoff to determine EN1 high vs. low to perform Fisher's exact test ($p$-val < 0.05). The cutoff was determined by a median value of EN1 expression in the squamous subtype. (E) GSEA of squamous (left) and progenitor (right) signatures in *EN1*-high vs. -low pancreatic cancer patients from Bian et al. (GSE89792). NES, *p*-value, and FDR *q*-value were determined by GSEA. (F) Squamous subtype markers, *TP63* and *KRT5* mRNA counts in *EN1*-high (T6, T14, T16, T17) vs. -low (T1, T2, T3, T5) PDA patients from Peng et al. scRNA-seq (CRA001160). *p*-values were determined by unpaired student's *t* test (two-tail) and *, **, ***, **** indicate $p$-val < 0.05, < 0.01, <0.001, <0.0001, respectively.

**EN1 promotes aggressive characteristics in PDA cells**

Given the association between EN1 expression and gene signatures of EMT and squamous subtype, we first hypothesized that EN1 could foster aggressive characteristics of PDA. To this end, we retrovirally introduced *En1* cDNA into murine KPC (mT-2D) cell lines (Figure 10A), and measured cell proliferation, invasion, migration, and anchorage-independent growth. While EN1 did not change the cell proliferation rate (Figure 10B), we found EN1 overexpression increased the cell invasion (Figure 10C), migration (Figure 10D-E), and anchorage-independent growth (Figure 10F), indicating that EN1 promotes the metastatic nature of PDA *in vitro*.

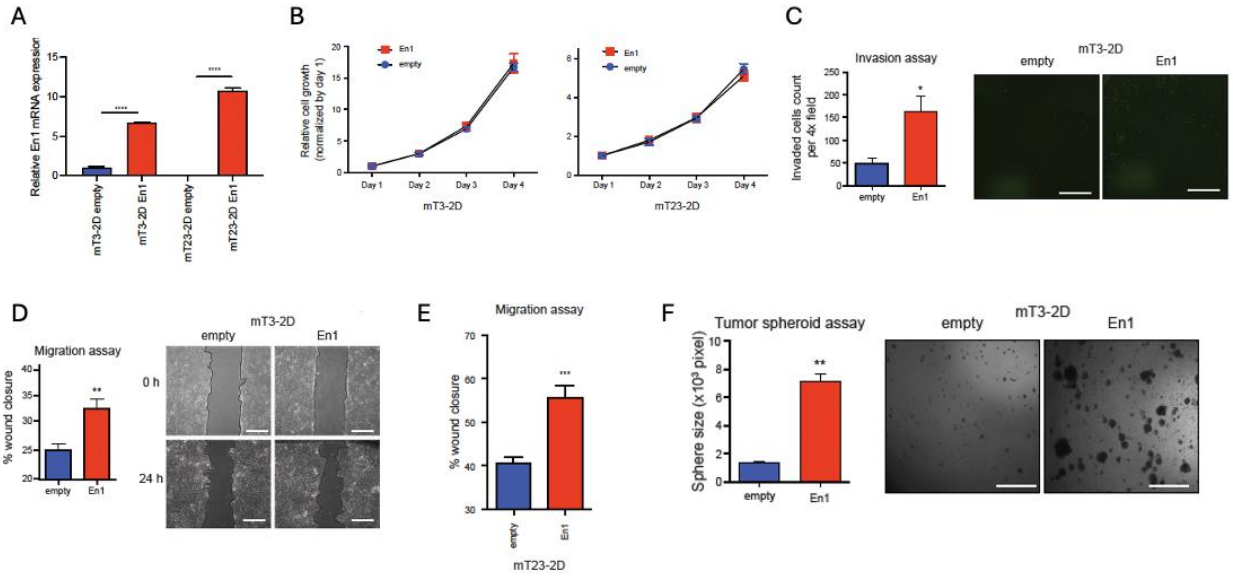


**Figure 10.** (A) Relative *En1* mRNA expression determined by RT-qPCR in mT3-2D and mT23-2D cell lines with (*En1*) and without (empty) *En1* cDNA overexpression. (B) mT3-2D and mT23-2D cells with *En1* cDNA were subjected to cell proliferation assay compared to empty vector control. Cell proliferation rate was determined

by ATP-based cell viability assay using CellTiterGlo and luminescence was measured daily for 4 days and normalized to day 1. n=3 per time point, mean ± SD. (C) mT3-2D cells with (En1) and without (empty) *En1* cDNA overexpression were subjected to Boyden-chamber invasion assay for 24 hours, and the cells migrating to across the transwell were stained by SYTO 13 (right) and quantified per 4x image field (left). n=3, mean ± SEM. (D) mT3-2D empty and *En1* cells were subjected to wound-healing assay, and the percentage of wound closure was monitored (right) and quantified (left) at 0- and 24-hour post-scratching. n=3, mean ± SEM. (E) mT23-2D with *En1* cDNA were subjected to wound-healing assay compared to empty vector control, and the area of the closed wound was quantified at 0- and 24-hour post-scratching, and the percentage of wound closure was calculated. n=3, mean ± SD. (F) mT3-2D cells with *En1* cDNA were subjected to anchorage-independent tumor spheroid formation assay for 72 hours, and the numbers of spheroids were monitored (right) and quantified (left). n=3, mean ± SEM. *p*-values were determined by student's *t* test (two-tail) and * and ** indicate *p*-val < 0.05, and < 0.01, respectively.

To further corroborate the role of EN1 in metastatic transitions, we used a two-channel microfluidic organotypic model[33] to investigate the role of EN1 in the intravasation potential of the cells (Figure 11A). In the model, the collagen-matrix embedded channel (green) contains mT-2D cells, and the other channel (red) contains a biomimetic blood vessel. As a result, EN1-expressing cells invaded the collagen matrix toward the blood vessels at a faster rate compared to the control. Furthermore, tail-vein injections of mT-2D cells revealed that EN1-expressing cells readily colonized in the lung parenchyma (Figure 11B), suggesting that EN1-mediated pro-survival and pro-migratory/invasive phenotypes conferred the metastatic ability necessary for lung colonization.

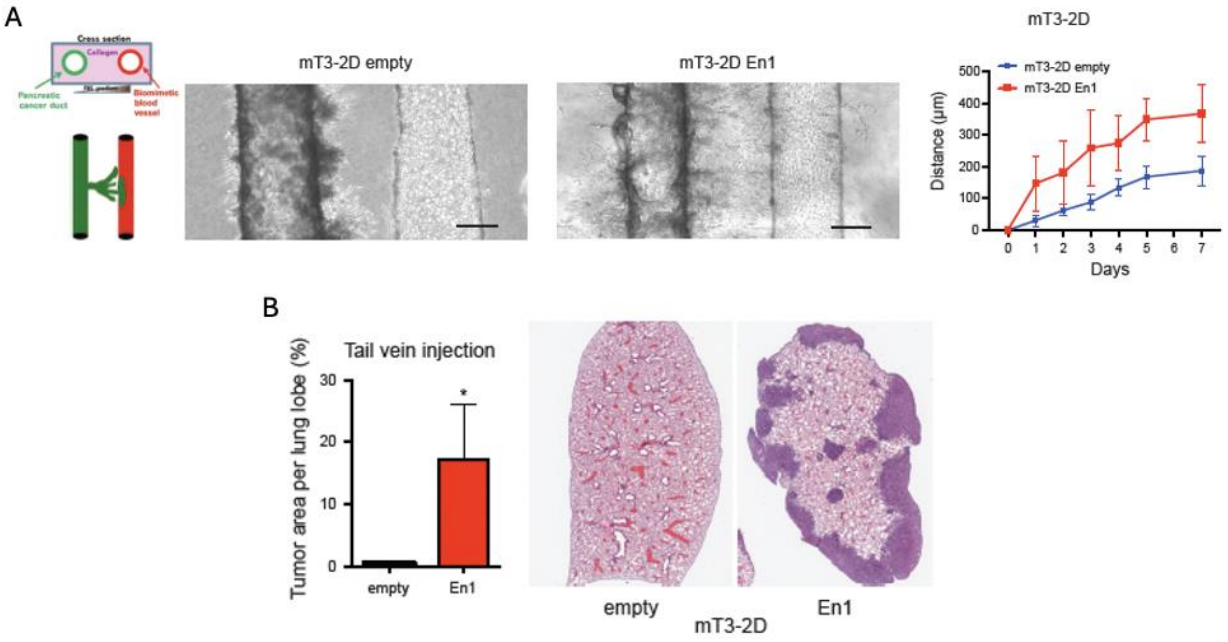


**Figure 11.** (A) mT3-2D empty (n=7) and *En1* (n=4) cells were subjected to organotypic tumor-on-a-chip assay (left) for 7 days, and the distance of the cell migrated toward to endothelial vessel was monitored (middle) and quantified (right) (n=8 per time point, mean ± SD). $p<0.001$; *p*-value were determined by Two-way ANOVA. Scale bar, 200 μm. (B) mT3-2D cells with *En1* cDNA were subject for tail-vein injection (n=5 per group) in C57BL/6 syngeneic mice. After 4 weeks, the animals were sacrificed, and the lung lobes were imaged (right) and quantified (left) for tumor area per lung lobe. n=5, mean ± SD. *p*-values were determined by student's *t* test (two-tail) and * and ** indicate *p*-val < 0.05, and < 0.01, respectively.

To test if EN1 plays similar roles in the human PDA cells, we chose CFPAC1 and PaTu 8988s human PDA cell lines that do not express EN1 (Figure 12A), and retrovirally introduced FLAG-tagged *EN1* cDNA (Figure 12B). In accordance with the data from murine mT-2D cells, EN1 overexpression increased clonogenic growth (Figure 12C-D, respectively) and anchorage-independent tumor-sphere formation (Figure 12E-F, respectively) in CFPAC1 and PaTu 8988s

cells. Taken together, the gain-of-function experiments showed that EN1 fosters aggressive characteristics of PDA, including cell survival, migration, and intravasation.

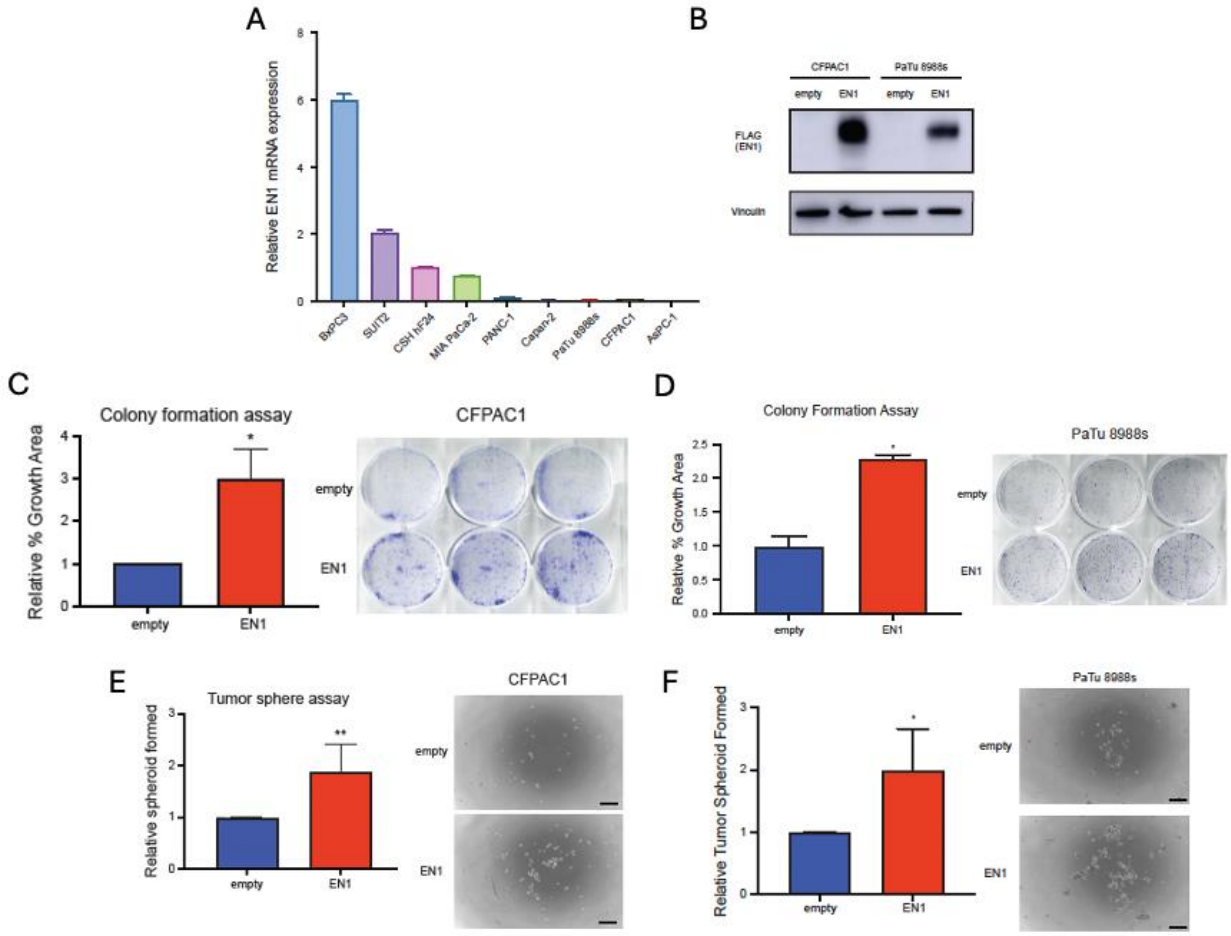


**Figure 12.** (A) Relative *EN1* mRNA expression in human PDA cell lines determined by RT-qPCR. n=3, mean ± SD. (B) Western blot analysis to determine the protein expression of FLAG-tagged EN1 compared to the plasmid without *EN1* cDNA (empty) control in CFPAC1 and PaTu 8988s cell lines. (C) CFPAC1 empty and *EN1* cells were subject for colony formation assay for 7 days, and the colonies were stained by crystal violet (right) and quantified (left) by percentage growth area. n=9, mean ± SD. (D) PaTu8988s empty and *EN1* cells were subjected for colony formation assay for 14 days, and the colonies were stained by crystal violet (right) and quantified (left) by percentage growth area. n=3, mean ± SD. (E) CFPAC1 empty and *EN1* cells were subject for

anchorage-independent tumor spheroid formation assay for 7 days, and the numbers of spheroids were monitored (right) and quantified (left). n=9, mean ± SD. Scale bars, 350 mm. (F) PaTu8988s empty and *EN1* cells were subjected for anchorage-independent tumor spheroid formation assay for 7 days, and the numbers of spheroids were monitored (right) and quantified (left). n=3, mean ± SEM. Scale bars, 350 mm. *p*-values were determined by student's *t* test (two-tail) and * and ** indicate *p*-val < 0.05, and < 0.01, respectively.

**EN1 deficiency attenuates PDA progression**

Since EN1 expression contributes to the aggressive natures of PDA cells, we reasoned that an EN1-targeting strategy might be therapeutically relevant. To investigate the effects of EN1 depletion in metastatic pancreatic cancer, we lentivirally introduced shRNAs against *En1* either targeting coding sequence (CDS) or 3'-untranslated regions (3' UTR) into mM3P and mM15 organoids (Figure 13A). We then subjected the mM organoids to the organoid survival and clonogenic cell growth assays. While EN1 depletion had no effect on cell growth in the complete organoid media (Figure 13B), we observed that the survival of the cells was markedly diminished in the reduced media upon EN1 depletion (Figure 13C-D).

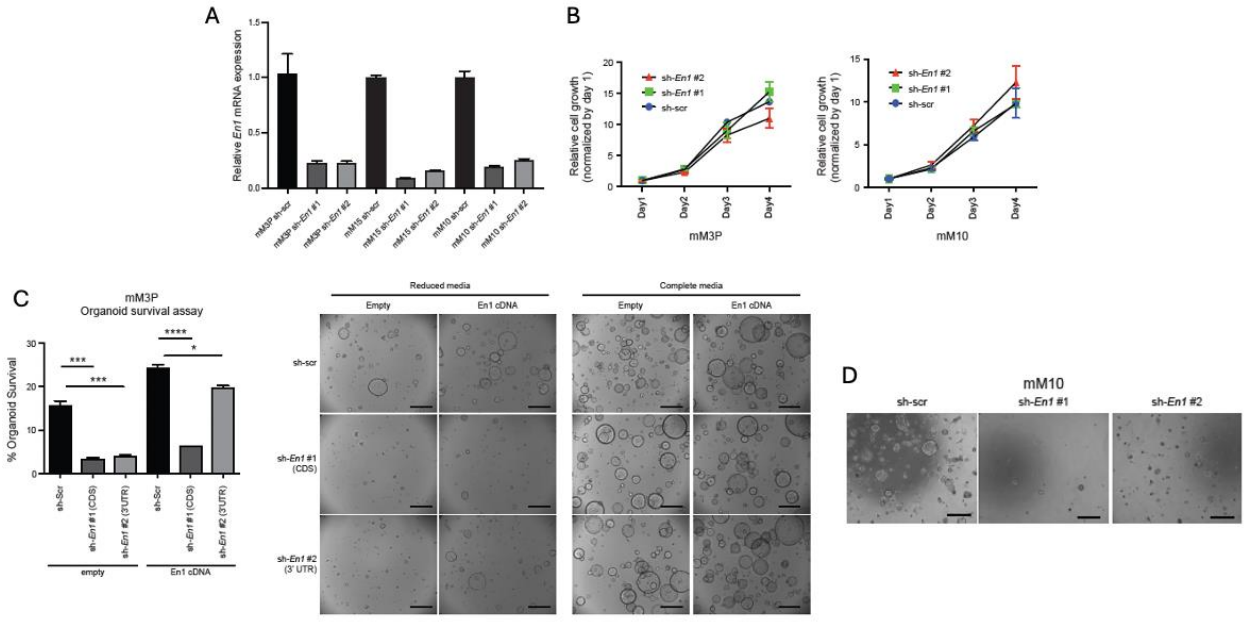


**Figure 13.** (A) Relative *En1* mRNA expressions determined by RT-qPCR in mM3P, mM15, and mM10 organoids with shRNA targeting *En1* mRNA coding region (sh*En1* #1 CDS) and *En1* mRNA 3' untranslated region (sh*En1*

#2 3'UTR) compared to the scramble shRNA (sh-scr) control organoid. n=3, mean ± SD. (B) Image-based quantification of organoid growth for mM3P and mM10 shScr, sh*En1* #1, and sh*En1* #2 organoids in the complete media. Organoid growth was normalized to day 1. n=3, mean ± SD. (C) mM3P organoids with scramble (shScr) and two *En1* (sh*En1*) shRNA constructs were subjected to organoid survival assay for 4 days. Depletion of EN1 impaired organoid survival in the reduced media, and *En1* cDNA rescued the EN1-depletion phenotype (middle). The complete media served as control (right). Quantification of organoid survival (left). n=3, mean ± SD. Scale bars, 1mm. (D) shScr and sh*En1* mM10 organoids were subjected to organoid survival assay for 4 days (top) and quantification of organoids (bottom). Scale bars, 1mm. *p*-values were determined by unpaired student's *t* test (two-tail) and *, **, ***, **** indicate *p*-val < 0.05, < 0.01, <0.001, <0.0001, respectively.

Moreover, the ability to grow clonogenicly in 2D was also impaired by the *En1* knockdown (Figure 14). To exclude the possibility of shRNA off-target effects, we performed a rescue experiment using retroviral *En1* cDNA. The phenotype of the reduced survival was rescued by *En1* cDNA in the shRNA-3'UTR organoids but not in the shRNA-CDS organoids (Figure 13C).

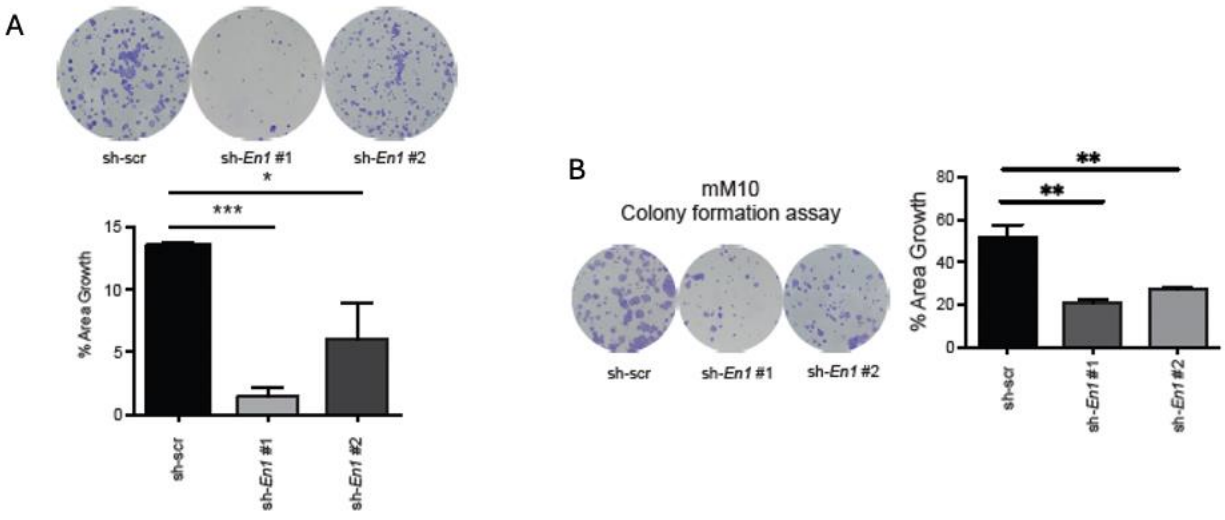

**Figure 14.** (A) shScr and sh*En1* mM3P organoids were subjected to colony formation assay for 7 days, and the colonies were stained by crystal violet (top) and quantified (bottom) by percentage growth area. n=3, mean ± SD. (B) (D) shScr and sh*En1* mM10 organoids were subjected to colony formation assay for 7 days, and the colonies were stained by crystal violet (left) and quantified (right) by percentage growth area.

To confirm the phenotype seen *in vitro*, we used subcutaneous and orthotopic transplantation models of PDA to determine the effects of *En1* knockdown in mM organoids *in vivo*. Previously, we showed mM organoids were highly metastatic compared to the paired mT organoids in orthotopic, tail-vein, and intrasplenic transplantation models[8]. Consistent with *in vitro* phenotypes, *En1* knockdown significantly reduced primary tumor burden in both subcutaneous and orthotopic models (Figure 15). In the orthotopic model, we observed reduced liver and lung metastases (Figure 16), suggesting EN1 possibly enhances the metastatic potentials of PDA.

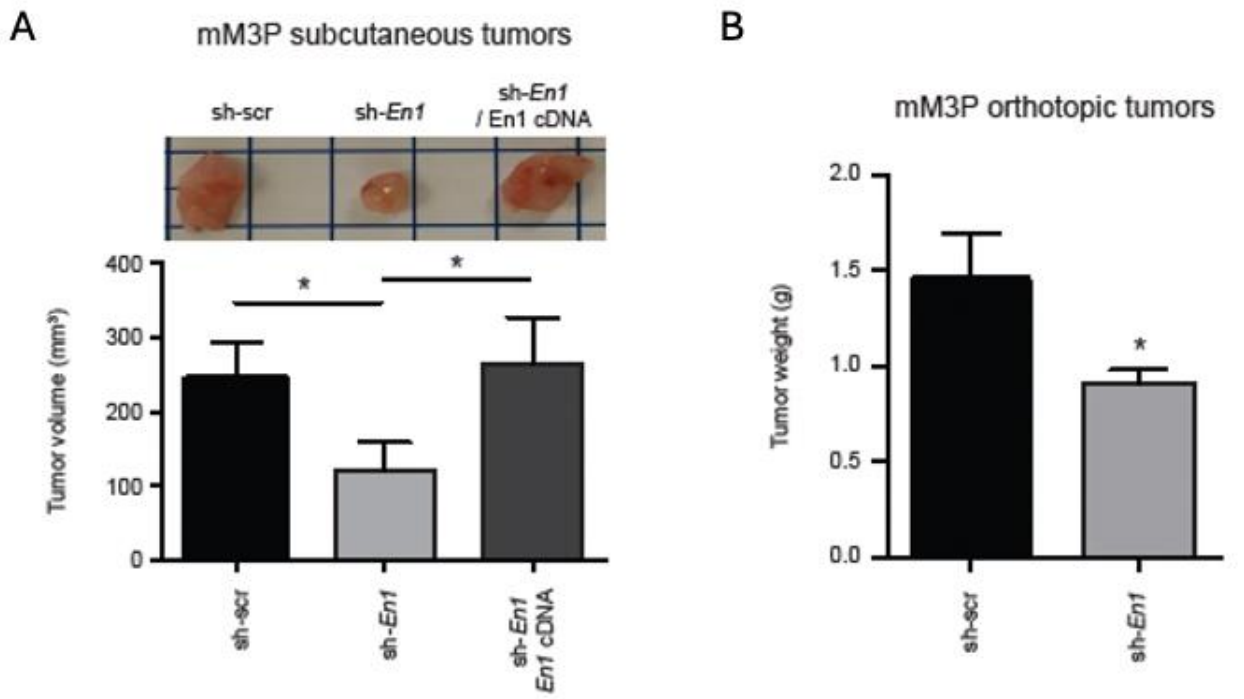


**Figure 15.** (A) 5x10$^5$ cells of dissociated shScr and sh*En1* mM3P organoids were subjected to subcutaneous transplantation in athymic NU/NU mice. The animals were sacrificed at 4-weeks post transplantation. EN1 depletion reduced the primary tumor burden and *En1* cDNA rescued the phenotype. Representative images of the subcutaneous tumors (top) and quantification (bottom) of the tumor volume. n=5 per group, mean ± SD. (B) 5x10$^5$ cells of dissociated shScr and sh*En1* mM3P organoids were subjected to orthotopic transplantation in athymic NU/NU mice for 7 weeks and quantified for primary tumor weight. The mean ± SD is shown (n=5 for shScr and n=4 for sh*En1*).

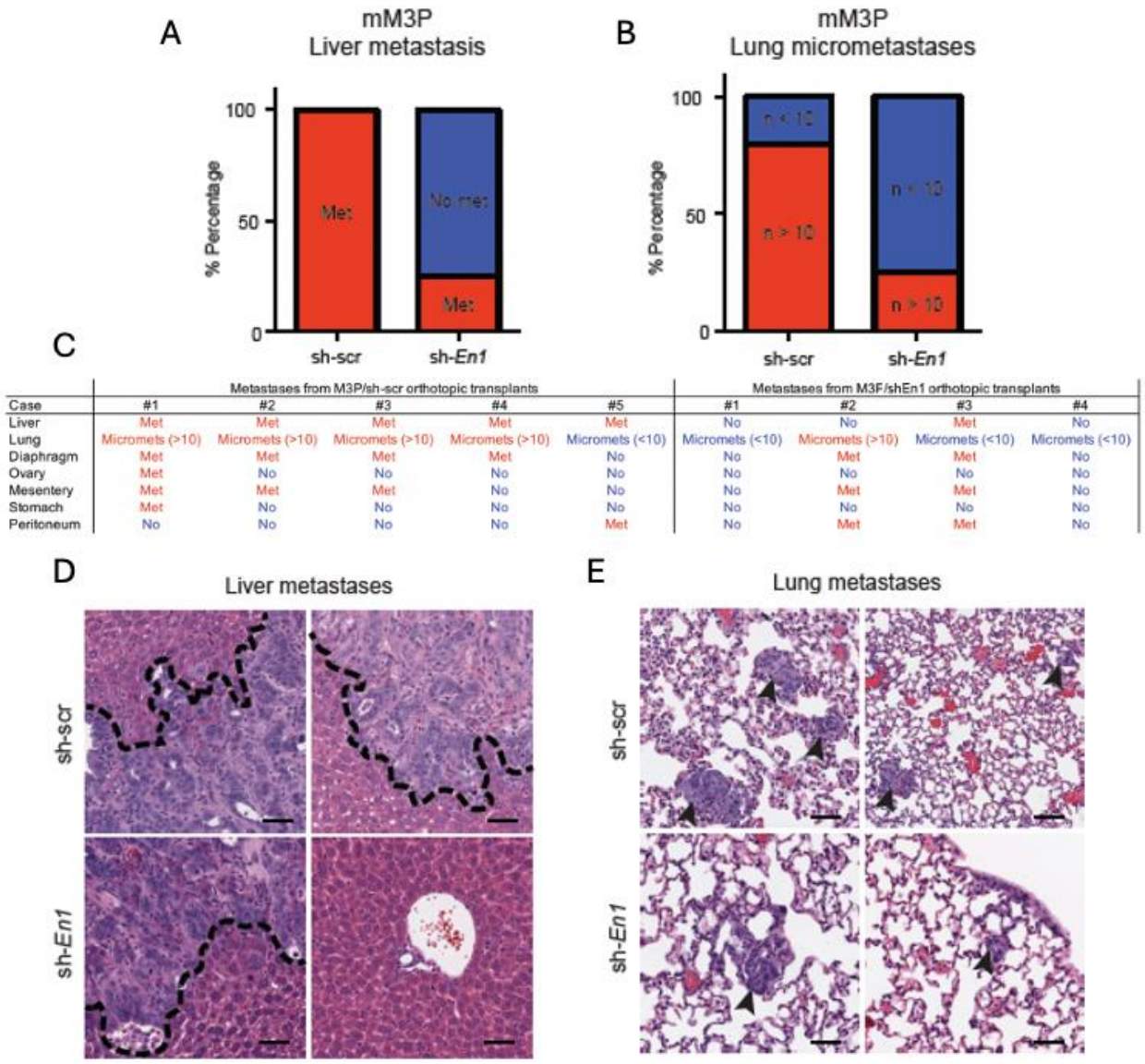


C

| Case | Metastases from M3P/sh-scr orthotopic transplants | | | | | Metastases from M3F/shEn1 orthotopic transplants | | | |
|---|---|---|---|---|---|---|---|---|---|
| | #1 | #2 | #3 | #4 | #5 | #1 | #2 | #3 | #4 |
| Liver | Met | Met | Met | Met | Met | No | No | Met | No |
| Lung | Micromets (>10) | Micromets (>10) | Micromets (>10) | Micromets (>10) | Micromets (<10) | Micromets (<10) | Micromets (>10) | Micromets (<10) | Micromets (<10) |
| Diaphragm | Met | Met | Met | Met | No | No | Met | Met | No |
| Ovary | Met | No | No | No | No | No | No | No | No |
| Mesentery | Met | Met | Met | No | No | No | Met | Met | No |
| Stomach | Met | No | No | No | No | No | No | No | No |
| Peritoneum | No | No | No | No | Met | No | Met | Met | No |




**Figure 16.** 5x10$^5$ cells of dissociated shScr and sh*En1* mM3P organoids were subjected to orthotopic transplantation in athymic NU/NU mice for 7 weeks. The number of animals with liver metastases (A) and the number of lung micrometastasis (n>10) (B) were quantified. The mean ± SD is shown (n=5 for shScr and n=4 for sh*En1*). (C) Summary of metastases from mM3P shScr (n=5) and sh-*En1* orthotopic transplants (n=5), 7 weeks post-transplantation. Depletion of En1 reduced liver metastasis frequency. Fisher's exact test, *p*-val <0.05. (D) Representative H&E staining of liver metastasis from the orthotopic injections of mM3P shScr and

sh*En1* organoids. Scale bar, 50 μm. (E) Representative H&E staining of lung metastasis from the orthotopic injections of mM3P shScr and sh*En1* organoids. Scale bar, 50 μm.

To address the role of EN1 in the human context, we depleted EN1 using two independent *EN1* shRNA constructs in *EN1*-expressing SUIT2 and BxPC3 human PDA cell lines (Figure 12A and 17A). As expected, EN1 depletion in human PDA cell lines led to reduced colony formation and anchorage-independent tumor-sphere formation (Figure 12B-E). Taken together, our results from the loss-of-function experiments showed that EN1 expression is required for cell survival and metastatic capabilities *in vitro* and *in vivo*, suggesting that EN1 and EN1-related pathways might be potential therapeutic targets for PDA.

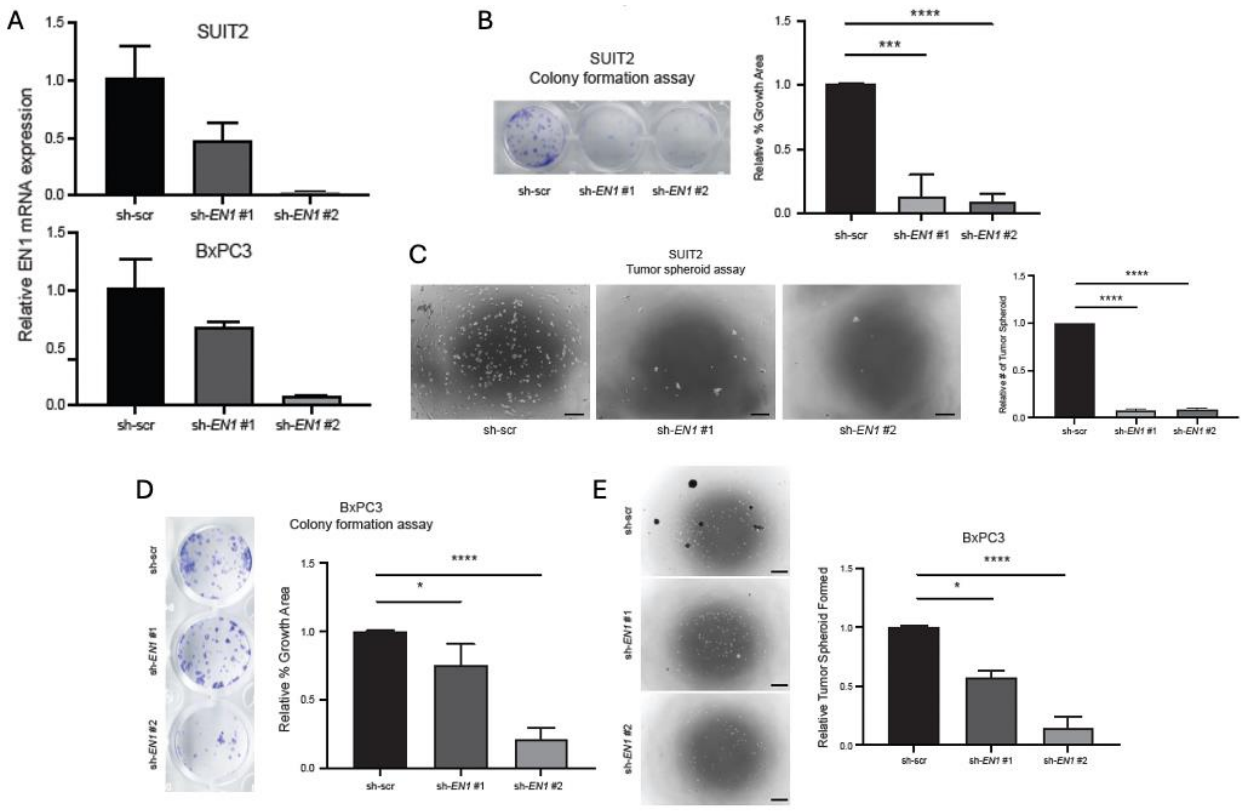

**Figure 17.** (A) Relative EN1 mRNA expressions are determined by RT-qPCR in SUIT2 (left) and BxPC3 (right) cell lines with shRNAs targeting *EN1* mRNA compared to the scramble shRNA. n=3, mean ± SD. (B) shScr and sh*EN1* SUIT2 cells were subjected to colony formation assay for 5 days, and the colonies were stained with crystal violet (top) and quantified (bottom) for the percentage growth area. n=3, mean ± SD. (C) shScr and sh*EN1* SUIT2 cells were subjected to anchorage-independent tumor spheroid formation assay for 7 days, and the numbers of spheroids were monitored (left) and quantified (right). n=3, mean ± SD. Scale bars, 350 mm. (D) shScr and sh*EN1* BxPC3 cells were subjected to colony formation assay for 2 weeks, and the colonies were stained with crystal violet (top) and quantified (bottom) for the percentage growth area. n=3, mean ± SD. (E) shScr and sh*EN1* BxPC3 cells were subjected to anchorage-independent tumor spheroid formation assay for 7 days, and the numbers of spheroids were monitored (left) and quantified (right). n=3, mean ± SD. Scale bars, 350 mm. *p*-values were determined by unpaired student's *t* test (two-tail) and *, **, ***, **** indicate *p*-val < 0.05, < 0.01, <0.001, <0.0001, respectively.

**Identifying genomic targets of EN1 in murine PDA cells**

Using gain- and loss-of-function experiments, we thus far demonstrated that EN1 is sufficient and necessary to develop aggressive characteristics in PDA. We reasoned that the underlying mechanisms of how EN1 confers these characteristics are likely dependent on its direct gene targets. Therefore, to dissect the underlying mechanism(s) by which EN1 endows the aggressive characteristics, we attempted to determine genome-wide EN1 binding sites and identify direct target genes of EN1. To address this, we first retrovirally introduced FLAG-tagged *En1* cDNA into mT-2D cell lines (Figure 18) and performed cleavage under target & release using nuclease followed by sequencing (CUT&RUN-seq) targeting the FLAG epitope in mT4-2D and mT5-2D cell lines.

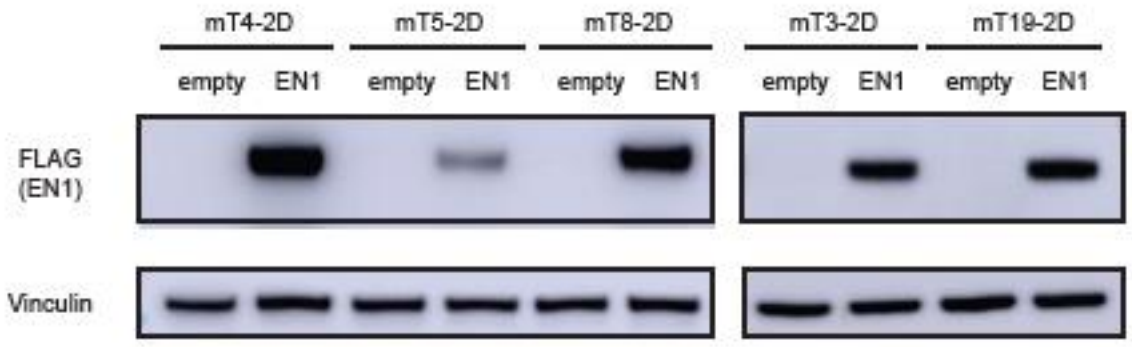


**Figure 18.** Western blot analysis to determine the protein expression of FLAG-tagged EN1 compared to the empty control in mT3-2D, mT4-2D, mT5-2D, mT8-2D, and mT19-2D cells.

From our bioinformatic analysis of CUT&RUN-seq, we identified 35,256 and 26,582 EN1 peaks in mT4-2D and mT5-2D KPC cells, respectively (Figure 19A). We then overlapped the two datasets and identified a total of 20,271 common peaks between these two cell lines. Among these peaks, most were located at gene promoters (41.74%) and intergenic/intron regions (54.26%) (Figure 19B), indicating that EN1 binds at gene promoters and enhancers. HOMER motif analysis of 20,271 common peaks showed the enrichment of known EN1 motif (GSE120957), other homeobox TFs motifs (LHX9 and ISL1) (Figure 20A), and *de novo* discovery of EN1 motif (Figure 20B).

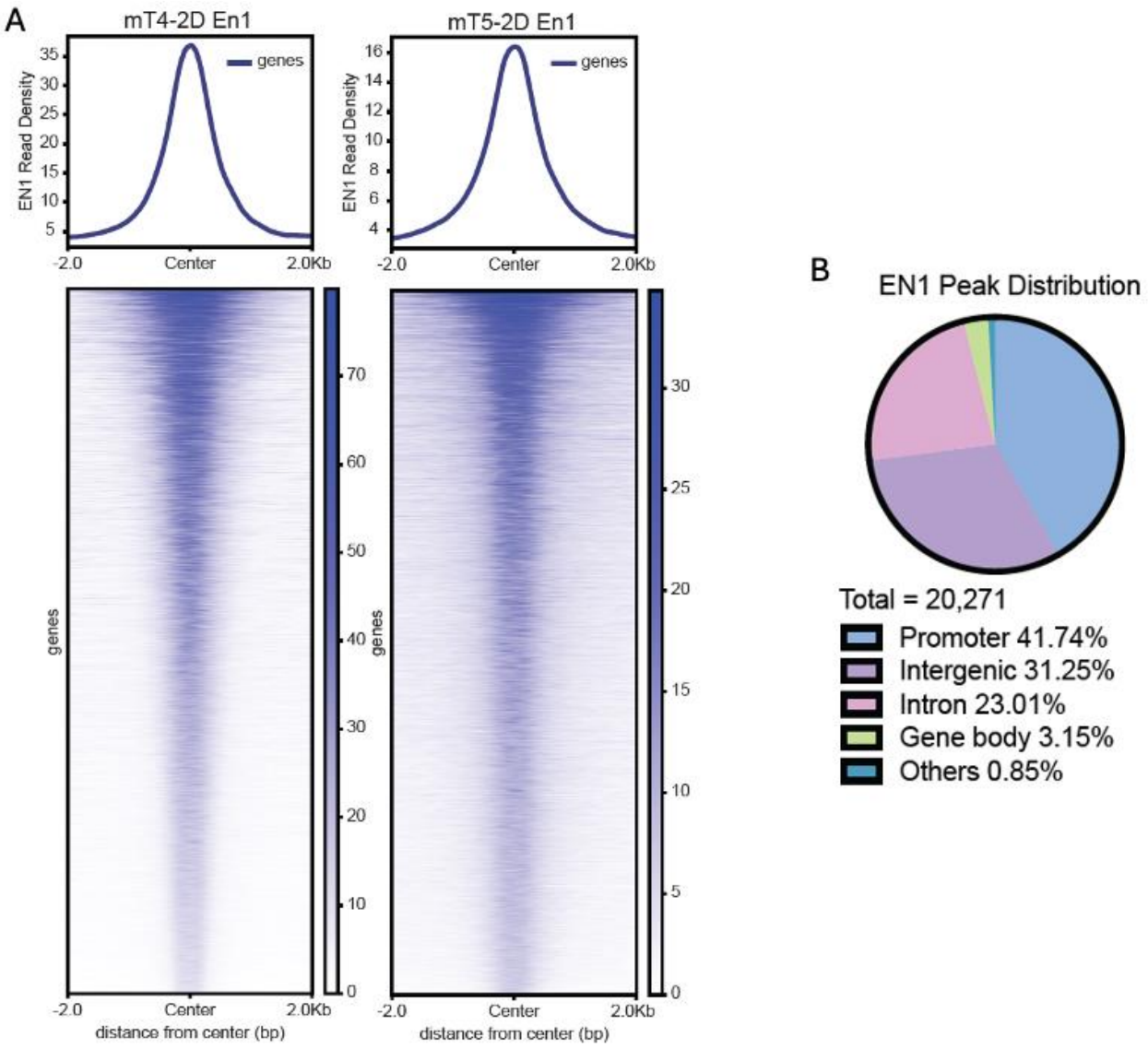


**Figure 19.** (A) Density plots of CUT&RUN-seq signal of the EN1 DNA-binding peaks in mT4-2D and mT5-2D cells with *FLAG-En1* cDNA. (B) Genome-wide distribution of the common EN1 peaks between mT4-2D *FLAG-EN1* and mT5-2D *FLAG-EN1* cells (n=20,271).

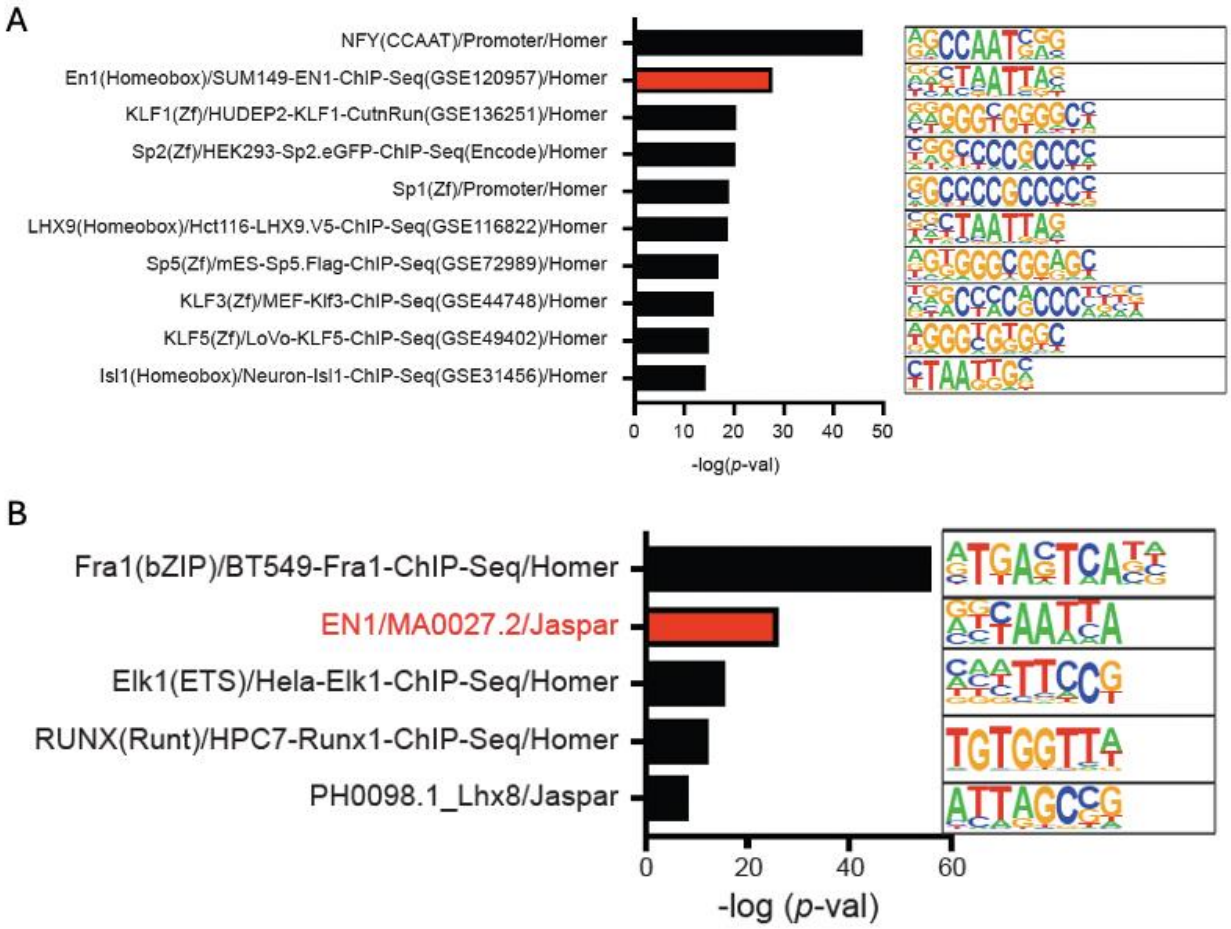


**Figure 20.** (A) Homer motif analysis for the known motifs using the overlapping mT4-2D and mT5-2D EN1 peaks. (B) Homer motif analysis for the *de novo* motifs using the overlapping mT4-2D and mT5-2D EN1 peaks. *p*-value was determined by HOMER.

While the known EN1 motif was enriched in the triple-negative breast cancer (TNBC) cell lines[23], we found minimum overlaps of EN1 peaks between PDA and TNBC cells (Figure 21A), suggesting EN1 genomic targets could differ depending on tissue or cell types. To understand the functional and biological importance of EN1 genomic targets and peak-associated genes, we performed gene ontology (GO) analysis using the Genomic Regions

Enrichment of Annotations Tool (GREAT) (Figure 21B) and the Database for Annotation, Visualization, and Integrated Discovery (DAVID) (Figure 21C). Both analyses showed the enrichment of apoptotic processes, cytoskeleton organizations, and cell cycle regulations.

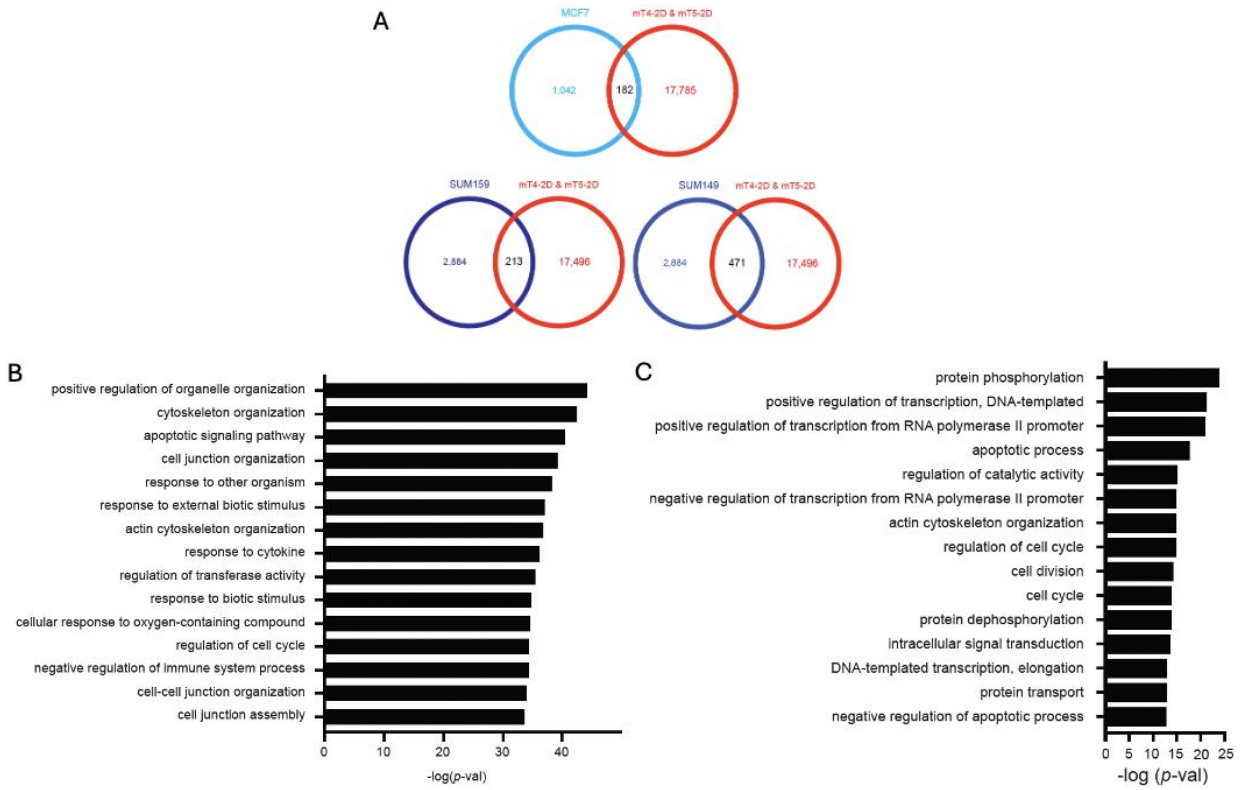


**Figure 21.** (A) Overlapping EN1 peaks identified in triple-negative breast cancer (TNBC) cells (MCF7, SUM149, and SUM159) and mT4-2D & mT5-2D cells. To properly compare murine and human genomes, we convert the EN1 peak positions identified in mT-2D cell lines (NCBI37/mm9) to human genome assembly (GRCh37/hg19) using UCSC Lift Genome Annotations tool. Of the 20,271 EN1 peaks identified in mT-2D cell lines, 17,967 peaks were LiftOver successfully. Among the TNBC cell lines, 182, 213, and 471 peak overlaps were identified in MCF7, SUM159, and SUM149 cells, respectively. (B) Genomic Regions Enrichment of Annotations Tool (GREAT) analysis of the overlapping mT4-2D and mT5-2D EN1 peaks showing the top 15 enriched pathways in biological functions. *p*-value was determined by GREAT. (C) Gene ontology (GO) analysis using the Database for

Annotation, Visualization, and Integrated Discovery (DAVID). The top 15 enriched pathways in biological functions were shown.

When the transcriptome profiles of PDA from the publicly available datasets were stratified into *EN1*-high and -low patient groups[29; 34-38], we identified the majority of genes associated with EN1 peaks were down-regulated in *EN1*-high patients (Figure 22), suggesting a predominant transcriptional repressive role of EN1 in PDA cells.

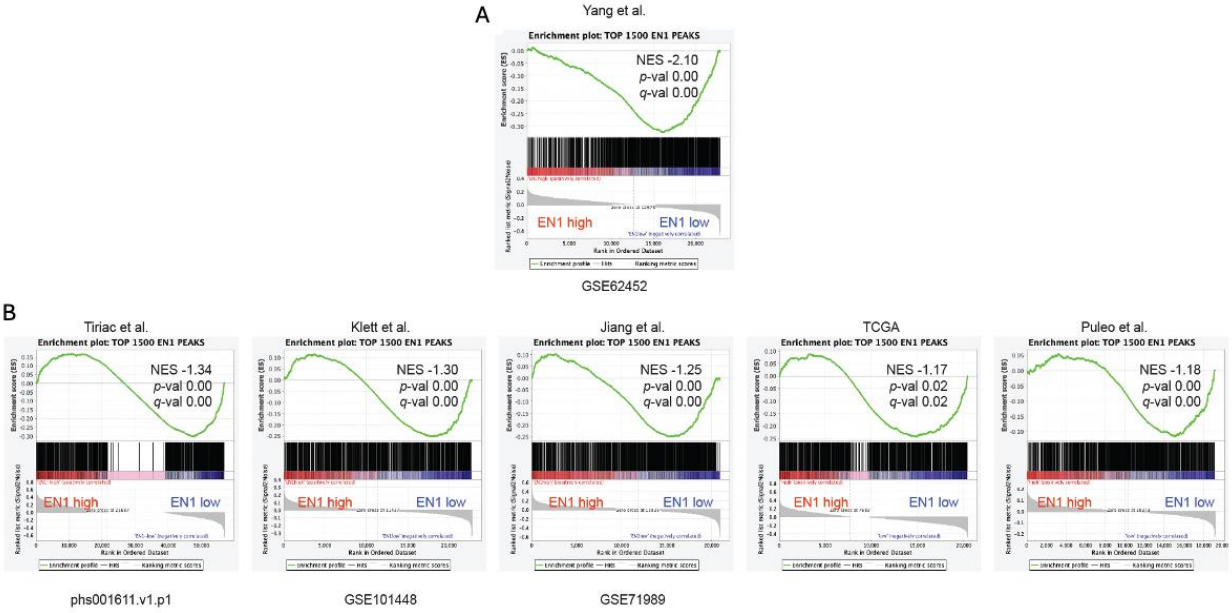


**Figure 22.** (A) GSEA of the genes associated with En1 peaks in *EN1*-high vs. -low pancreatic cancer patients from Yang et al. (GSE62452). The genes associated with top 1,500 EN1 peaks among 20,271 common peaks were used for GSEA. NES, *p*-value, and FDR *q*-value were determined by GSEA. (B) GSEA of the top 1500 EN1 peak-associated genes in *EN1*-high vs. -low pancreatic cancer patients, organoids, or cell lines from Tiriac et al. (phs001611.v1.p1), Klett et al. (GSE101448), Jiang et al. (GSE71989), TCGA-PAAD, and Puleo et al. NES, *p*-value, and FDR *q*-value were determined by GSEA.

**Identifying transcriptional targets of EN1 in PDA cells**

Once EN1 genomic targets were identified, we next sought to pinpoint the transcriptional targets of EN1 in order to stratify if and/or how EN1 governs the expressions of its gene targets. To address this, we performed RNA-seq analysis of mM3P and mM15 organoids introduced with scramble or *En1*-targeting shRNAs (Figure 13A). Differentially expressed gene analysis resulted in 154 differentially expressed genes (DEGs) with a statistical significance (*p*-val <0.05) (Figure 23). Of the total DEGs, 120 genes (79%) were upregulated upon *En1* knockdown, suggesting a transcriptional repressive role of EN1 in PDA.

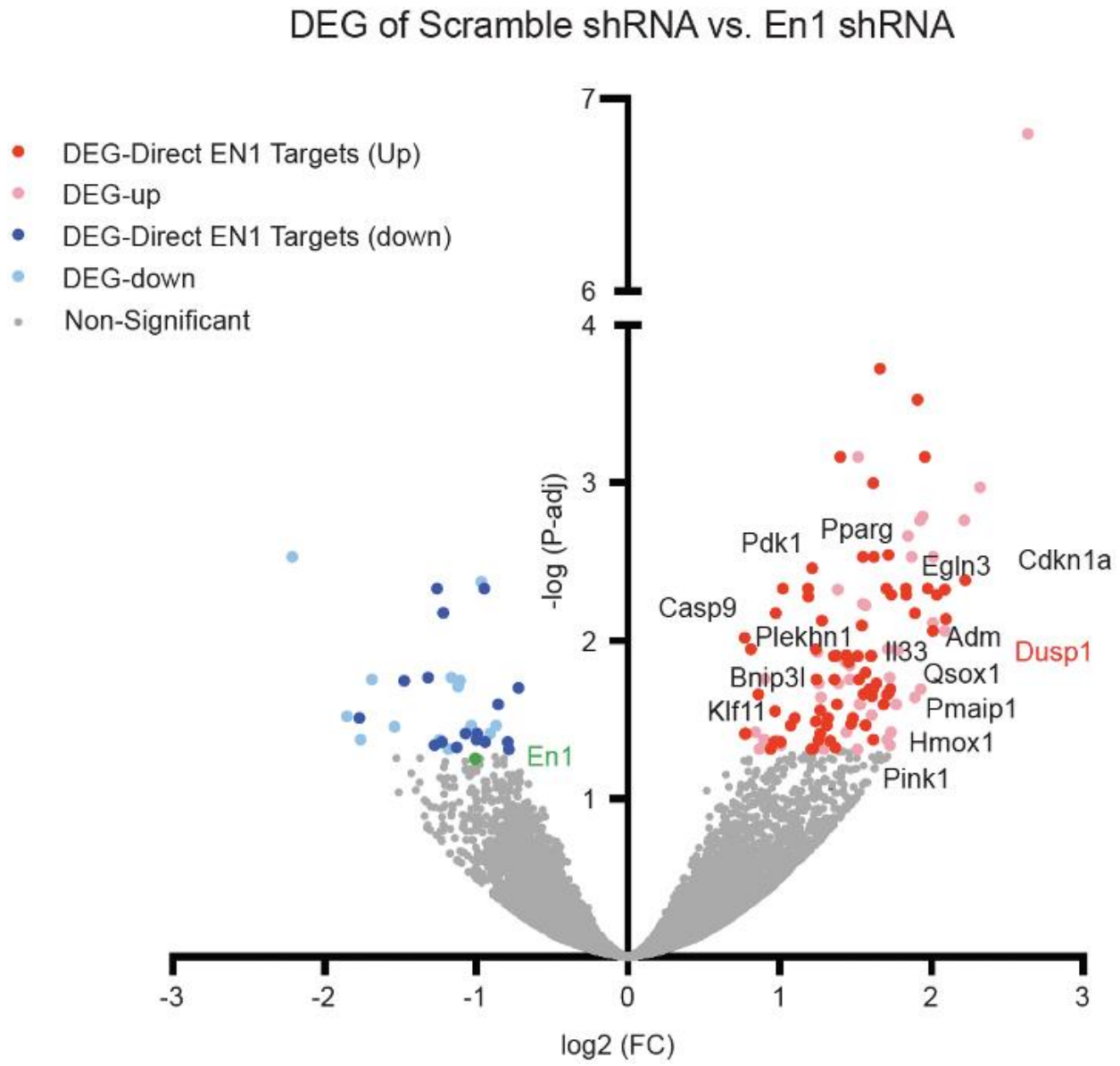


**Figure 23.** Volcano plot representing RNA-seq of mM3P and mM15 organoids with scramble (shScr) and two *En1* (sh*En1*) shRNA constructs. Differentially expressed gene analysis identified 154 differentially expressed genes (DEG). Among the DEGs, 120 genes were upregulated (red), and 32 genes were downregulated (blue) upon *En1* depletion; among which, 92 DEGs (dark red or dark blue) were the direct EN1 targets. DEG-direct EN1 target genes involved in cell death pathways were annotated.

To then understand the functional significance of differentially expressed genes, we performed GO analysis using DAVID and GSEA (Figure 24). Both analyses showed the enrichment of apoptotic signaling pathways, in agreement with the functional annotations of EN1 genomic targets (Figure 21B-C).

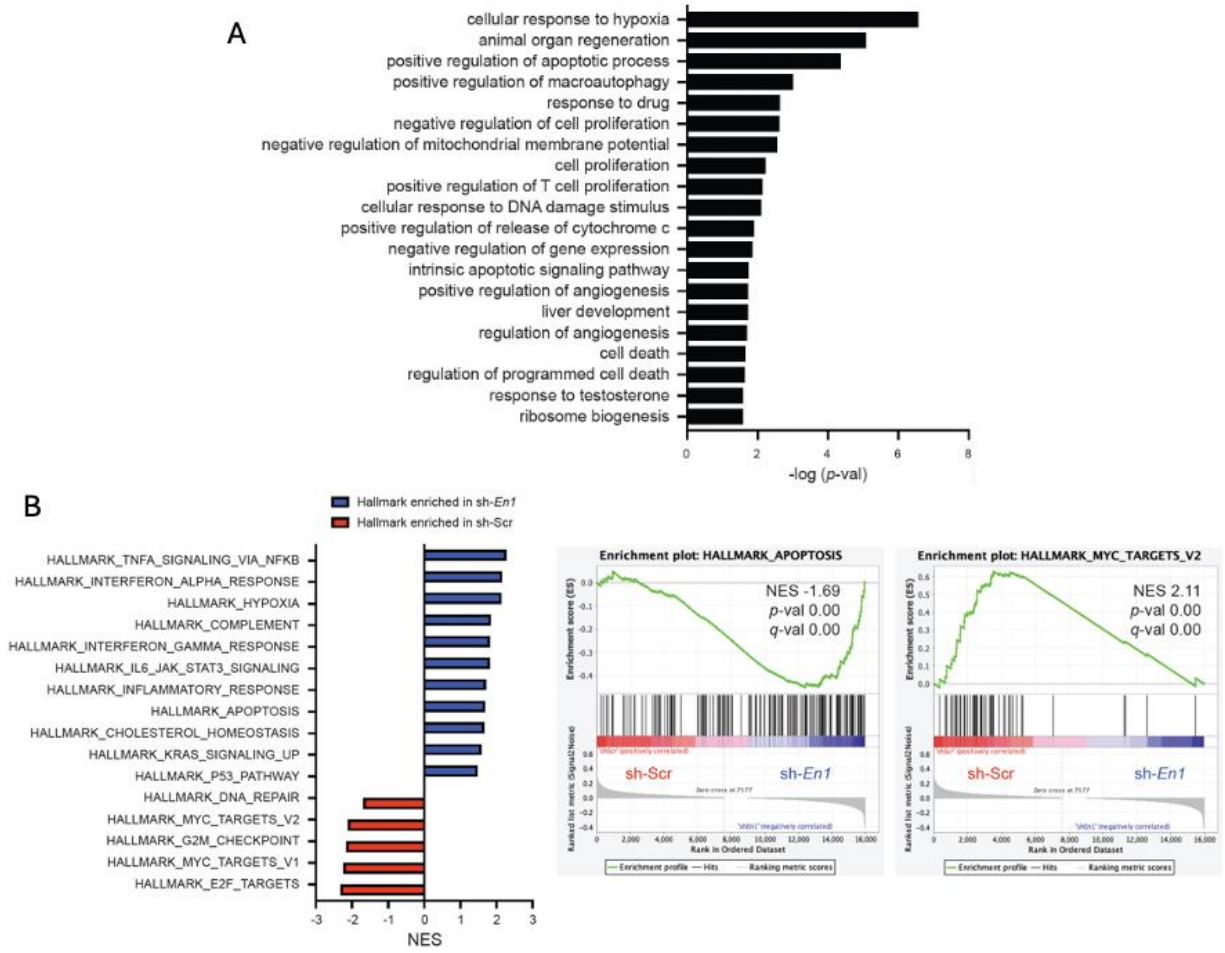


**Figure 24.** (A) GO analysis of the DEGs using DAVID. Top 20 significantly enriched biological functions were shown. (B) Normalized enrichment score (NES) of the GSEA Hallmark gene set in mM3P and mM15 organoids upon En1 knock-down. The top 16 significantly enriched hallmarks (left) and examples of the GSEA plots (right)

are shown. Hallmark_Apoptosis and Hallmark_Myc_Targets_V2 gene sets were enriched in sh*En1* and shScr, respectively.

We also found that *En1* depletion increased cleaved Caspase 3 expression without any change in DNA damage-related protein expressions (Figure 25A), consistent with the observation that regulations of cell death pathways were significantly enriched in the upregulated DEGs upon *En1* knockdown (Figure 25B). Among the downregulated DEGs, metabolic processes, including amino acid transport, regulation of TOR signaling, and transmembrane transport, were enriched (Figure 25B). Collectively, the data suggest EN1 is a multifaceted regulator of various cellular processes involved not only in pro-survival and cell death but also in metabolism. Furthermore, hallmarks for E2F and MYC targets were also enriched in shScr organoids (Figure 24B), well correlated with molecular signatures enriched in *EN1*-high patients from the TCGA-PAAD dataset (Figure 9B). While EN1 expression was associated with EMT signature in the TCGA-PAAD dataset (Figure 9C), we did not find any enrichment of EMT signatures in RNA-seq analyses of *En1*-depleted mM organoids, suggesting that EMT-related genes are not direct targets of EN1. Interestingly, upon orthotopic transplantations of mM organoids, En1 depletion resulted in the down-regulation of Vimentin, a mesenchymal marker in the primary tumors, and increased CK-19 positivity in the metastatic PDA cells (Figure 25C), indicating that EN1 may play a permissive role of the expression of EMT-related genes *in vivo*.

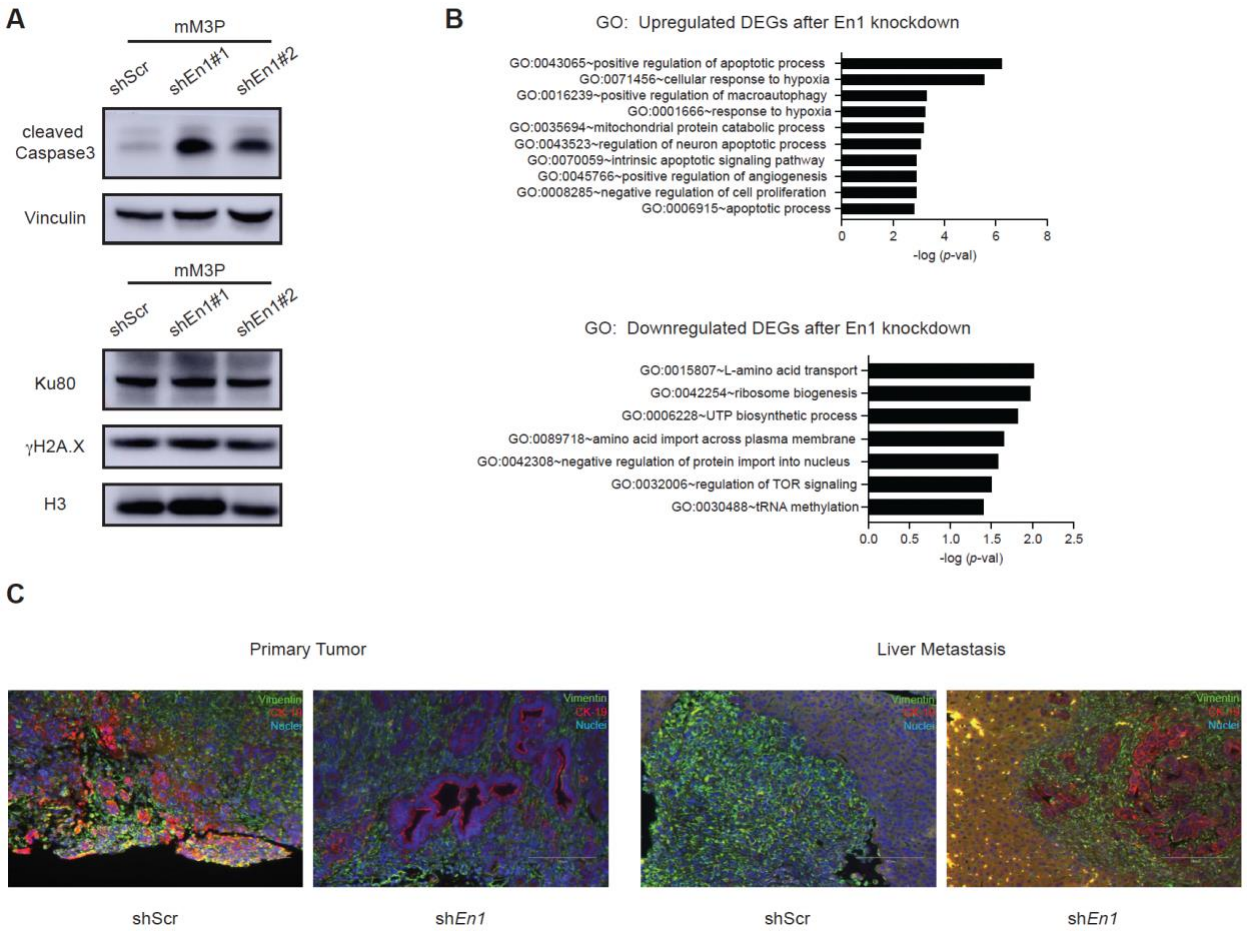


**Figure 25.** (A) Western blot analysis to determine the protein expression of cleaved Caspase 3, KU80 and gH2A.X. in mM3P organoids with scramble (shScr) and two independent *En1* (sh*En1*) shRNA constructs cultured in the reduced media for 24 hours before harvesting. (B) DAVID analysis of the upregulated DEGs (top) and downregulated DEGs (bottom) after *En1* knockdown in mM3P and mM15 organoids showing the top enriched pathways in biology functions. *p*-value was determined by DAVID. (C) Immunofluorescence staining of vimentin and CK-19 in the tissue sections collected from orthotopically transplanted mM3P organoids (figure 3D-F), comparing shScr and sh*En1* conditions, depicting primary tumor (left) and distant liver metastasis (right). Scale bar, 150 mm.

To further elucidate the correlation between EN1 genomic and transcriptional targets, we performed GSEA and showed EN1 peak-associated genes were significantly enriched after *En1* knockdown (Figure 26A), highlighting that EN1 governs the gene expression predominantly through transcription repression. We also performed RNA-seq analysis for SUIT2 cells after *EN1* knockdown and identified 1,057 DEGs (Figure 26B). Similar to murine cells, gene ontology analysis showed apoptosis, cell adhesion, and migration process were enriched in the DEGs (Figure 27C), indicating the functional similarities of EN1 between murine and human PDA cells. Taken together, our data showed that as a TF, the major role of EN1 is transcription repression; in turn, the differentially expressed EN1 gene targets regulate anti-apoptotic, EMT, cell-cycle regulations, and metabolic programs.

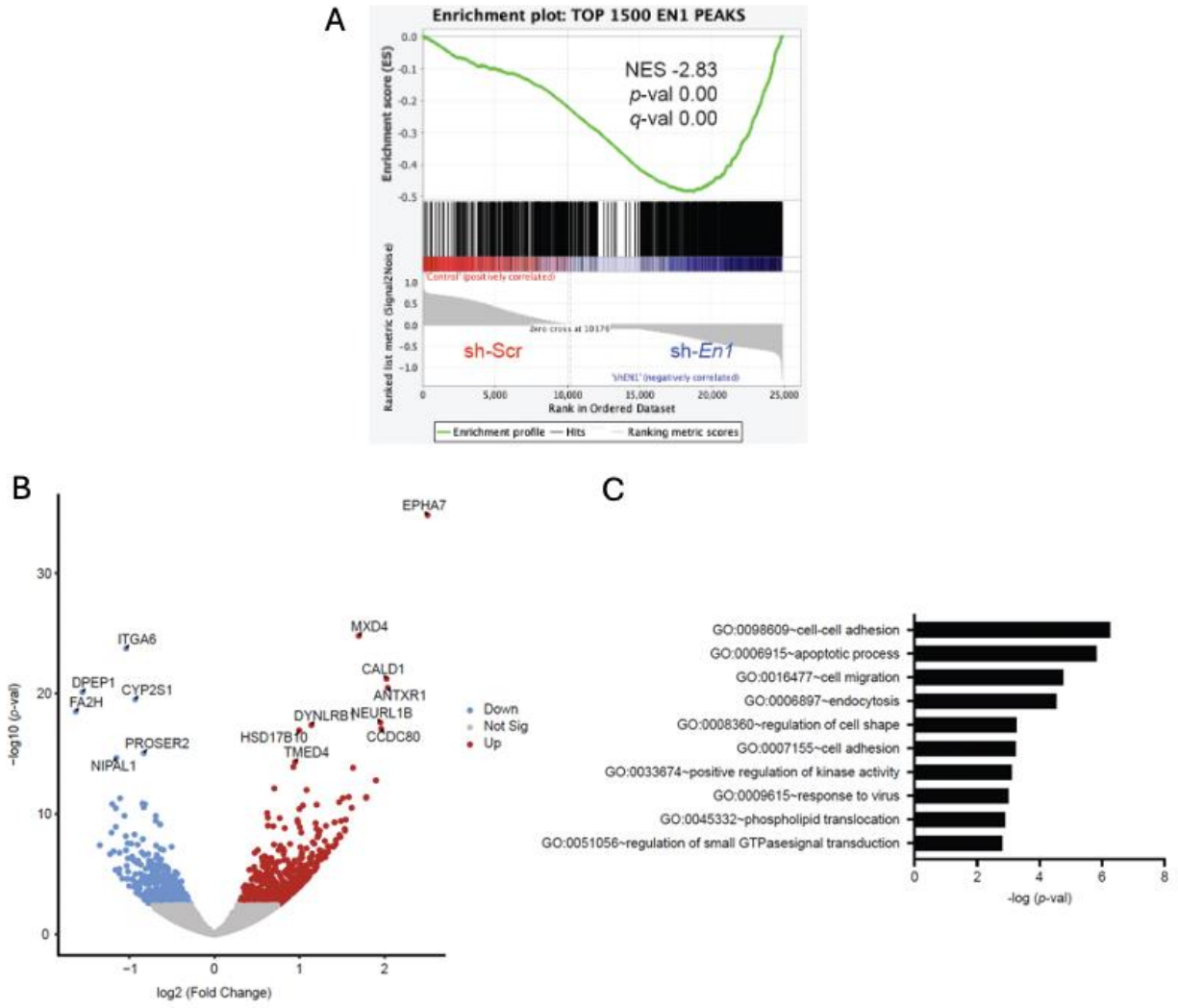


**Figure 26.** (A) GSEA of the genes associated with top 1,500 EN1 peaks revealed that putative EN1 target genes were up-regulated upon *En1* depletion in mM organoids. (B) Volcano plot representing RNA-sequencing of SUIT2 shScr and two independent sh*EN1* constructs identified 1056 differentially expressed genes (DEG). Among the DEGs, 638 genes were upregulated, and 418 genes were downregulated after *En1* knockdown. (C) DAVID analysis of the DEGs after *EN1* knockdown in SUIT2 cells showing the top 10 enriched pathways in biology functions. *p*-value was determined by DAVID.

**EN1 modulates gene promoter and enhancer activities to promote PDA progression**

Our analysis of the EN1 binding regions in the pancreatic cancer genome strongly suggested that EN1 targets promoters and enhancers through its DNA-binding domain. Since the majority of EN1 transcriptional targets were upregulated upon EN1 knockdown (Figure 23), we reasoned that EN1 could repress gene transcription by altering promoter and enhancer activities. To better understand how EN1 regulates its target gene expression, we performed CUT&RUN-seq targeting active promoter marker tri-methylation of lysine 4 on histone H3

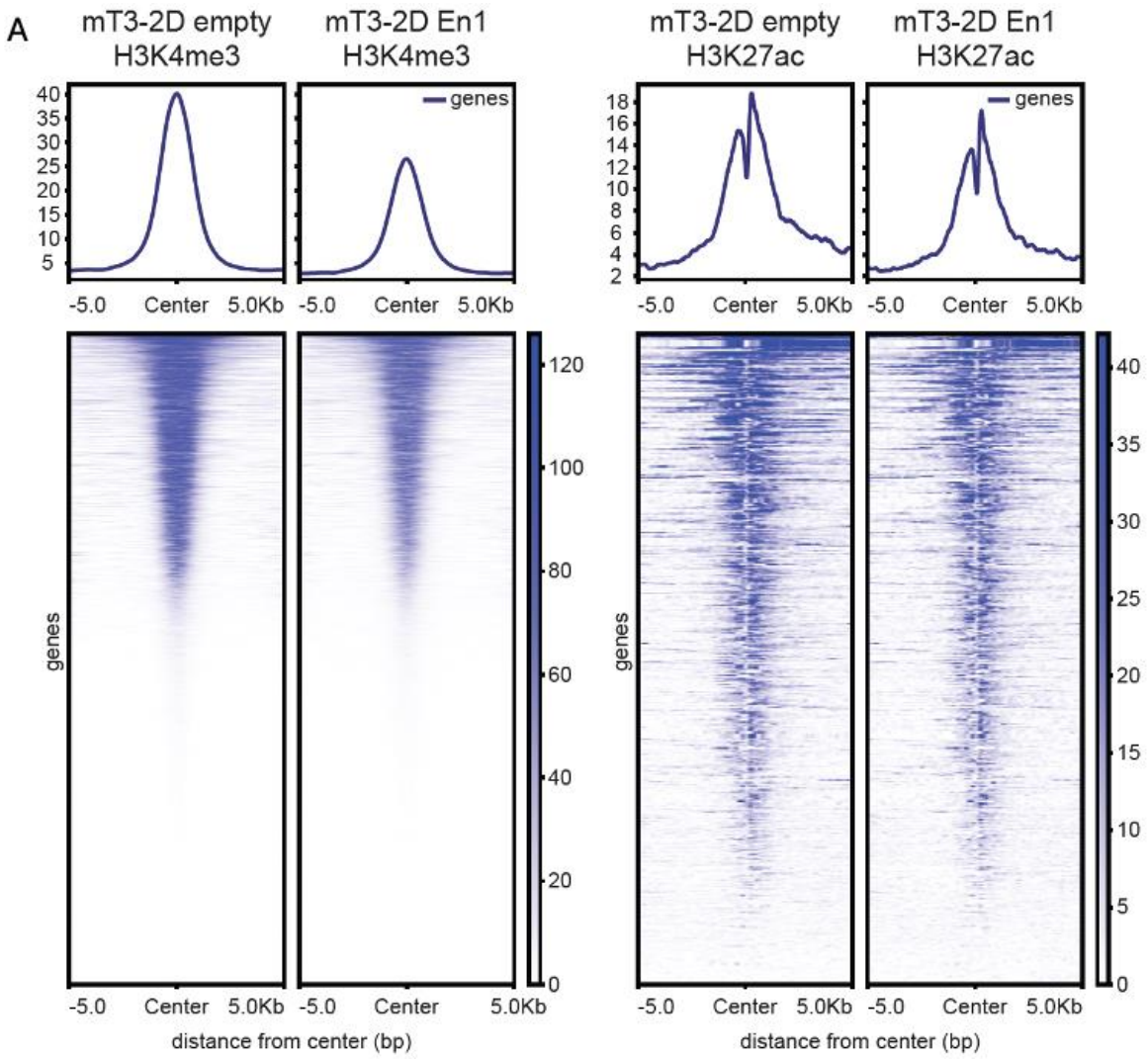

protein subunit (H3K4me3) and active enhancer marker acetylation of lysine 27 on histone H3 protein subunit (H3K27ac) using mT3-2D cell line overexpressing EN1. We then asked the question whether EN1 expression would alter H3K4me3 and H3K27ac occupancy in EN1 binding regions. H3K4me3 and H3K27ac CUT&RUN-seq analysis in mT3-2D cells revealed that H3K4me3 and H3K27ac occupancy were reduced surrounding EN1 binding sites (Figure 27A) and the promoters of EN1 gene targets (Figure 27B), indicating that EN1 binding reduced the activities of the target gene promoter and enhancer.

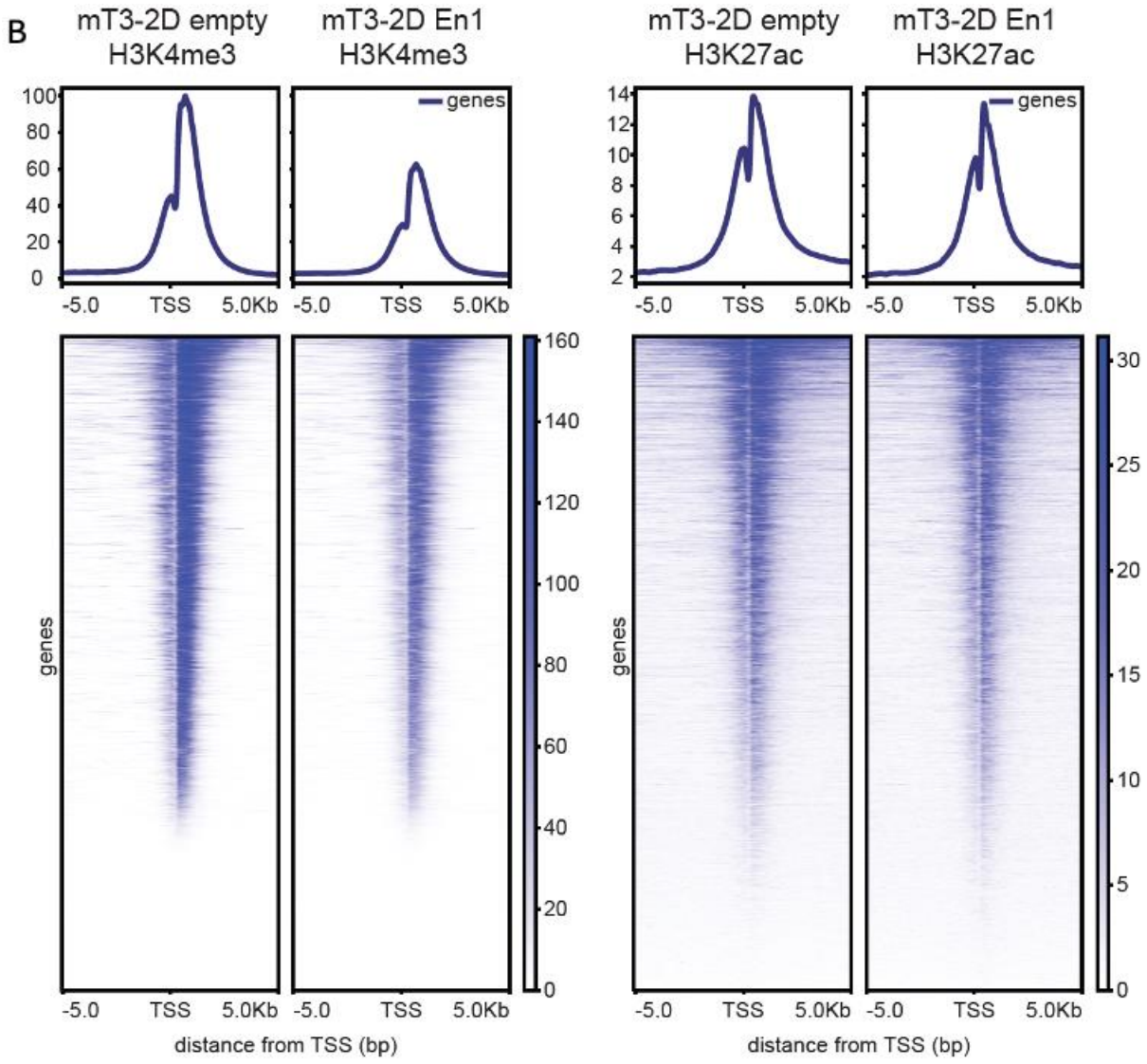

**Figure 27.** (A) Density plots of H3K4me3 (left) and H3K27ac (right) CUT&RUN-seq signals at EN1 genomic binding sites in mT3-2D empty | *FLAG-En1* cells. (B) Density plots of H3K4me3 (left) and H3K27ac (right) CUT&RUN-seq signals at EN1 peak-associated gene promoters and the transcription start sites (TSS) in mT3-2D empty | *FLAG-En1* cells.

Next, we performed H3K4me3 and H3K27ac CUT&RUN-seq with three additional biological replicates (mT4-2D, mT5-2D, and mT8-2D cell lines) upon EN1 overexpression and generated averaged meta-profiles (Figure28). Similar to mT3-2D cells, upon EN1 overexpression, H3K4me3 and H3K27ac occupancies were decreased around EN1 binding regions and promoters of EN1 gene targets, suggesting EN1 can repress gene expression through modulating promoter and enhancer activities of its target genes.

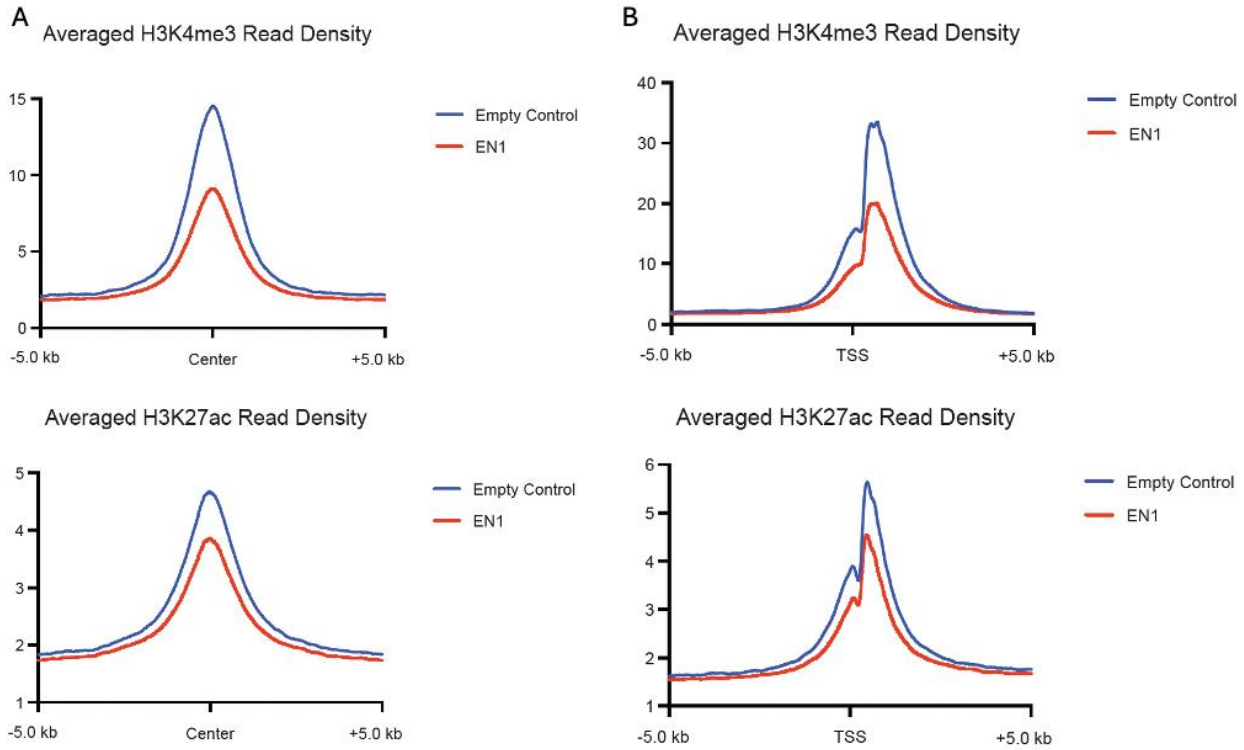

**Figure 28.** (A) Averaged density plots of H3K4me3 (left) and H3K27ac (right) CUT&RUN-seq signals at EN1 genomic binding sites in mT4-2D, mT5-2D, and mT8-2D empty | *FLAG-EN1* cells. (B) Averaged density plots of H3K4me3 (left) and H3K27ac (right) CUT&RUN-seq signals at EN1 peak-associated gene promoters and the TSS in mT4-2D, mT5-2D, and mT8-2D empty | *FLAG-EN1* cells.

For instance, EN1 binds the promoter and distal enhancer of dual specificity phosphatase 1, *Dusp1* gene, and H3K4me3 and H3K27ac occupancies at these loci were reduced upon En1 overexpression (Figure 29A), suggesting that EN1 could repress *Dusp1* expression through limiting the promoter and/or enhancer activities of *Dusp1*. Indeed, EN1 could bind to the *Dusp1* promoter in CUT&RUN-qPCR assay and repressed the promoter activity (Figure 29B-C).

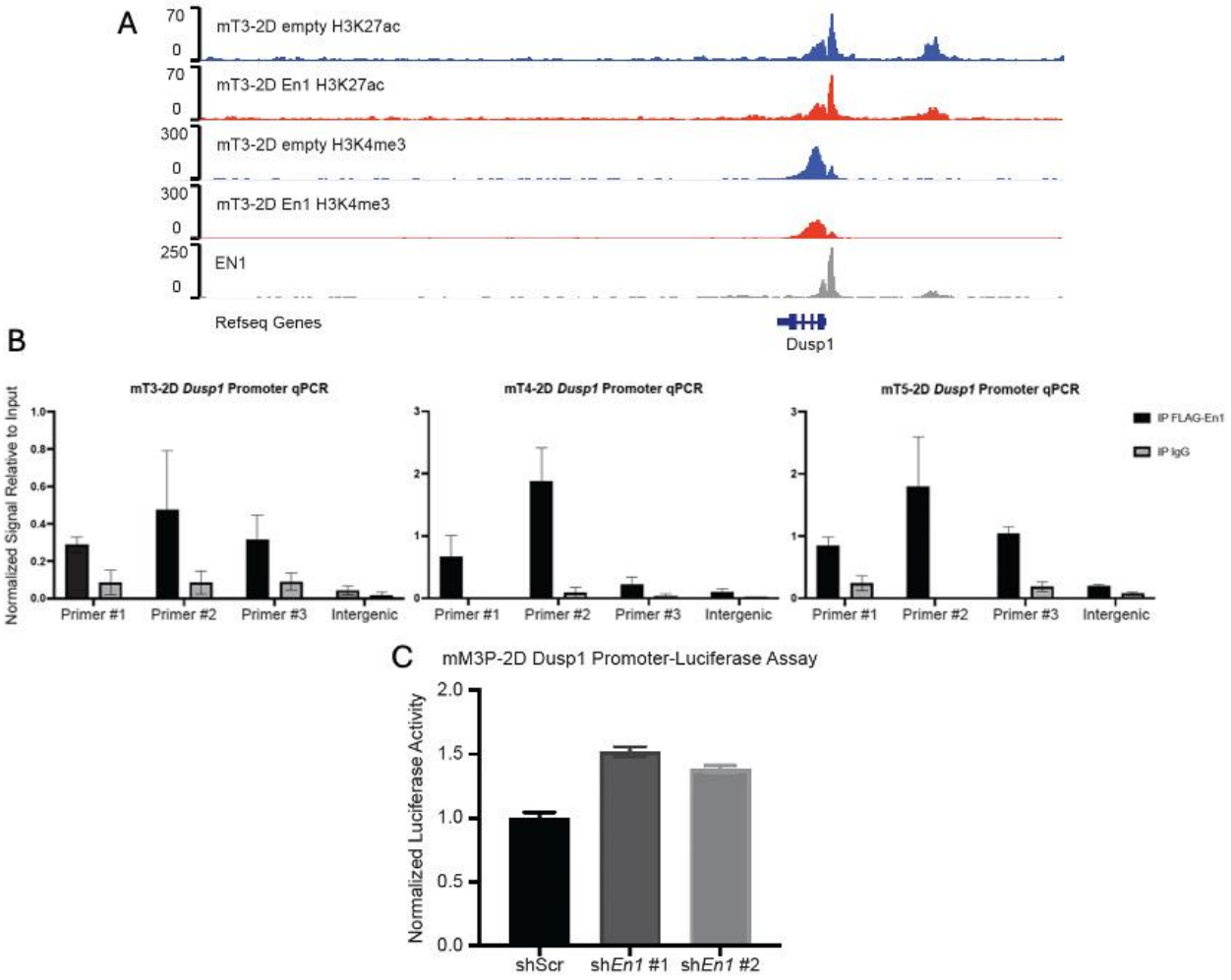


**Figure 29.** (A) Representative gene browser track of H3K27ac, H3K4me3, and EN1 CUT&RUN-seq signal at *Dusp1* gene in mT3-2D empty (blue) and *FLAG-EN1* (red) cells. (B) CUT&RUN assay targeting FLAG-tagged EN1 in three mT-2D cell lines, followed by qPCR analysis employing three primer pairs spanning *Dusp1* promoter EN1 binding sites identified in figure 6E. (C) Luciferase activity assay assessing the *Dusp1* promoter activity in mM3P-2D cell line with scramble (shScr) and two independent *En1* (sh*En1*) shRNA constructs (n=3).

DUSP1 is known to play a role in regulating cell death by dephosphorylating MAPKs[39; 40]. Indeed, En1 depletion upregulated Dusp1 expression (Figure 23 and 30A-B). Furthermore,

other *Dusp* family genes were also upregulated upon En1 knockdown, including *Dusp4*, *Dusp5*, *Dusp6*, *Dusp8*, *Dusp10*, *Dusp16*, and *Dusp19* (Figure 30C).

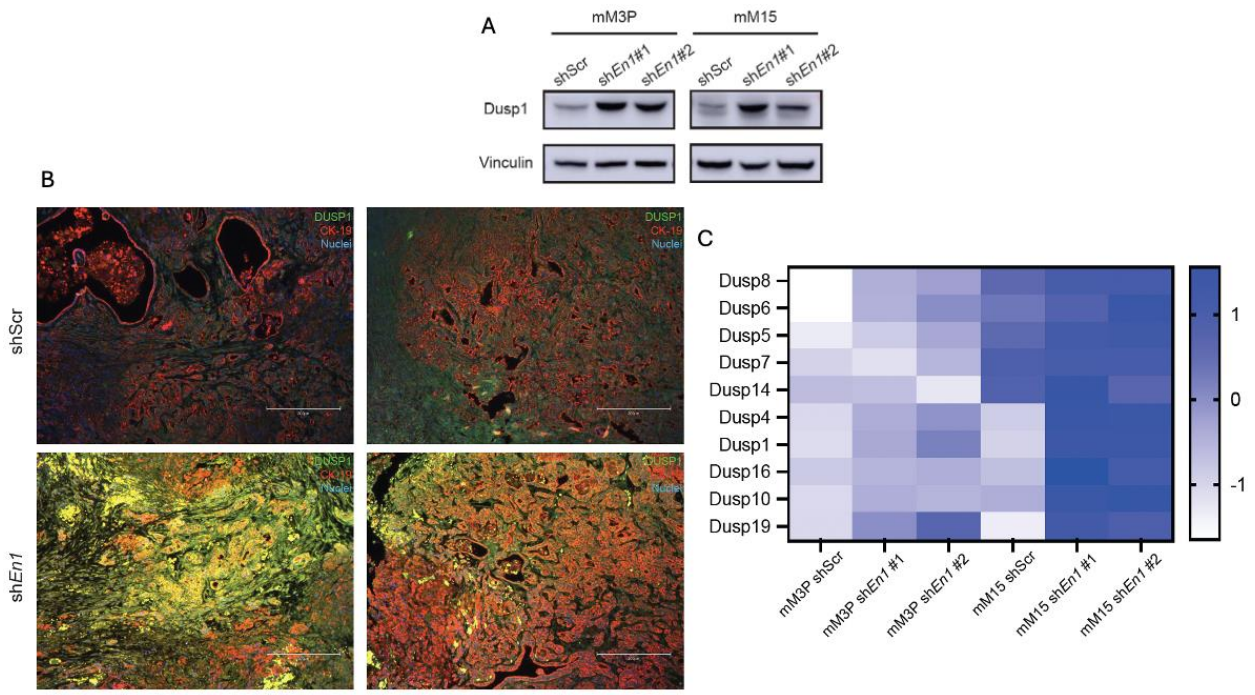


**Figure 30.** (A) Western blot analysis to determine the protein expression of DUSP1 in mM3P and mM15 organoids with shScr and two independent sh*En1* constructs. (B) Immunofluorescence staining of DUSP1 and CK-19 in primary tumor tissue sections collected from shScr (top) and sh*En1* (bottom) mM3P orthotopically transplanted organoids. Scale bar, 150 mm. (C) Heatmap showing the expressions of *Dusp* genes in shScr and sh*En1* mM3P and mM15 organoids, as derived from the RNA-seq dataset presented in figure 23.

To examine if EN1 affects ERK signaling activities, we performed phospho-ERK1/2 Western blotting in mM3P and mM15 organoids (Figure 31A-B). En1 depletion resulted in decreased phospho-ERK1/2 signals, which was more pronounced in the reduced media (Figure 31A),

suggesting that EN1 positively regulates MAPK via repressing a negative regulator of MAPK pathway. These findings offer a potential personalized medicine approach for EN1-high PDA patients with MAPK inhibitors (e.g., ERK inhibitor) to improve the treatment efficacy and patient survival outcomes. Although EN1 genomic and transcriptomic targets are involved in cellular response to hypoxia and MYC pathways (Figure 23), we did not observe any significant change in HIF-1a and c-MYC protein expressions upon *En1* knockdown (Figure 31C).

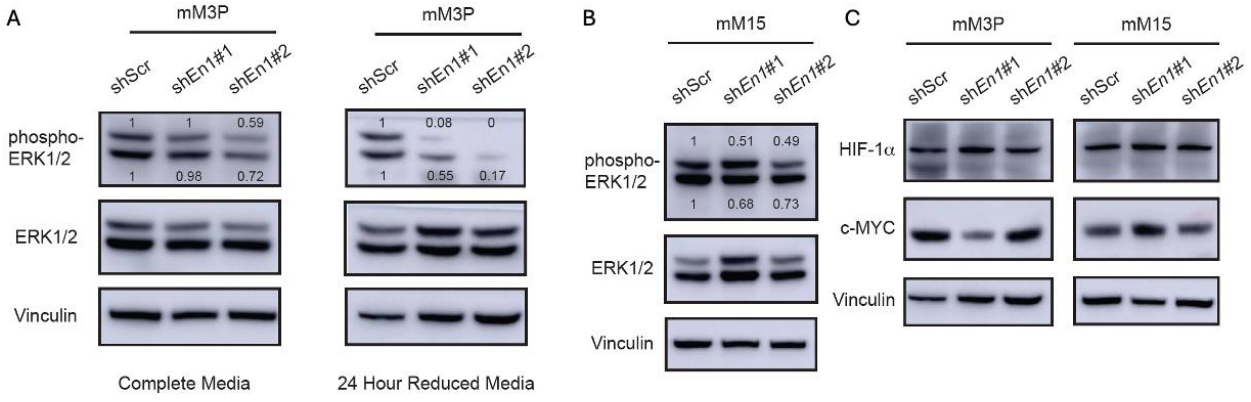


**Figure 31.** (A) Western blot analysis to determine the protein expression of phospho-ERK1/2 (Thr202/Tyr204) and total ERK1/2 in mM3P organoids with scramble (shScr) and two independent En1 (shEn1) shRNA constructs. Blots on the left showed organoids cultured in the complete organoid media and on the right showed organoids cultured in the reduced media for 24 hours before harvesting. Band intensity was determined by ImageJ. (B) Western blot analysis to determine the protein expression of phospho-ERK1/2 (Thr202/Tyr204) and total ERK1/2 in mM15 organoids cultured in the complete media with scramble (shScr) and two independent *En1* (sh*En1*) shRNA constructs. (C) Western blot analysis to determine the protein expression of HIF-1a and c-MYC in mM3P and mM15 organoids cultured in the reduced media for 24 hours with

scramble (shScr) and two independent *En1* (sh*En1*) shRNA constructs. Vinculin data for mM3P was duplicated as Figure 31A right panel.

It has been shown that *En1* mutant mice shared a similar phenotype with *Ezh2* mutant mice[41; 42]. Given the role of EZH2 in H3K27me3[43] and the role of EN1 in transcriptional repression, we performed H3K27me3 CUT&RUN-seq with mT4-2D, mT5-2D, and mT8-2D cell lines upon EN1 overexpression. While we observed the enriched H3K27me3 occupancy at the known EZH2 binding regions[44], we saw negligible H3K27me3 occupancy at EN1 binding regions and no discernible changes upon EN1 overexpression (Figure 32), suggesting EN1-mediated transcription repression is independent of EZH2 catalytic activities.

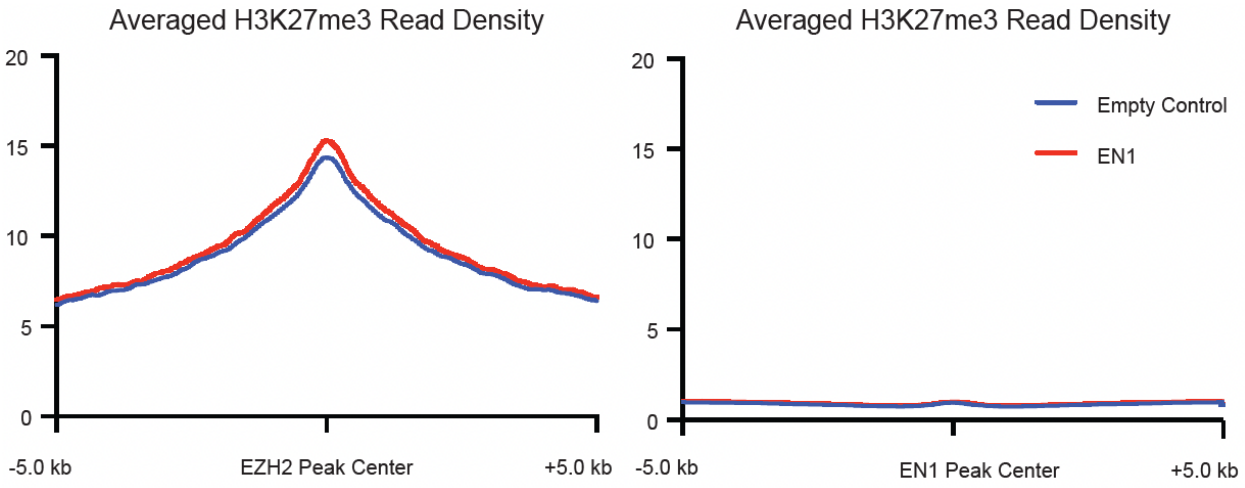


**Figure 32.** Averaged density plots of H3K27me3 CUT&RUN-seq signals around EZH2 genomic binding sites (left) and EN1 genomic binding sites (right) in mT4-2D, mT5-2D, and mT8-2D empty | *FLAG-EN1* cells.

To further explore the potential mechanisms by which EN1 interacts with transcriptional repressors to repress its gene targets, we performed nuclear co-immunoprecipitation of FLAG-tagged EN1 followed by mass spectrometry with mT3-2D and mT19-2D cell lines upon EN1 overexpression and identified 68 significantly enriched EN1 interacting proteins (Figure 33A). GO analysis identified negative regulation of transcription as the top enriched biological pathway (Figure 33B), which includes ARID4B, KAT2A, SINHCAF, WDR5, EZH2, MED9, MCPH1, SIRT7, and ZFP819. These findings shed light on potential mechanisms of how EN1 exerts transcriptional repression of its target genes, which warrants further investigations.

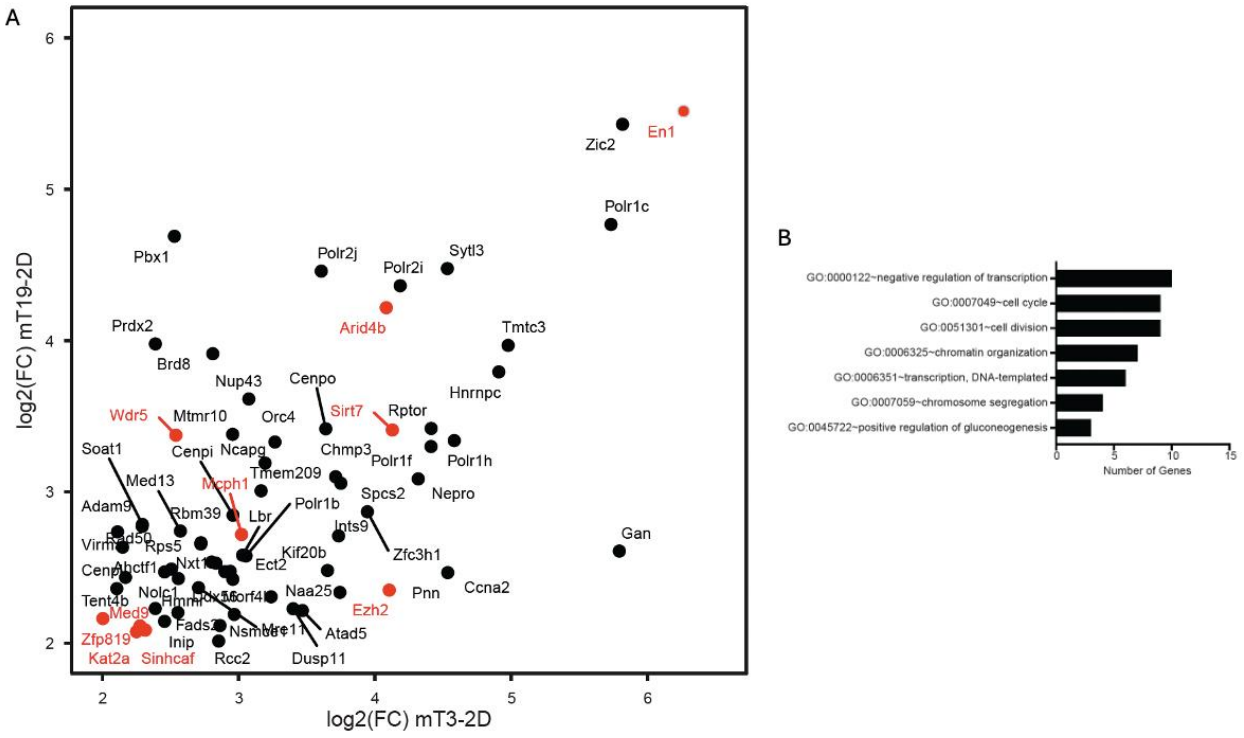

**Figure 33.** (A) Nuclear co-immunoprecipitation assay of FLAG-tagged EN1 followed by mass spectrometry in mT3-2D and mT19-2D EN1 overexpressed cell lines identified 68 EN1-interacting proteins. Proteins involved in transcription repression were highlighted in red. (B) DAVID analysis of the EN1 interacting proteins showing the top significantly enriched pathways in biological functions.

**EN1 promotes PDA progression in GEMMs and PDA patients**

Next, we asked whether EN1 deficiency in pancreatic epithelial cells could delay PDA progression in genetically modified mouse models (GEMMs). To this end, we crossed the conditional knock-out alleles of *En1* (aka *En1*$^{flox/flox}$) with KPC mice to generate KPEC (*Kras*$^{+/LSL\text{-}G12D}$*; Trp53*$^{+/LSL\text{-}R172H}$*; En1*$^{flox/flox}$*; Pdx1-Cre*) mice (Figure 34).

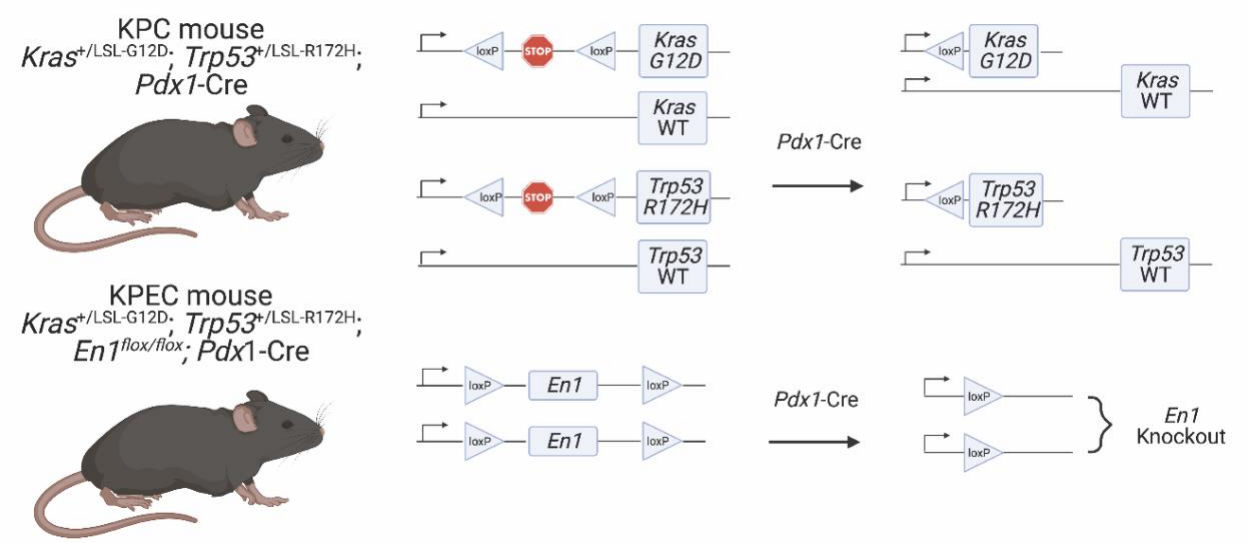


**Figure 34.** Schematic representation of the genetically engineered mouse models with *Kras*$^{+/LSL\text{-}G12D}$*, Trp53*$^{+/LSL\text{-}R172H}$*, Pdx1-Cre* (KPC) and *En1*$^{flox/flox}$ (KPEC) alleles.

There was no gross defect in pancreatic development when inactivating EN1 in the pancreas of EC mice (Figure 35A). Long-term survival analysis showed that EN1 inactivation extended the animal overall survival (Figure 35B), with the medium survival of 191 days for the KPEC mice and 125 days for the KPC mice.

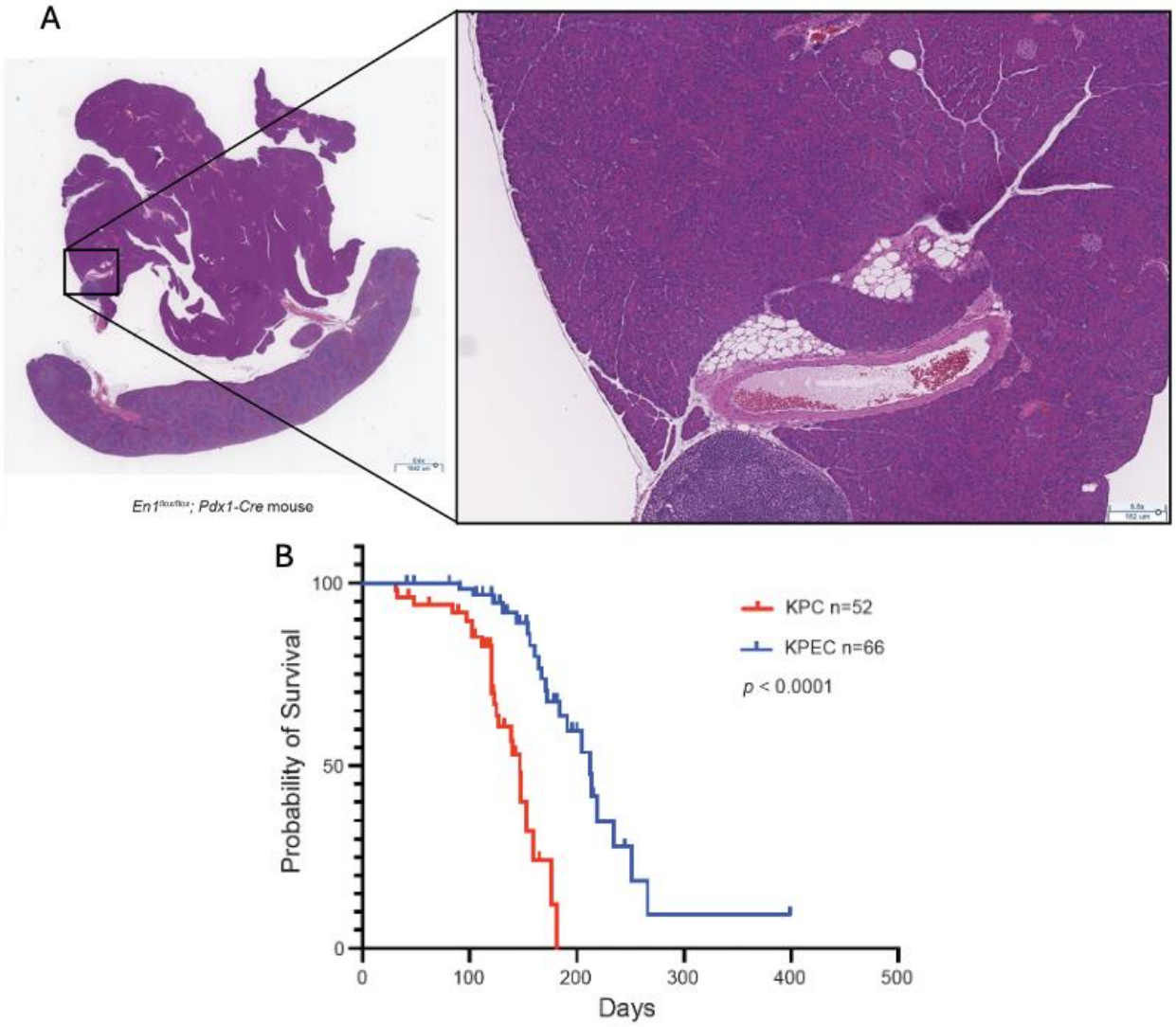


**Figure 35.** (A) H&E staining of pancreas isolated from *En1*$^{flox/flox}$*; Pdx1-Cre* (EC) mouse at 67 days age. (B) Kaplan-Meier plot of KPC (n = 52) and KPEC (n = 66) mice survival. The median survival of KPC mice is 147 days and the median survival of KPEC mice is 212 days. ****$p$<0.0001 was determined by Log-rank (Mantel-Cox) test and GehIBreslow-Wilcoxon test.

To illustrate the effect of *En1* inactivation in PDA progression, we sacrificed 10 mice per genotype at 120 days age for histopathological analysis. Histopathological analysis of KPC and KPEC mice showed the KPEC mice had significantly less percentage of abnormal pancreata, including acinar to ductal metaplasia (ADM), PanIN, and PDA, compared to KPC pancreata at 120 days of age (Figure 36).

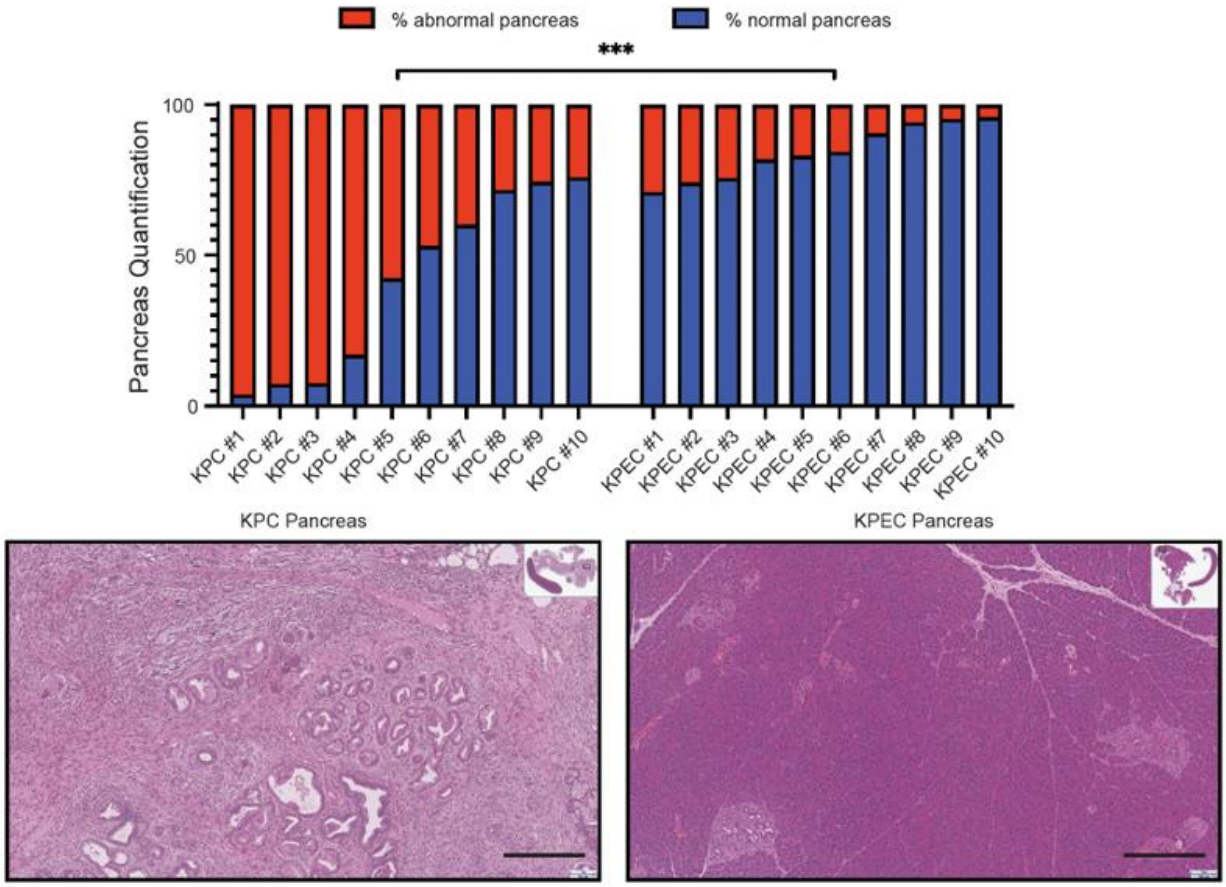


**Figure 36.** Bar plot representing the percentage of abnormal pancreata (red) and normal pancreata (blue) from the KPC mice (n=10) and KPEC mice (n=10) at 120-day age. Representative H&E staining of KPC pancreas (bottom left, scale bar, 300 mm) and KPEC pancreas (bottom right, scale bar, 300 mm).

Of the examined animals at 120 days of age, 80% of KPC mice developed PDA compared to only 40% of the KPEC mice that had developed PDA (Figure 37A). One tumor-derived organoid (1 out of 4) from KPEC mice that we tested harbored unrecombined alleles of En1 (Figure 37B), suggesting that there might be a selective advantage for the unrecombined allele of En1 during the PDA progression of certain KPEC mice. Overall, *En1* deficiency significantly attenuated PDA progression in our autochthonous mouse model.

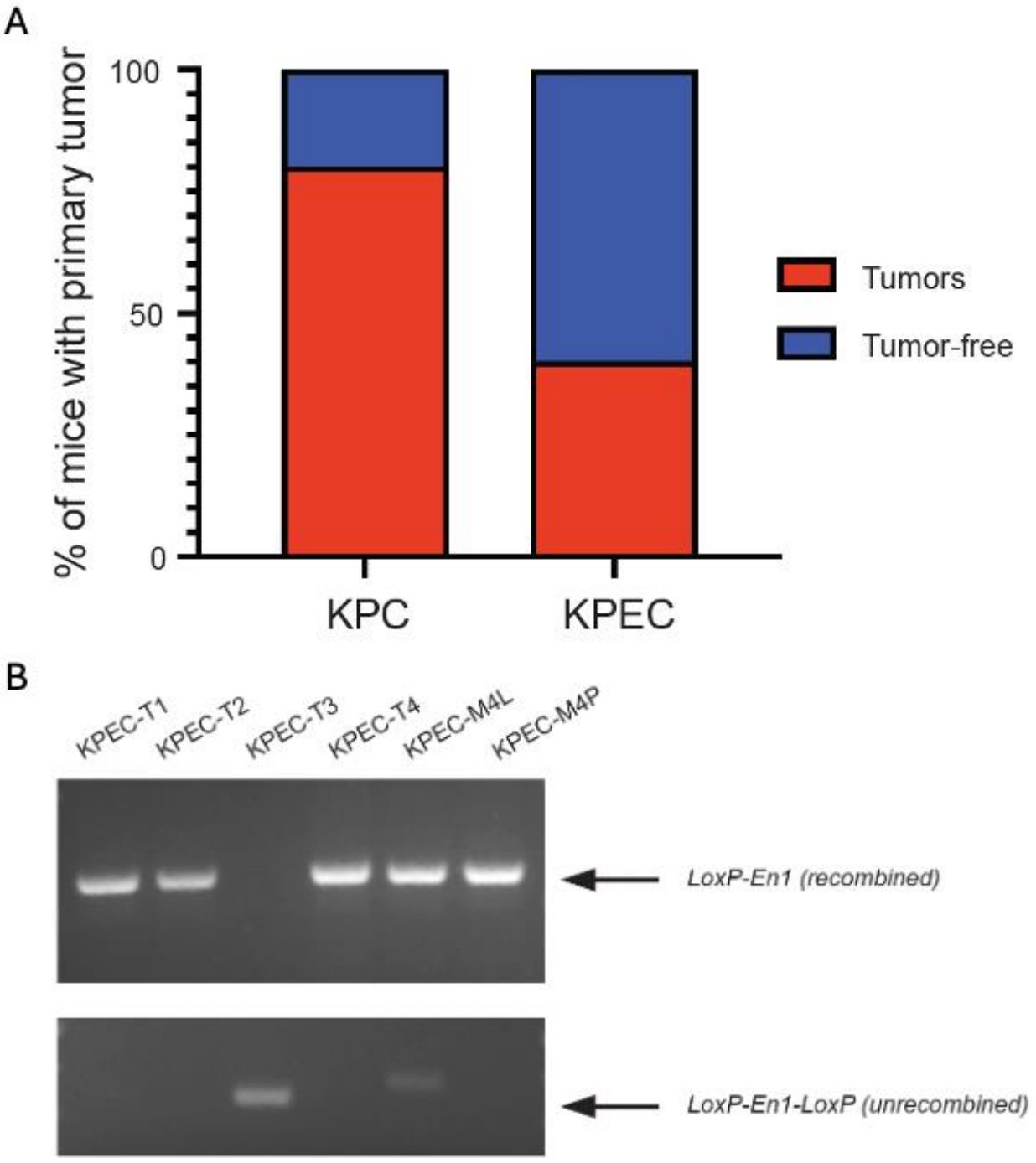


**Figure 37.** (A) Quantification of the number of mice bearing tumors at 120-day age from KPC (n=10) and KPEC (n=10) mice. (B) PCR analysis of 1 loxP-*En1* (recombined, top) and LSL-*En1* cassette (unrecombined, bottom)

using tumor and metastasis organoids derived from KPEC mice. T: tumor; M: metastasis; L: liver; and P: peritoneum. Expected En1 1 loxP size: 600 bp; expected LSL-En1 size: 380 bp.

To confirm our findings in human PDA patient setting, we performed EN1 immunohistochemistry in the paired primary tumors and liver metastases tissue microarray from 19 PDA patients of the Rapid Autopsy Program (Figure 38A). We found 7 out of 19 patients had a higher EN1 protein expression in the metastatic lesions compared to their paired primary tumors. Consistent with our finding that EN1 is a prognostic factor in PDA, EN1 protein expression level in the primary tumor was inversely correlated with the patient survival data (Figure 38B). Taken together, our data showed that aberrant expression of EN1 facilitates PDA progression, resulting in poor survival of PDA GEMMs and patients.

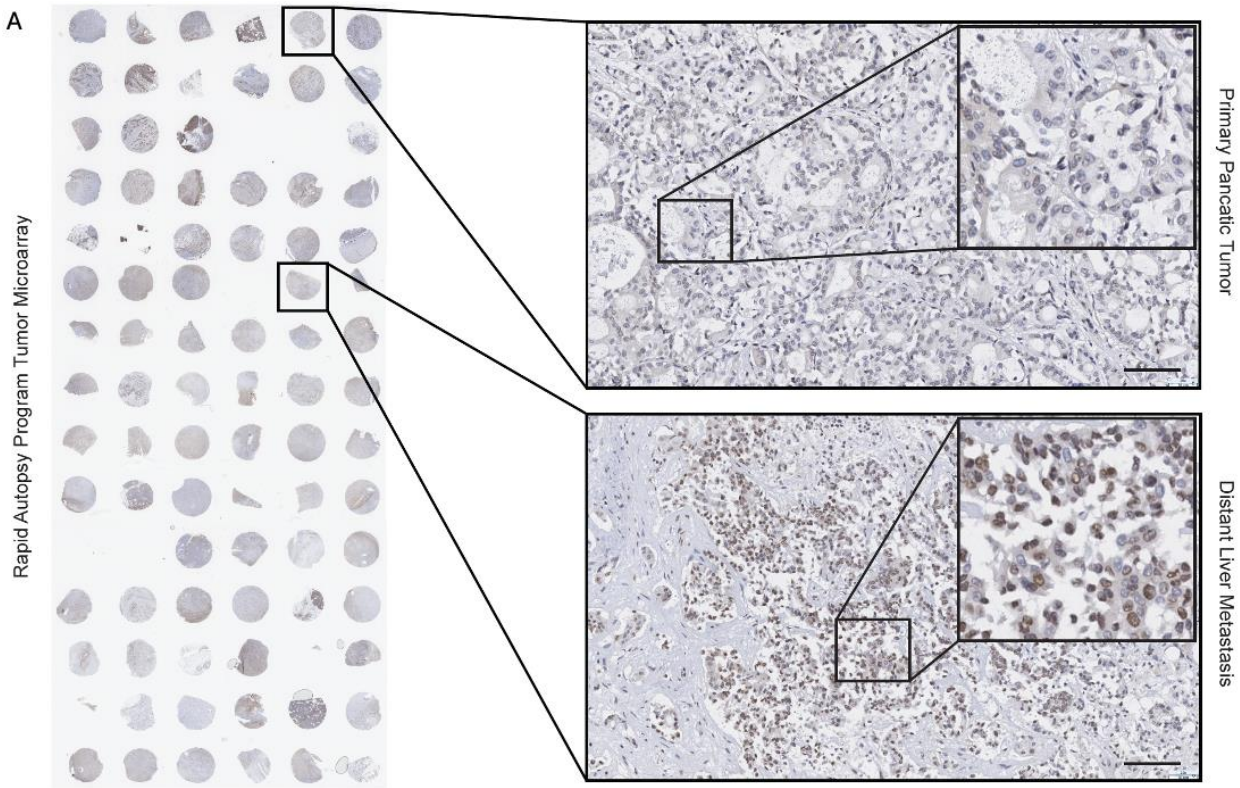

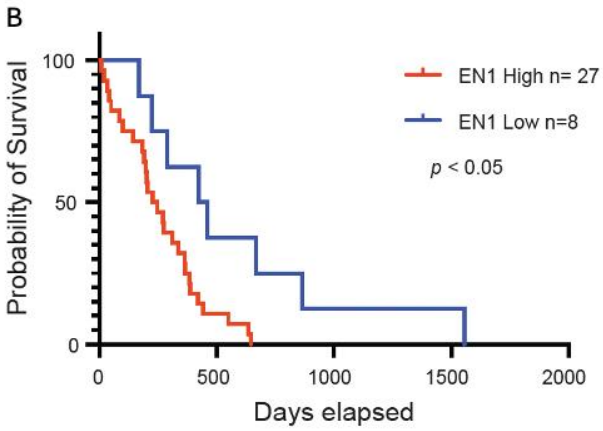


**Figure 38.** (A) Immunohistochemistry staining of EN1 in 19 human pancreatic and metastatic specimens from rapid autopsies (left). Representative image of a primary tumor EN1 IHC staining from patient #55 (Top right, scale bar, 100 mm). Representative image of a liver metastasis EN1 IHC staining from patient #55 (Bottom right, scale bar, 100 mm). (B) Kaplan-Meier plot of patient days survived after diagnosis corresponding to EN1-high (n=27) vs. -low (n=8) from the tissue microarray IHC. *$p$<0.05 was determined by Log-rank (Mantel-Cox) test and Gehan-Breslow-Wilcoxon test.

## Discussion

Non-mutational epigenetic reprogramming is one of the hallmarks of cancer[45]. A growing body of evidence highlights the critical roles of epigenetic alterations in carcinogenesis, including PDA. Previously, we and others have shown that aberrantly expressed transcription factors (e.g., TP63, FOXA1, EVI1, and TEAD2) alter the pancreatic epigenome, thereby promoting PDA progression and a molecular subtype transition[4; 5; 8; 46; 47]. Patients with metastatic PDA have a strikingly poor prognosis and limited response rate to current first-line chemotherapies, including FOLFIRINOX and gemcitabine/nab-Paclitaxel[48; 49]. The poor clinical outcome could be attributed to intrinsic chemoresistance of the cancer cell or the pro-survival program acquired during pancreatic carcinogenesis, which might be mediated through aberrant expressions of TFs and subsequent alteration in epigenetic landscapes and gene expressions. A better understanding of these mechanisms would allow us to identify potential targets and improve patient survival.

Here, we identified aberrant expressions of EN1, a neuro-development TF in the late stage of PDA, resulting in enhancer reprogramming and endowing aggressive characteristics in PDA progression. EN1 has been shown to be a pro-survival factor in brain development and associated with poor prognosis in multiple cancer types, such as adenoid cystic sarcoma, triple-negative breast cancer, nasopharyngeal carcinoma, and osteosarcoma[17-23]. Our data showed that EN1 perturbations altered the expression of a number of genes involved in apoptosis-, MYC-, hypoxia- and E2F-related pathways. For instance, we found that EN1

depletion altered MAPK pathways likely through the up-regulation of negative regulators such as DUSP1, promoting cell survival. Collectively, EN1-mediated transcriptional alterations render the aggressive characteristics seen in our *in vitro* and *in vivo* studies. This observation highlights the critical role of developmental TF-mediated epigenetic reprogramming in cancer and might offer a unique therapeutic opportunity to exploit EN1-mediated epigenetic vulnerability in PDA.

While TFs are generally thought to be undruggable, it would be feasible to target the critical interacting proteins or functionally important downstream genes of the TFs[50]. EN1 is known to function as a transcription repressor via the EH1 domain[51; 52]. Consistent with the known role as a transcriptional repressor, we showed a majority of EN1 target genes (79%) were upregulated upon EN1 depletion, suggesting that EN1 is predominantly a transcription repressor in the PDA context. The detailed molecular mechanisms of how EN1 reduced H3K27ac and H3K4me3 occupancy remain unknown and should be further explored. Thus, it would be worthwhile to identify repressive protein complexes that EN1 recruits to its genomic binding sites in PDA. For instance, in triple-negative breast cancer (TNBC), synthetic peptides targeting EN1 protein-protein interaction domains have been shown to induce cellular apoptotic responses *in vitro*[18]. Likewise, targeting strategies of other interacting proteins in TNBC, such as TLE3, TRIM24-TRIM28-TRIM33 complex[23] , and BRD4-S[53], might attenuate EN1-mediated aggressive cancer phenotypes in the breast cancer context.

In addition, inhibition of direct EN1 downstream target genes might also be a novel therapeutic strategy. For example, *Dusp1*, a phosphatase negatively regulating ERK, JNK, and p38 MAPK activities[39], was identified as a direct repressive target of EN1 in our study. Thus, En1 depletion resulted in an anti-survival phenotype, likely through up-regulation of DUSP1, a negative regulator of MAPK. A previous study has also shown that DUSP1 can antagonize a pro-survival signal upon gemcitabine treatment in PDA[54]. Similarly, the downregulation of DUSP1 has been shown to confer pro-tumorigenic and metastatic characteristics (e.g., proliferation, migration, invasion, anti-apoptosis) in other cancer types, such as bladder and prostate cancers[55-57]. It should be noted that EN1 genomic binding sites appear to be context-dependent since we did not find the EN1 target genes associated with WNT and Hedgehog signaling pathways that were previously identified in TNBC[21; 23]. It is possible that the pre-existing epigenetic landscape in different cell types dictates the EN1 binding sites.

EN1 is an essential gene during embryonic development, and its expression in the neuroepithelium is required to form the midbrain and hindbrain[58]. Within the adult central nervous system, the mesodiencephalic dopaminergic neurons constitutively utilize EN1 to maintain cellular identity, survival, outgrowth, and pathfinding[59-63]. A line of evidence appears to point out that PDA exhibits neurodevelopment-related programs, such as axon guidance pathways, for their survival and tumorigenicity[11], while cancer cells generally utilize transcriptional programs associated with the cell lineage for survival[9]. In addition, a recent single-nucleus analysis of PDA samples identified a distinct neural-like progenitor

(NRP) tumor cell type from patients who received the neoadjuvant therapies. Genes enriched in the NPR subtype were linked to axon guidance pathways, cell-cell adhesions, migrations, and negative regulations of cell death[64]. Although EN1 was not differentially expressed in the NRP PDA subpopulation, the *EN1*-mediated transcriptional program, including axon guidance, cell-cell junction organizations, negative regulation of apoptosis, cell migration, and cytoskeleton organizations, may exert similar functions to the NRP-related programs in PDA as the neural-related genes were expressed within invasive epithelia of PDA to support cell survival and the development of therapeutic resistance. This observation highlights the clinical significance of aberrantly expressed TFs and their contributions to the pancreatic epigenome, in turn promoting PDA progression, metastasis, and chemotherapeutic resistance.

In summary, we provided new evidence that EN1, a neurodevelopmental TF, could be aberrantly expressed in the late stage of PDA progression. EN1 can regulate a set of genes that govern pro-survival signals, contributing to metastatic characteristics of PDA. Importantly, we identified the direct targets of EN1 in PDA and elucidated the effect of EN1 in pancreatic cancer epigenome, which provides path to develop novel and exploitable drug targets in the future.

**Reference**

1. Siegel RL, Miller KD, Wagle NS, Jemal A. 2023. Cancer statistics, 2023. CA Cancer J Clin.

2. Maitra A, Hruban RH. 2008. Pancreatic cancer. Annu Rev Pathol. 3:157-188.

3. Yachida S, Jones S, Bozic I, Antal T, Leary R, Fu B, Kamiyama M, Hruban RH, Eshleman JR, Nowak MA et al. 2010. Distant metastasis occurs late during the genetic evolution of pancreatic cancer. Nature. 467(7319):1114-1117.

4. Wang SS, Xu J, Ji KY, Hwang CI. 2021. Epigenetic alterations in pancreatic cancer metastasis. Biomolecules. 11(8).

5. Somerville TDD, Xu Y, Miyabayashi K, Tiriac H, Cleary CR, Maia-Silva D, Milazzo JP, Tuveson DA, Vakoc CR. 2018. Tp63-mediated enhancer reprogramming drives the squamous subtype of pancreatic ductal adenocarcinoma. Cell Rep. 25(7):1741-1755.e1747.

6. Boj SF, Hwang CI, Baker LA, Chio II, Engle DD, Corbo V, Jager M, Ponz-Sarvise M, Tiriac H, Spector MS et al. 2015. Organoid models of human and mouse ductal pancreatic cancer. Cell. 160(1-2):324-338.

7. Hingorani SR, Wang L, Multani AS, Combs C, Deramaudt TB, Hruban RH, Rustgi AK, Chang S, Tuveson DA. 2005. Trp53r172h and krasg12d cooperate to promote chromosomal instability and widely metastatic pancreatic ductal adenocarcinoma in mice. Cancer Cell. 7(5):469-483.

8. Roe JS, Hwang CI, Somerville TDD, Milazzo JP, Lee EJ, Da Silva B, Maiorino L, Tiriac H, Young CM, Miyabayashi K et al. 2017. Enhancer reprogramming promotes pancreatic cancer metastasis. Cell. 170(5):875-888.e820.

9. Garraway LA, Sellers WR. 2006. Lineage dependency and lineage-survival oncogenes in human cancer. Nat Rev Cancer. 6(8):593-602.

10. Chédotal A, Kerjan G, Moreau-Fauvarque C. 2005. The brain within the tumor: New roles for axon guidance molecules in cancers. Cell Death Differ. 12(8):1044-1056.

11. Biankin AV, Waddell N, Kassahn KS, Gingras MC, Muthuswamy LB, Johns AL, Miller DK, Wilson PJ, Patch AM, Wu J et al. 2012. Pancreatic cancer genomes reveal aberrations in axon guidance pathway genes. Nature. 491(7424):399-405.

12. Albéri L, Sgadò P, Simon HH. 2004. Engrailed genes are cell-autonomously required to prevent apoptosis in mesencephalic dopaminergic neurons. Development. 131(13):3229-3236.

13. Simon HH, Saueressig H, Wurst W, Goulding MD, O'Leary DD. 2001. Fate of midbrain dopaminergic neurons controlled by the engrailed genes. J Neurosci. 21(9):3126-3134.

14. Simon HH, Thuret S, Alberi L. 2004. Midbrain dopaminergic neurons: Control of their cell fate by the engrailed transcription factors. Cell Tissue Res. 318(1):53-61.

15. Logan C, Wizenmann A, Drescher U, Monschau B, Bonhoeffer F, Lumsden A. 1996. Rostral optic tectum acquires caudal characteristics following ectopic engrailed expression. Curr Biol. 6(8):1006-1014.

16. McGrath SE, Michael A, Pandha H, Morgan R. 2013. Engrailed homeobox transcription factors as potential markers and targets in cancer. FEBS Lett. 587(6):549-554.

17. Frerich CA, Brayer KJ, Painter BM, Kang H, Mitani Y, El-Naggar AK, Ness SA. 2018. Transcriptomes define distinct subgroups of salivary gland adenoid cystic carcinoma with different driver mutations and outcomes. Oncotarget. 9(7):7341-7358.

18. Beltran AS, Graves LM, Blancafort P. 2014. Novel role of engrailed 1 as a prosurvival transcription factor in basal-like breast cancer and engineering of interference peptides block its oncogenic function. Oncogene. 33(39):4767-4777.

19. Qin G, Hu B, Li X, Li R, Meng Y, Wang Y, Zou D, Wei F. 2020. Identification of key differentially expressed transcription factors in glioblastoma. J Oncol. 2020:9235101.

20. Wiggins GAR, Black MA, Dunbier A, Morley-Bunker AE, Pearson JF, Walker LC, Investigators k. 2021. Increased gene expression variability in brca1-associated and basal-like breast tumours. Breast Cancer Res Treat. 189(2):363-375.

21. Chang J, Guo C, Li J, Liang Z, Wang Y, Yu A, Liu R, Guo Y, Chen J, Huang S. 2022. En1 regulates cell growth and proliferation in human glioma cells via hedgehog signaling. Int J Mol Sci. 23(3).

22. Kim YJ, Sung M, Oh E, Vrancken MV, Song JY, Jung K, Choi YL. 2018. Engrailed 1 overexpression as a potential prognostic marker in quintuple-negative breast cancer. Cancer Biol Ther. 19(4):335-345.

23. Peluffo G, Subedee A, Harper NW, Kingston N, Jovanović B, Flores F, Stevens LE, Beca F, Trinh A, Chilamakuri CSR et al. 2019. *En1* is a transcriptional dependency in triple-negative breast cancer associated with brain metastasis. Cancer Res. 79(16):4173-4183.

24. Chen J. 2016. The cell-cycle arrest and apoptotic functions of p53 in tumor initiation and progression. Cold Spring Harb Perspect Med. 6(3):a026104.

25. Oni TE, Biffi G, Baker LA, Hao Y, Tonelli C, Somerville TDD, Deschênes A, Belleau P, Hwang CI, Sánchez-Rivera FJ et al. 2020. Soat1 promotes mevalonate pathway dependency in pancreatic cancer. J Exp Med. 217(9).

26. Moffitt RA, Marayati R, Flate EL, Volmar KE, Loeza SG, Hoadley KA, Rashid NU, Williams LA, Eaton SC, Chung AH et al. 2015. Virtual microdissection identifies distinct tumor- and stroma-specific subtypes of pancreatic ductal adenocarcinoma. Nat Genet. 47(10):1168-1178.

27. Franses JW, Philipp J, Missios P, Bhan I, Liu A, Yashaswini C, Tai E, Zhu H, Ligorio M, Nicholson B et al. 2020. Pancreatic circulating tumor cell profiling identifies lin28b as a metastasis driver and drug target. Nat Commun. 11(1):3303.

28. Peng J, Sun BF, Chen CY, Zhou JY, Chen YS, Chen H, Liu L, Huang D, Jiang J, Cui GS et al. 2019. Single-cell rna-seq highlights intra-tumoral heterogeneity and malignant progression in pancreatic ductal adenocarcinoma. Cell Res. 29(9):725-738.

29. Tiriac H, Belleau P, Engle DD, Plenker D, Deschênes A, Somerville TDD, Froeling FEM, Burkhart RA, Denroche RE, Jang GH et al. 2018. Organoid profiling identifies common responders to chemotherapy in pancreatic cancer. Cancer Discov. 8(9):1112-1129.

30. Bian B, Bigonnet M, Gayet O, Loncle C, Maignan A, Gilabert M, Moutardier V, Garcia S, Turrini O, Delpero JR et al. 2017. Gene expression profiling of patient-derived pancreatic cancer xenografts predicts sensitivity to the bet bromodomain inhibitor jq1: Implications for individualized medicine efforts. EMBO Mol Med. 9(4):482-497.

31. Network CGAR. 2017. Integrated genomic characterization of pancreatic ductal adenocarcinoma. Cancer Cell. 32(2):185-203.e113.

32. Bailey P, Chang DK, Nones K, Johns AL, Patch AM, Gingras MC, Miller DK, Christ AN, Bruxner TJ, Quinn MC et al. 2016. Genomic analyses identify molecular subtypes of pancreatic cancer. Nature. 531(7592):47-52.

33. Nguyen DT, Lee E, Alimperti S, Norgard RJ, Wong A, Lee JJ, Eyckmans J, Stanger BZ, Chen CS. 2019. A biomimetic pancreatic cancer on-chip reveals endothelial ablation via alk7 signaling. Sci Adv. 5(8):eaav6789.

34. Network. CGAR. 2017. Integrated genomic characterization of pancreatic ductal adenocarcinoma. Cancer Cell. 32(2):185-203.e113.

35. Puleo F, Nicolle R, Blum Y, Cros J, Marisa L, Demetter P, Quertinmont E, Svrcek M, Elarouci N, Iovanna J et al. 2018. Stratification of pancreatic ductal adenocarcinomas based on tumor and microenvironment features. Gastroenterology. 155(6):1999-2013.e1993.

36. Yang S, He P, Wang J, Schetter A, Tang W, Funamizu N, Yanaga K, Uwagawa T, Satoskar AR, Gaedcke J et al. 2016. A novel mif signaling pathway drives the malignant character of pancreatic cancer by targeting nr3c2. Cancer Res. 76(13):3838-3850.

37. Klett H, Fuellgraf H, Levit-Zerdoun E, Hussung S, Kowar S, Küsters S, Bronsert P, Werner M, Wittel U, Fritsch R et al. 2018. Identification and validation of a diagnostic and prognostic multi-gene biomarker panel for pancreatic ductal adenocarcinoma. Front Genet. 9:108.

38. Jiang J, Azevedo-Pouly AC, Redis RS, Lee EJ, Gusev Y, Allard D, Sutaria DS, Badawi M, Elgamal OA, Lerner MR et al. 2016. Globally increased ultraconserved noncoding rna expression in pancreatic adenocarcinoma. Oncotarget. 7(33):53165-53177.

39. Shen J, Zhang Y, Yu H, Shen B, Liang Y, Jin R, Liu X, Shi L, Cai X. 2016. Role of dusp1/mkp1 in tumorigenesis, tumor progression and therapy. Cancer Med. 5(8):2061-2068.

40. Yue J, López JM. 2020. Understanding mapk signaling pathways in apoptosis. Int J Mol Sci. 21(7).

41. Mesman S, Smidt MP. 2020. Acquisition of the midbrain dopaminergic neuronal identity. Int J Mol Sci. 21(13).

42. Wever I, Wagemans CMRJ, Smidt MP. 2019. Ezh2 is essential for fate determination in the mammalian isthmic area. Front Mol Neurosci. 12:76.

43. Gan L, Yang Y, Li Q, Feng Y, Liu T, Guo W. 2018. Epigenetic regulation of cancer progression by ezh2: From biological insights to therapeutic potential. Biomark Res. 6:10.

44. Patil S, Steuber B, Kopp W, Kari V, Urbach L, Wang X, Küffer S, Bohnenberger H, Spyropoulou D, Zhang Z et al. 2020. Ezh2 regulates pancreatic cancer subtype identity and tumor progression via transcriptional repression of. Cancer Res. 80(21):4620-4632.

45. Hanahan D. 2022. Hallmarks of cancer: New dimensions. Cancer Discov. 12(1):31-46.

46. Kim HR, Yim J, Yoo HB, Lee SE, Oh S, Jung S, Hwang CI, Shin DM, Kim T, Yoo KH et al. 2021. Evi1 activates tumor-promoting transcriptional enhancers in pancreatic cancer. NAR Cancer. 3(2):zcab023.

47. Yoo HB, Moon JW, Kim HR, Lee HS, Miyabayashi K, Park CH, Ge S, Zhang A, Tae YK, Sub Y et al. 2023. A tead2-driven endothelial-like program shapes basal-like differentiation and metastasis of pancreatic cancer. Gastroenterology.

48. Conroy T, Desseigne F, Ychou M, Bouché O, Guimbaud R, Bécouarn Y, Adenis A, Raoul JL, Gourgou-Bourgade S, de la Fouchardière C et al. 2011. Folfirinox versus gemcitabine for metastatic pancreatic cancer. N Engl J Med. 364(19):1817-1825.

49. Von Hoff DD, Ervin T, Arena FP, Chiorean EG, Infante J, Moore M, Seay T, Tjulandin SA, Ma WW, Saleh MN et al. 2013. Increased survival in pancreatic cancer with nab-paclitaxel plus gemcitabine. N Engl J Med. 369(18):1691-1703.

50. Bushweller JH. 2019. Targeting transcription factors in cancer - from undruggable to reality. Nat Rev Cancer. 19(11):611-624.

51. Serrano N, Maschat F. 1998. Molecular mechanism of polyhomeotic activation by engrailed. EMBO J. 17(13):3704-3713.

52. Tolkunova EN, Fujioka M, Kobayashi M, Deka D, Jaynes JB. 1998. Two distinct types of repression domain in engrailed: One interacts with the groucho corepressor and is preferentially active on integrated target genes. Mol Cell Biol. 18(5):2804-2814.

53. Wu SY, Lee CF, Lai HT, Yu CT, Lee JE, Zuo H, Tsai SY, Tsai MJ, Ge K, Wan Y et al. 2020. Opposing functions of brd4 isoforms in breast cancer. Mol Cell. 78(6):1114-1132.e1110.

54. Liu F, Gore AJ, Wilson JL, Korc M. 2014. Dusp1 is a novel target for enhancing pancreatic cancer cell sensitivity to gemcitabine. PLoS One. 9(1):e84982.

55. Pan W, Han J, Wei N, Wu H, Wang Y, Sun J. 2022. Linc00702-mediated dusp1 transcription in the prevention of bladder cancer progression: Implications in cancer cell proliferation and tumor inflammatory microenvironment. Genomics. 114(4):110428.

56. Guo F, Zhang C, Wang F, Zhang W, Shi X, Zhu Y, Fang Z, Yang B, Sun Y. 2020. Deubiquitinating enzyme usp33 restrains docetaxel-induced apoptosis via stabilising the phosphatase dusp1 in prostate cancer. Cell Death Differ. 27(6):1938-1951.

57. Zhang Y, Chen M, Liu C, Xiang C. 2018. Dusp1 is involved in the progression of small cell carcinoma of the prostate. Saudi J Biol Sci. 25(5):858-862.

58. Davidson D, Graham E, Sime C, Hill R. 1988. A gene with sequence similarity to drosophila engrailed is expressed during the development of the neural tube and vertebrae in the mouse. Development. 104(2):305-316.

59. Condron BG, Patel NH, Zinn K. 1994. Engrailed controls glial/neuronal cell fate decisions at the midline of the central nervous system. Neuron. 13(3):541-554.

60. Lundell MJ, Chu-LaGraff Q, Doe CQ, Hirsh J. 1996. The engrailed and huckebein genes are essential for development of serotonin neurons in the drosophila cns. Mol Cell Neurosci. 7(1):46-61.

61. Saueressig H, Burrill J, Goulding M. 1999. Engrailed-1 and netrin-1 regulate axon pathfinding by association interneurons that project to motor neurons. Development. 126(19):4201-4212.

62. Marie B, Cruz-Orengo L, Blagburn JM. 2002. Persistent engrailed expression is required to determine sensory axon trajectory, branching, and target choice. J Neurosci. 22(3):832-841.

63. Alvarez-Fischer D, Fuchs J, Castagner F, Stettler O, Massiani-Beaudoin O, Moya KL, Bouillot C, Oertel WH, Lombès A, Faigle W et al. 2011. Engrailed protects mouse midbrain dopaminergic neurons against mitochondrial complex i insults. Nat Neurosci. 14(10):1260-1266.

64. Hwang WL, Jagadeesh KA, Guo JA, Hoffman HI, Yadollahpour P, Reeves JW, Mohan R, Drokhlyansky E, Van Wittenberghe N, Ashenberg O et al. 2022. Single-nucleus and spatial transcriptome profiling of pancreatic cancer identifies multicellular dynamics associated with neoadjuvant treatment. Nat Genet. 54(8):1178-1191.

65. Hingorani SR, Petricoin EF, Maitra A, Rajapakse V, King C, Jacobetz MA, Ross S, Conrads TP, Veenstra TD, Hitt BA et al. 2003. Preinvasive and invasive ductal pancreatic cancer and its early detection in the mouse. Cancer Cell. 4(6):437-450.

66. Sgaier SK, Lao Z, Villanueva MP, Berenshteyn F, Stephen D, Turnbull RK, Joyner AL. 2007. Genetic subdivision of the tectum and cerebellum into functionally related regions based on differential sensitivity to engrailed proteins. Development. 134(12):2325-2335.

67. Hwang CI, Boj SF, Clevers H, Tuveson DA. 2016. Preclinical models of pancreatic ductal adenocarcinoma. J Pathol. 238(2):197-204.

68. Langmead B, Trapnell C, Pop M, Salzberg SL. 2009. Ultrafast and memory-efficient alignment of short dna sequences to the human genome. Genome Biol. 10(3):R25.

69. Li H, Handsaker B, Wysoker A, Fennell T, Ruan J, Homer N, Marth G, Abecasis G, Durbin R, Subgroup GPDP. 2009. The sequence alignment/map format and samtools. Bioinformatics. 25(16):2078-2079.

70. Ramírez F, Ryan DP, Grüning B, Bhardwaj V, Kilpert F, Richter AS, Heyne S, Dündar F, Manke T. 2016. Deeptools2: A next generation web server for deep-sequencing data analysis. Nucleic Acids Res. 44(W1):W160-165.

71. Zhang Y, Liu T, Meyer CA, Eeckhoute J, Johnson DS, Bernstein BE, Nusbaum C, Myers RM, Brown M, Li W et al. 2008. Model-based analysis of chip-seq (macs). Genome Biol. 9(9):R137.

72. Feng J, Liu T, Qin B, Zhang Y, Liu XS. 2012. Identifying chip-seq enrichment using macs. Nat Protoc. 7(9):1728-1740.

73. Yu G, Wang LG, He QY. 2015. Chipseeker: An r/bioconductor package for chip peak annotation, comparison and visualization. Bioinformatics. 31(14):2382-2383.

74. Kim D, Langmead B, Salzberg SL. 2015. Hisat: A fast spliced aligner with low memory requirements. Nat Methods. 12(4):357-360.

75. Liao Y, Smyth GK, Shi W. 2014. Featurecounts: An efficient general purpose program for assigning sequence reads to genomic features. Bioinformatics. 30(7):923-930.

76. Love MI, Huber W, Anders S. 2014. Moderated estimation of fold change and dispersion for rna-seq data with deseq2. Genome Biol. 15(12):550.

77. Mootha VK, Lindgren CM, Eriksson KF, Subramanian A, Sihag S, Lehar J, Puigserver P, Carlsson E, Ridderstråle M, Laurila E et al. 2003. Pgc-1alpha-responsive genes involved in oxidative phosphorylation are coordinately downregulated in human diabetes. Nat Genet. 34(3):267-273.

78. Subramanian A, Tamayo P, Mootha VK, Mukherjee S, Ebert BL, Gillette MA, Paulovich A, Pomeroy SL, Golub TR, Lander ES et al. 2005. Gene set enrichment analysis: A knowledge-based approach for interpreting genome-wide expression profiles. Proc Natl Acad Sci U S A. 102(43):15545-15550.

79. Tanigawa Y, Dyer ES, Bejerano G. 2022. Whichtf is functionally important in your open chromatin data? PLoS Comput Biol. 18(8):e1010378.

80. Huang DW, Sherman BT, Tan Q, Kir J, Liu D, Bryant D, Guo Y, Stephens R, Baseler MW, Lane HC et al. 2007. David bioinformatics resources: Expanded annotation database and novel algorithms to better extract biology from large gene lists. Nucleic Acids Res. 35(Web Server issue):W169-175.

81. Sherman BT, Hao M, Qiu J, Jiao X, Baseler MW, Lane HC, Imamichi T, Chang W. 2022. David: A web server for functional enrichment analysis and functional annotation of gene lists (2021 update). Nucleic Acids Res.

82. Guzmán C, Bagga M, Kaur A, Westermarck J, Abankwa D. 2014. Colonyarea: An imagej plugin to automatically quantify colony formation in clonogenic assays. PLoS One. 9(3):e92444.

83. Choudhry P. 2016. High-throughput method for automated colony and cell counting by digital image analysis based on edge detection. PLoS One. 11(2):e0148469.

84. Jonkman JE, Cathcart JA, Xu F, Bartolini ME, Amon JE, Stevens KM, Colarusso P. 2014. An introduction to the wound healing assay using live-cell microscopy. Cell Adh Migr. 8(5):440-451.

85. Nguyen DH, Stapleton SC, Yang MT, Cha SS, Choi CK, Galie PA, Chen CS. 2013. Biomimetic model to reconstitute angiogenic sprouting morphogenesis in vitro. Proc Natl Acad Sci U S A. 110(17):6712-6717.

## Chapter Three—Nucleoplasmic Macromolecular Crowding and Pancreatic Cancer Metastasis

### Summary

Pancreatic ductal adenocarcinoma (PDA) represents a formidable challenge in oncology due to its aggressive nature and high metastatic propensity. Despite its grim prognosis, most patients are diagnosed at an advanced stage, leading to a dismal 5-year survival rate below 5%. This study endeavors to unravel the unexplored relationship between PDA progression and nucleoplasmic macromolecular crowding, a critical yet often overlooked factor in biological processes. Utilizing innovative tools, including nucleoplasmic genetically encoded multimeric nanoparticles and a 3D PDA organoid model, we investigated nucleoplasmic macromolecular crowding in PDA progression and metastasis. We first observed differential nucleoplasmic macromolecular crowding in murine metastatic PDA organoids. We then unveiled the up-regulation of nesprin-3, a crucial component of the outer nuclear membrane and the linker of the nucleoskeleton and cytoskeleton complex, in metastatic PDA organoids. Perturbation of nesprin-3 leads to alterations in nucleoplasmic macromolecular crowding and attenuations of metastatic potential in vitro, indicating the significant role of nesprin-3 in regulating nuclear macromolecular crowding and cancer metastasis. By bridging the gap between genetic and biophysical factors, this preliminary study provides insights and warrants further investigations into the biophysical properties of the nucleoplasm and its influence on the aggressive traits of PDA.

## Introduction

Pancreatic ductal adenocarcinoma (PDA) is one of the most challenging malignancies. PDA represents a formidable challenge in oncology due to its aggressive nature and high metastatic propensity. Despite incremental improvements of the 5-year relative survival rate of PDA patients to 12.5% over the past few years[1], the 5-year survival rate for metastatic PDA patients remains unchanged at a dismal 3.2%[2]. Gain-of-function mutations of KRAS in pancreatic epithelial cells, leading to the formation of pancreatic intraepithelial neoplasia (PanIN), initiate PDA progression, followed by loss-of-function mutations of tumor suppressor genes, such as CDKN2A, TP53, and SMAD4[3]. However, no known recurrent genetic mutations drive PDA metastasis[4]. In fact, metastatic lesions are genetically similar to the primary tumor, suggesting that non-genetic factors are responsible for metastatic transitions. Metastasis is a multistep process requiring cancer cells to overcome various physical barriers. This involves acquiring migratory and invasive characteristics, intravasating, surviving systemic circulation, extravasating, and colonizing secondary organ sites. One possible mechanism for metastatic PDA cells to overcome these challenges involves fluctuations in gene expression caused by epigenetic alterations to acquire invasive traits. Additionally, an emerging research field indicates that the mechanical properties of the cell nucleus play a crucial role in cancer metastasis. More specifically, the nuclear lamina acts as a mechanical scaffold for chromosome positioning, chromatin remodeling, and transcriptional regulations[5]. However, it remains unknown if the biophysical properties of the nucleus, including macromolecular crowding, affect PDA metastasis.

Macromolecular crowding is implicated in various biological and cellular processes, including chromatin compaction, epigenetic regulation, and gene expression regulation[6]. Nuclei, constituting 20-40% of the cellular volume, are densely packed with biological macromolecules such as proteins and nucleic acids[7]. A balanced concentration of these crowding agents energetically favors intermolecular interactions, thereby accelerating reaction rates. Alterations in macromolecular crowding can significantly impact biological functions within nuclei, including RNA synthesis[8], chromatin interaction and compaction[9], and the transcription rate of specific genes[7]. Consequently, macromolecular crowding impacts cell differentiation[10] and nuclear volume[11], a hallmark of cancer. Despite the implication of cytosolic macromolecular crowding in cancer progression and therapeutic resistance[12], the role of nucleoplasmic macromolecular crowding in tumor progression and metastasis remains unexplored.

To study macromolecular crowding, we employ the ectopic expression and single-particle tracking of nucleoplasmic genetically encoded multimeric nanoparticles (nucGEMs)[13]. NucGEMs are comprised of the *Pyrococcus furiosus* encapsulin scaffold protein fused with a green fluorescent protein (GFP) and a nuclear localization signal (NLS) from the large T-antigen of SV40, assembling into stable 40 nm in diameter particles that are similar in size compared to RNA Polymerase II within the nucleus[14]. Once nucGEM is expressed, the motion of the GEMs can be observed to infer various biophysical properties within the

nucleus, such as viscosity, elasticity, and structure based on the characteristic motion of the nucGEM[14].

Until recently, studying the dynamic changes of biophysical and molecular dynamics during cancer progression has been challenging due to the lack of relevant in vitro models capable of recapitulating different stages of PDA. To address this obstacle, we previously established an in vitro organoid model derived from a genetically engineered mouse model harboring *Kras*$^{+/LSL\text{-}G12D}$*; Trp53*$^{+/LSL\text{-}R172H}$*; Pdx1-Cre* (hereinafter referred to as KPC) alleles[15]. The organoid models derived from the normal murine pancreas and the KPC PDA tissues allow a direct comparison of the normal (mN)-, tumor (mT)- and paired metastasis (mM)-derived organoids at biochemical, biophysical, and cell biological levels at each stage of the diease progression. Furthermore, 2D cell lines can be derived from the mT and mM organoids, enabling a direct comparison of the biophysical and cell biological properties of the cancer cells during adaptation to the plastic petri dish.

In this study, we identified Nesprin-3 as a potential oncogene and regulator of nucleoplasmic macromolecular crowding in pancreatic cancer cells. The gene *Syne3* encodes nesprin-3 and is a crucial member of the outer nuclear membrane and the linker of the nucleoskeleton and cytoskeleton (LINC) complex. LINC complexes are nuclear envelope-spanning molecular bridges that physically couple the nucleus to cytoskeletal structures and play critical roles in regulating nuclear-cytoplasmic transport via nuclear pore complexes, mechanotransduction, genome stability, chromatin organization, and gene

transcription[16,17]. Furthermore, disruptions of the LINC complex, known to impair force transmission between the nucleus and cytoskeleton, are associated with defects in cell migration[18,19], suggesting a potential influence of nucleoplasmic biophysical properties on cancer cell metastasis. Moreover, disruption in the LINC complex altered cytoplasmic stiffness[20], a factor implicated in cellular plasticity and the induction of epithelial-to-mesenchymal transition (EMT)[21]. Perturbation of Nesprin-3 leads to alterations in nucleoplasmic macromolecular crowding and attenuations of metastatic potential in vitro, indicating the significant role of nesprin-3 in regulating nuclear macromolecular crowding and cancer metastasis. Therefore, targeting Nesprin-3 and nucleoplasmic macromolecular crowding could be effective therapeutic strategies against PDA metastasis.

## Materials and Methods

### Tissue culture conditions

Murine pancreatic normal organoids (mN11, mN12, and mN13), primary tumor organoids (mT3, mT19, and mT23), metastatic organoids (mM1, mM6, and mM10), and tumor 2D cell lines (mT19-2D and mM6-2D) from the tumor-bearing KPC mice were established and characterized previously[22]. . Murine pancreatic organoid culture media contains Advanced DMEM/F-12 (Thermo Fisher 12634028), 10mM HEPES (Thermo Fisher 15630080), 1% Penicillin-Streptomycin (Thermo Fisher 15140122), 1% GlutaMAX Supplement (Thermo Fisher 35050061), 0.5mM A 83-01 (Fisher Scientific 29-391-0), 0.05mg/mL mEGF (Fisher Scientific PMG8043), 0.1mg/mL hFGF-10 (Pepro Tech 100-26), 0.01mM hGastrin I (Fisher Scientific 30-061), 0.1mg/mL mNoggin (Pepro Tech 250-38), 1.25mM *N*-Acetyl-L-cysteine (Millipore Sigma A9165), 10mM Nicotinamide (Millipore Sigma N0636), 1X B-27 Supplement (Fisher Scientific 17-504-044), and 1x RSPO1-conditioned medium. Murine 2D culture media contains DMEM (Corning 10-013-CV), 10% FBS (Gen Clone 25-550H), and 1% Penicillin-Streptomycin.

### Cloning

Scramble shRNA was obtained previously[22]. *Syne3* shRNAs sequences were obtained from the TRC shRNA library available at the Broad Institute (sh*Syne3* CDS TRCN0000283060 and sh*Syne3* 3'UTR TRCN0000283064) and cloned in the pLKO.1 puro construct (Addgene 8453). 8 μg of pLKO.1 plasmid was first digested overnight at 37 ℃ using 2μL AgeI-HF (NEB R3552L)

and 2μL EcoRI-HF (NEB R3101L). The digested plasmid was then dephosphorylated using 2μL Quick CIP (NEB M0525L) at 37 ℃ for 3 hours and purified using PureLink™ PCR purification kit (Thermo Fisher K310001) and diluted to 50ng/μL. 1μL of each paired oligonucleotide stocks (100 μM) was first phosphorylated using T4 Polynucleotide Kinase (NEB M0201L) at 37 ℃ for 30 minutes and then heated to 95 ℃ for 5 minutes followed by ramping down to 25 ℃ at 5 ℃/minute for annealing and diluted at 1:200 dilution factor. 1μL of annealed primers were ligated with the pLKO.1 vector using Quick Ligation™ kit (NEB M2200L) at room temperature for 30 minutes. Sanger sequencing was performed by Genewiz using U6 primer (5' ACTATCATATGCTTACCGTAAC 3') for validation. pLV V5-tagged *Syne3* puro was obtained from Addgene (Addgene 175136), and pLV mCherry puro was obtained from VectorBuilder.

**Reverse transcription and quantitative PCR**

Total RNA was extracted using TRIzol reagents per the manufacturer's instructions as described in the RNA preparation for sequencing. RNA concentration was measured using NanoDrop 1000 (Thermo Fisher). 1500 ng of RNA was used for cDNA synthesis with a high-capacity cDNA reverse transcription kit (Thermo Fisher 4368814). 1 mL of the cDNA or CUT&RUN DNA was used for qPCR with PowerTrack™ SYBR green qPCR master mix (Thermo Fisher 446109) on LightCycler 480 instrument II (Roche Diagnostics). The qPCR results were quantified using the 2^(delta)(delta)Ct method with housekeeping gene *Gapdh* and *Actb* for data normalization. qPCR primer sequences used in the study include *Gapdh* Forward 5' TTCACCACCATGGAGAAGGC 3', *Gapdh* Reverse 5' CCCTTTTGGCTCCACCCT 3', *Actb*

Forward 5' GTGACGTTGACATCCGTAAAGA 3', *Actb* Reverse 5' GCCGGACTCATCGTACTCC 3', *Syne3* Forward 5' GCAGGTGACAAGTTCTGTGAGG 3', *Syne3* Reverse 5' TGGAGGTCTAGGAGCTTCCTGT 3'.

**Lentivirus production and infection**

Lentivirus was produced in HEK293T (ATCC CRL-3216) via X-tremeGENE9 (Millipore Sigma 6365809001) transfection using psPAX2 (Addgene 12260) and pMD2.G (Addgene 12259). Detailed protocols for transfection and infection procedures were described previously[22].

**Colony formation assay**

KPC-2D cell lines were trypsinized to generate single-cell suspensions and counted three times to average the cell counts. 1000 cells were resuspended in DMEM supplemented with 10% FBS and 1% Penicillin-Streptomycin and plated in 6-well tissue culture plates (Celltreat 229105) for 14 days. Colonies were stained at room temperature for 1 hour with 2% crystal violet (Thomas Scientific 30430001-1) diluted in 100% methanol to reach the 0.5% final concentration, followed by tap water wash three times and running water wash for five minutes. The plates were imaged with iPhone 12 Pro Max (Apple), and clonogenic growth was analyzed using the ImageJ (NIH) plugin ColonyArea[23].

**Tumor spheroid formation assay**

All cell lines were trypsinized to generate single cell suspensions and counted three times to average the cell counts. 15,000 cells of KPC-2D cells were resuspended in 3D Tumorsphere

Medium XF (PromoCell C-28075) and plated in ultra-low attachment 24-well plates (Millipore Sigma CLS3473-24EA) for 14 days. Culture suspensions were mixed well before imaging using the EVOS M5000 imaging system (Fisher Scientific) under a 4x bright field. Spheroids were analyzed using the ImageJ plugin Cell Colony Edge[24].

**Wound-healing assay**

Cells were grown to 100% in 6-well tissue culture plates and wounded linearly using a 200 μL tip followed by three washes of PBS. Cell migration was imaged every 6 hours for 18 hours under 4x bright field. The percentage of migration was determined by the ImageJ plugin MRI Wound Healing Tool[25].

**Cell proliferation assay**

All cell lines were trypsinized to generate single cell suspensions and counted three times to average the cell counts. 5000 cells were plated in 100 μL of the culture media and serial diluted 7 times at 1:2 dilution factor in 96-well plates for 36 or 60 hours. 100 μL of diluted AlamarBlue solution prepared by mixing 180 μL of Resazurin (Fisher Scientific, AC418900010) in 50 mL of PBS was added to each well and incubated at 37 ℃ for 2 hours. Absorbance at 570nm was measured using a SpectraMax iD5 microplate reader (Molecular Devices). Data analysis was performed as previously described[26].

**Boyden chamber invasion assay**

Matrigel (Corning 356231) was first diluted in DMEM at 1:10 dilution. 100 μL diluted Matrigel was placed in a transwell insert (Neta Scientific SIAL-CLS3464), incubated in the tissue culture incubator for 3 hours, and removed completely using vacuum suctioning. 600 μL of DMEM supplemented with 10% FBS was added to the lower chamber. 50,000 per 200 μL of cells were then added on top of the solidified Matrigel and incubated for 36 hours. After, the transwell was removed and gently scrubbed with a cotton swab and washed twice with PBS. Cells were then stained with Giemsa stain (Millipore Sigma G5637).

**RNA sequencing data analysis**

mT3, mT19, mT23, and paired mM1, mM6, and mM10 organoid RNA sequencing data were obtained from a publicly available database[27]. Pair-end raw data was aligned to mm10 reference genome using HISAT2[28]. Sequencing reads were counted and normalized using featureCounts[29]. DESeq2[30] was then used to identify differentially expressed genes.

**nucGEM Imaging and data analysis**

A pipeline for imaging nucGEM and the subsequent data analysis was developed by the Starr & Luxton Labs at the University of California, Davis.

## Results

To investigate whether metastatic PDA organoids exhibit differential nucleoplasmic macromolecular crowding from tumor PDA organoids, we lentivirally introduced nucGEMs into three pairs of mT and mM organoids from KPC mice. Using spinning-disk confocal microscopy for live cell imaging, we first optimized the quantification of molecular crowding, characterized by the effective diffusion rate, in the nucleoplasm of single cells within 3D organoids (Figure 39).

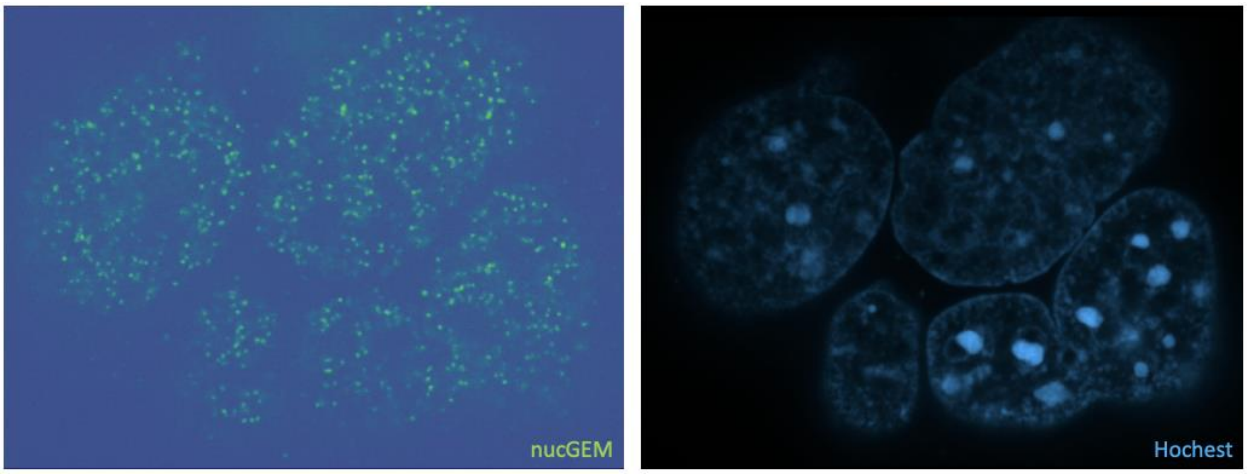


**Figure 39.** A representative image of nucGEM (left) in the mM6 organoid. Single nuclei are contrasted by Hochest staining (right). The nucGEM is imaged using a 100x Nikon HCA Spinning Disc Confocal Microscope at the UC Davis Light Microscopy Core.

We observed a higher diffusion rate in the nuclei of mM organoids at the 40 nm length scale, indicating a reduced collision frequency and a lower molecular reaction rate at the mesoscale compared to mT organoids (Figure 40).

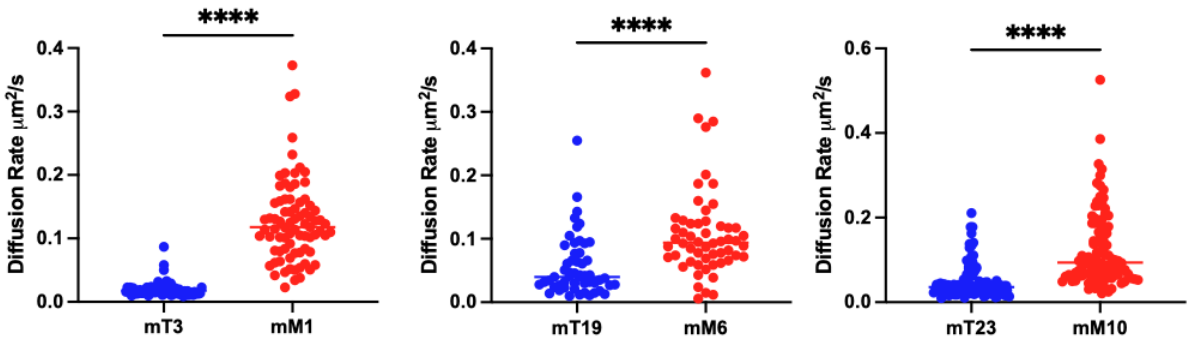


**Figure 40.** Nucleoplasmic macromolecular crowding in paired murine KPC tumor and metastasis PDA organoids. Each data point represents the average effective diffusion of nucGEMs in a single nucleus from the indicated organoids. mT3 n = 69, mT19 n = 54, mT23 n = 99, mM1 n = 79, mM6 n = 56, and mM10 n = 99. **** $p < 0.0001$, one-way ANOVA.

Given that 2D cell culture is a prevalent model for cancer research, we asked if the process of adapting a plastic petri dish would alter the biophysical properties of the cell nuclei from in vivo-mimicking 3D culture to 2D monolayer culture. To address this, we lentivirally expressed nucGEMs into organoid-derived 2D cell lines, including mT3-2D, mT19-2D, mT23-2D, mM1-2D, mM6-2D, and mM10-2D cells (Figure 41). We observed only the mT23-2D/mM10-2D pair of cell lines recapitulated the findings in 3D organoid and that the mesoscale macromolecular diffusion rate was higher in mT3-2D and mT19-2D cell lines.

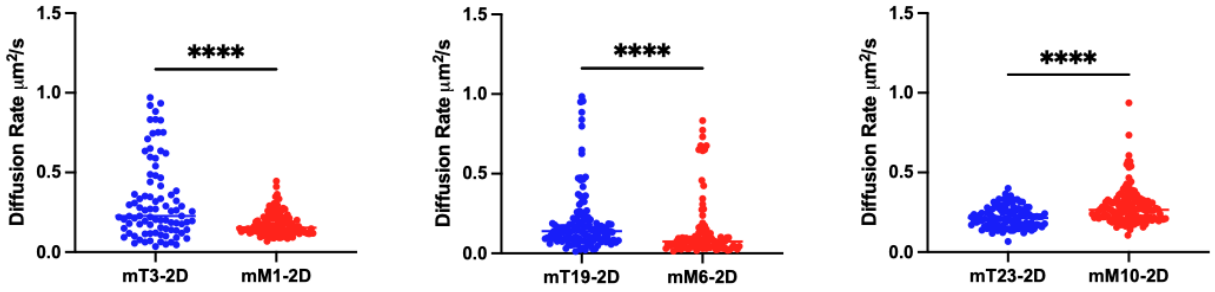


**Figure 41.** Nucleoplasmic macromolecular crowding in paired murine KPC tumor and metastasis PDA organoid-derived 2D cell lines. Each data point represents the average effective diffusion of nucGEMs in a single nucleus from the indicated organoids. mT3 n = 109, mT19 n = 148, mT23 n = 113, mM1 n = 126, mM6 n = 110, and mM10 n = 133. **** $p < 0.0001$, one-way ANOVA.

Interestingly, when comparing between 3D organoids and 2D cell lines, we observed that the nucleoplasmic macromolecular diffusion was significantly higher in the 2D cell lines compared to the parental 3D organoid, with the exception of the mM6-2D/3D pair (Figure 42). Furthermore, the diffusion rate in 2D cells had a larger range of distribution compared to the parental 3D organoids.

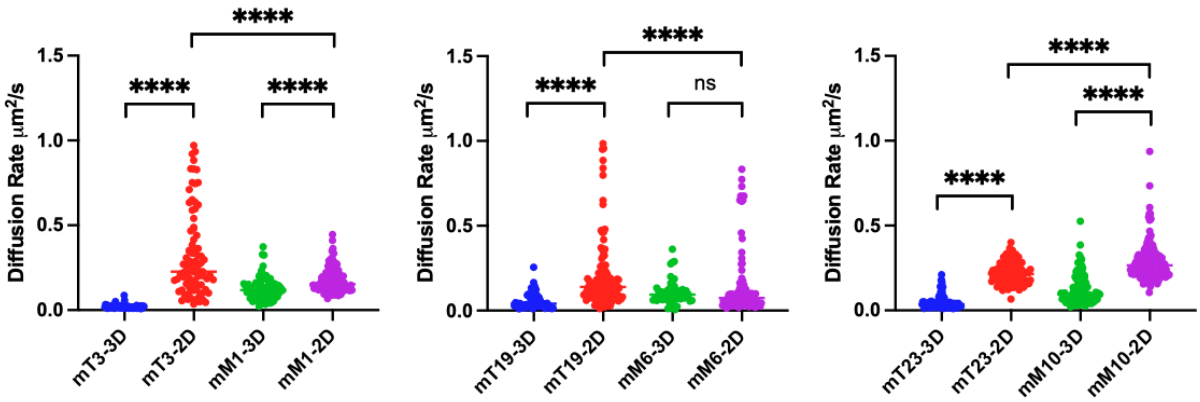

**Figure 42.** Comparison of nucleoplasmic macromolecular crowding in 3D organoid and organoid-derived 2D cell lines. **** $p < 0.0001$, one-way ANOVA.

It has been shown that alteration of the extracellular environment can influence the biophysical properties within the cell, including metabolism, signaling, cellular, and nuclear stiffness[31,32]. Therefore, we asked if the observed difference in nuclear diffusion between the 3D organoid and 2D cell lines was due to the difference in the extracellular environment. To address this, we plated the nucGEM-expressing mT19-2D cell into Matrigel, allowed the cells to form organoids, and imaged the nucGEMs after three weeks of passaging. Interestingly, we observed that the averaged nuclear macromolecular diffusion rate did not change after 2D cells grew into 3D organoids (mT19 2-3D) (Figure 43), indicating that the observed increase in nuclear macromolecular diffusion during organoid adaptation to 2D plastic petri dish was not due to the change in extracellular environment but the intrinsic properties of the cell. It is worth noting that comparing mT19 2D and mT19 2-3D, the range of diffusion coefficient was reduced when cells were in the 3D matrix form, resembling the parental organoid (Figure 43).

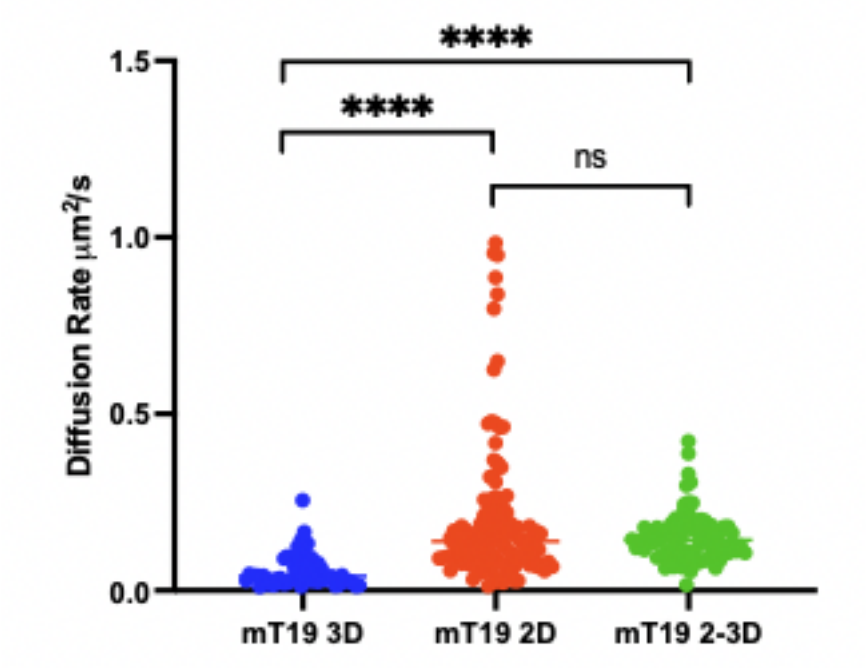


**Figure 43.** Nucleoplasmic macromolecular crowding in mT19 organoid, organoid-derived 2D cells, and 2D cells reformed into organoids. Each data point represents the average effective diffusion of nucGEMs in a single nucleus from the indicated organoids. mT19 3D n = 54, mT19 2D n = 148, and mT19 2-3D n = 85. **** $p < 0.0001$, one-way ANOVA.

To identify potential regulators of nuclear crowding, we analyzed publicly available RNA-seq datasets of pancreatic organoid models for PDA progression[27]. We observed differential expression of LINC complex protein-encoding genes, with nuclear envelope spectrin repeat protein 3 (nesprin-3, encoded by the *Syne3* gene) up-regulated and nesprin-4 (encoded by the *Syne4* gene) down-regulated in mM relative to mT organoids (Figure 44). We also observed the upregulation of other LINC complex genes, including *Tor1a*, *Tor1b*, *Sun1*, and *Sun2* (Figure 44).

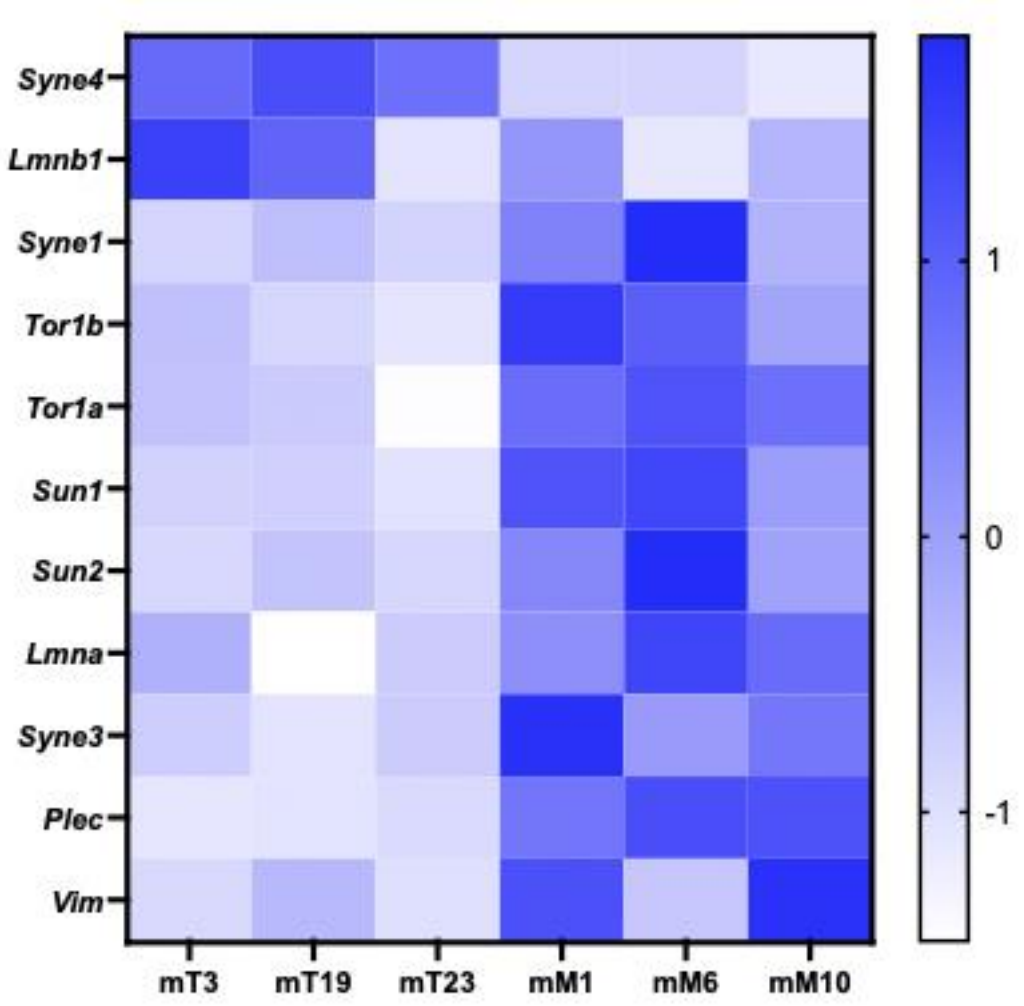


**Figure 44.** A heatmap of significantly differentially expressed genes from the RNA-sequencing analysis of paired mT and mM PDA organoids[27]. $p < 0.05$, the p-value was determined by DESeq2[30].

LINC complexes are nuclear envelope-spanning molecular bridges that physically couple the nucleus to cytoskeletal structures and play critical roles in regulating nuclear-cytoplasmic transport via nuclear pore complexes, mechanotransduction, genome stability, chromatin organization, and gene transcription[16,17]. In addition, disruption in the LINC complex altered cytoplasmic stiffness[20], a factor implicated in cellular plasticity and the

induction of epithelial-to-mesenchymal transition (EMT)[21]. Furthermore, Nesprin-3 indirectly interacts with vimentin (*Vim*) intermediate filaments via the cytoskeletal crosslinker protein plectin (*Plec*)[33], both of which are crucial for cell polarity and EMT[34]. Given the upregulation of *Syne3*, *Vim,* and *Plec* in mM vs. mT PDA organoids (Figure 44), we hypothesized that Nesprin-3 regulates nuclear molecular crowding to promote pancreatic cancer metastasis. To address this hypothesis, we ectopically introduced V5-tagged Syne3 in the mT19-2D cell line (Figure 45) and measured cell proliferation, migration, and anchorage-independent growth.

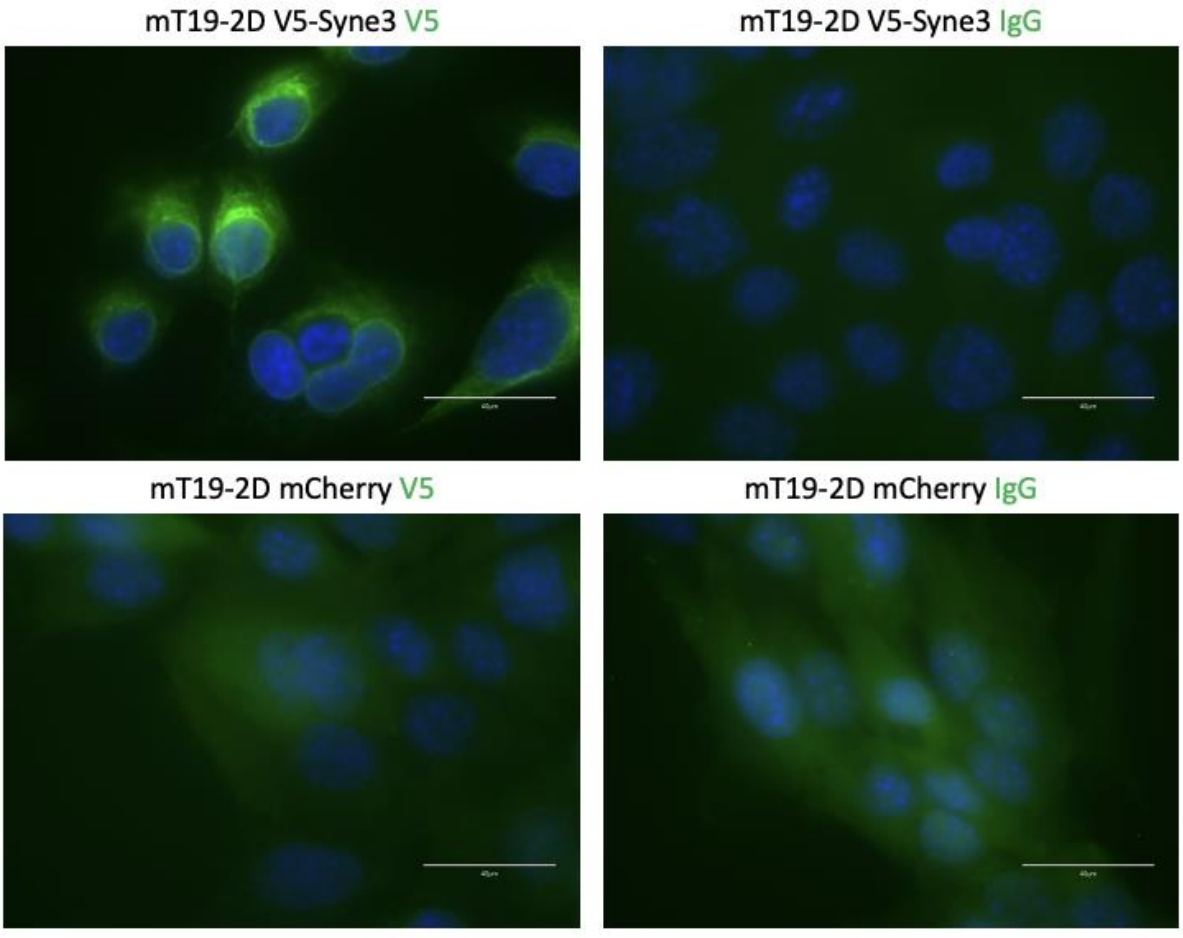

**Figure 45.** Immunofluorescence staining of anti-V5 in mT19-2D cells that lentivirally introduced with V5-tagged Nesprin-3 or mCherry control. Nesprin-3 was localized at the nuclear membrane. Scale bar: 40 μm.

While Nesprin-3 did not change cell proliferation (Figure 46), survival (Figure 47), or anchorage-independent growth (Figure 48), we found that Nesprin-3 overexpression increased cell migration (Figure 49) and invasion (Figure 50), indicating that Nesprin-3 is sufficient to promote PDA aggressive characteristics in vitro.

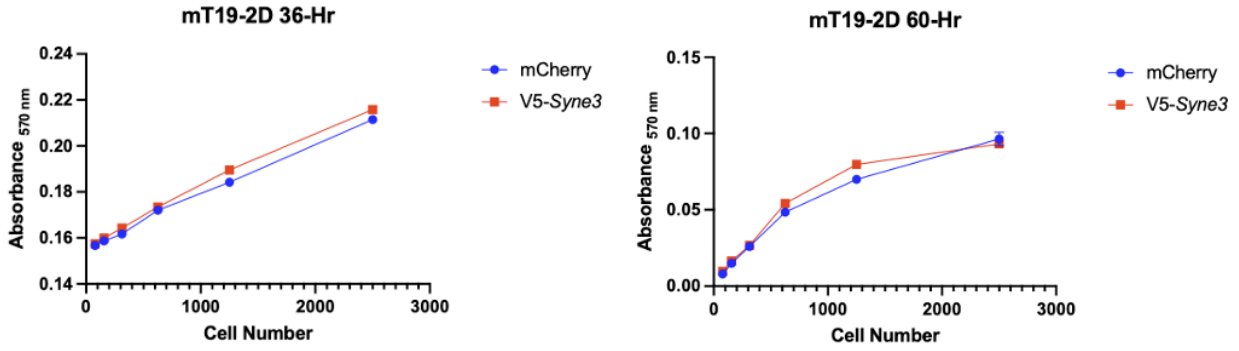


**Figure 46.** mT19-2D cells with *V5-Syne3* cDNA were subjected to cell proliferation assay compared to the mCherry vector control. Cell proliferation rate was determined by cell viability assay using Alamar blue, and absorbance was measured at 36- and 60-hours post-seeding. n=6 per cell number, mean ± SD.

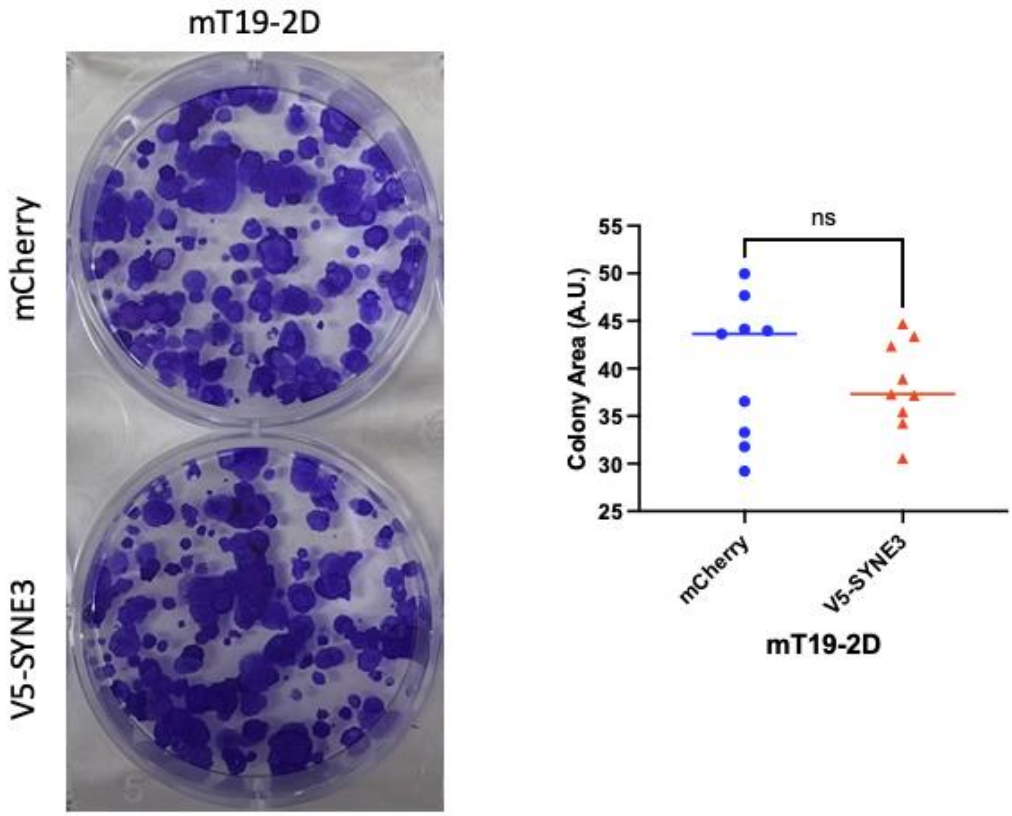


**Figure 47.** mT19-2D mCherry and *SYNE3*-overexpression cells were subject to colony formation assay for 14 days, and the colonies were stained by crystal violet (right) and quantified (left) by percentage growth area. n=9, mean ± SD.

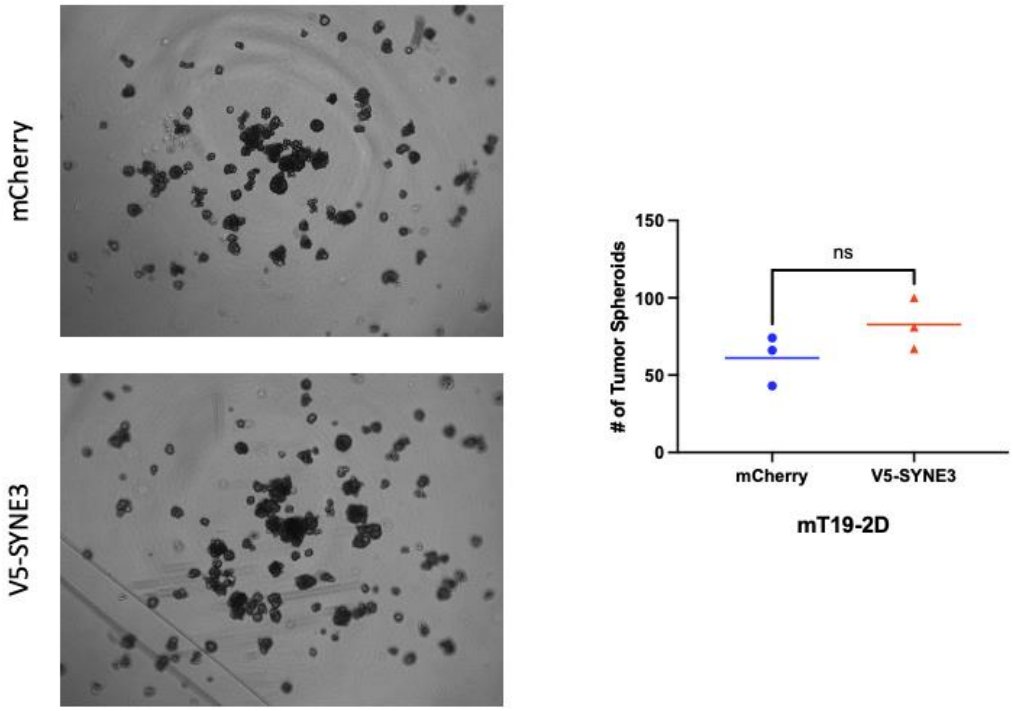


**Figure 48.** mT19-2D mCherry and *SYNE3*-overexpression cells were subject for anchorage-independent tumor spheroid formation assay for 14 days, and the numbers of spheroids were monitored (right) and quantified (left). n=3, mean ± SD.

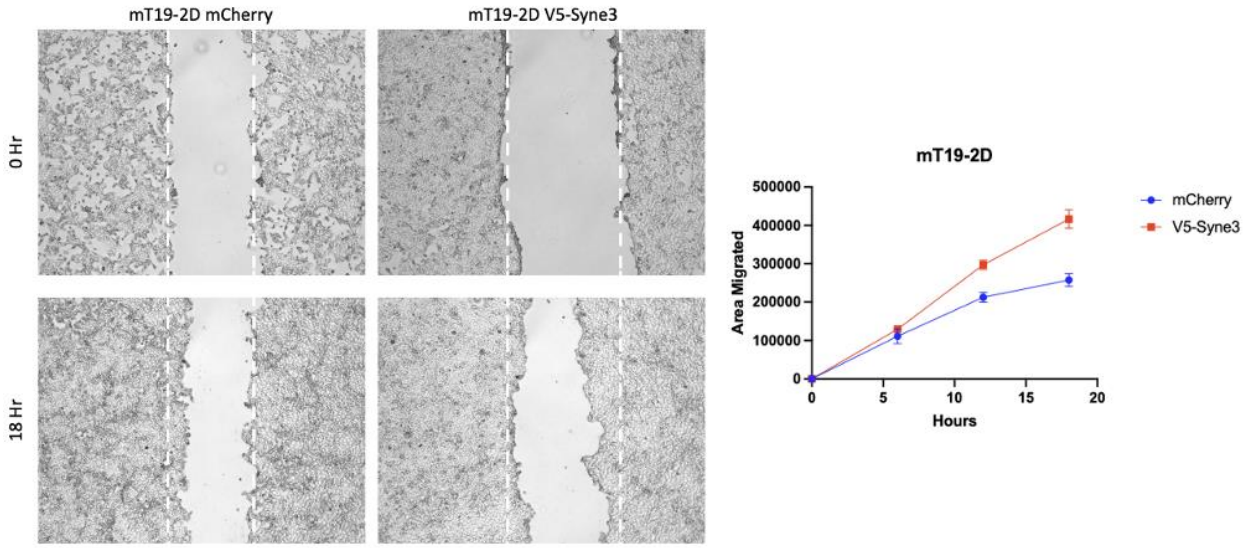

**Figure 49.** mT19-2D mCherry and *SYNE3*-overexpression cells were subjected to wound-healing assay, and the percentage of wound closure was monitored (right) and quantified (left) at 0-, 6-, 12-, and 18-hour post-scratching. n=3, mean ± SD.

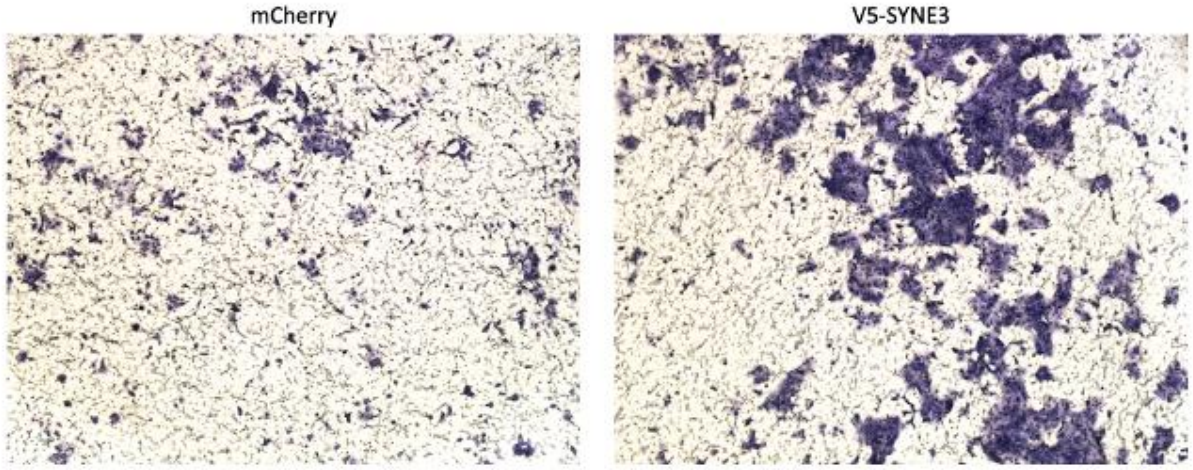


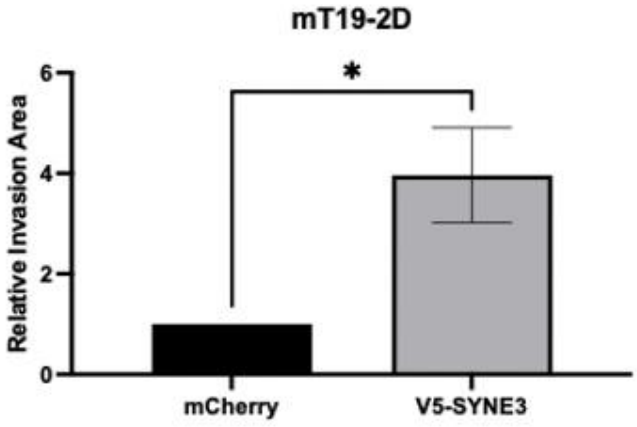


**Figure 50.** mT19-2D mCherry and *SYNE3*-overexpression cells were subjected to Boyden-chamber Matrigel invasion assay for 36 hours, and the cells migrating across the transwell were fixed with methanol, stained by Giemza (top), and quantified per 4x image field (bottom). n=3, mean ± SD. * $p < 0.01$, student t-test.

Since Nesprin-3 expression contributed to the aggressive natures of PDA cells, we reasoned that a SYNE3-targeting strategy might be therapeutically relevant. To investigate the effects of Nesprin-3 depletion in metastatic pancreatic cancer, we lentivirally introduced shRNAs against *Syne3* either targeting coding sequence (CDS) or 3'-untranslated regions (3' UTR) into the mM6-2D cell line (Figure 51).

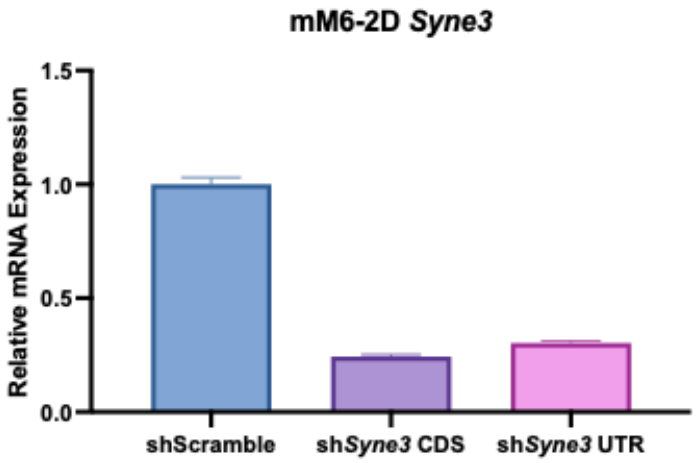


**Figure 51.** Relative *Syne3* mRNA expressions determined by RT-qPCR in mM6-2D cells with shRNA targeting *Syne3* mRNA coding region (sh*Syne3* CDS) and *Syne3* mRNA 3' untranslated region (sh*Syne3* 3'UTR) compared to the scramble shRNA (shScr) control cells. n=3, mean ± SD.

We then subjected the cells to cell proliferation, migration, invasion, and anchorage-independent growth assays. While Nesprin-3 knockdown did not change cell proliferation (Figure 52) or survival (Figure 53), we found that it impaired anchorage-independent growth (Figure 54), cell migration (Figure 55), and invasion (Figure 56), indicating that Nesprin-3 is necessary for PDA transformation, migration, and invasion in vitro.

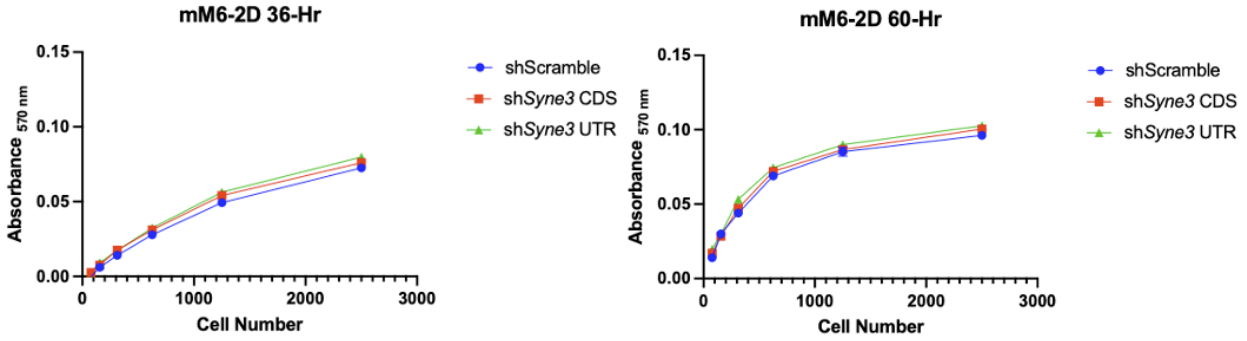


**Figure 52.** mM6-2D cells with shScr, shSyne3 CDS, and shSyne3 UTR were subjected to cell proliferation assay compared to the mCherry vector control. Cell proliferation rate was determined by cell viability assay using Alamar blue, and absorbance was measured at 36- and 60-hours post-seeding. n=6 per cell number, mean ± SD.

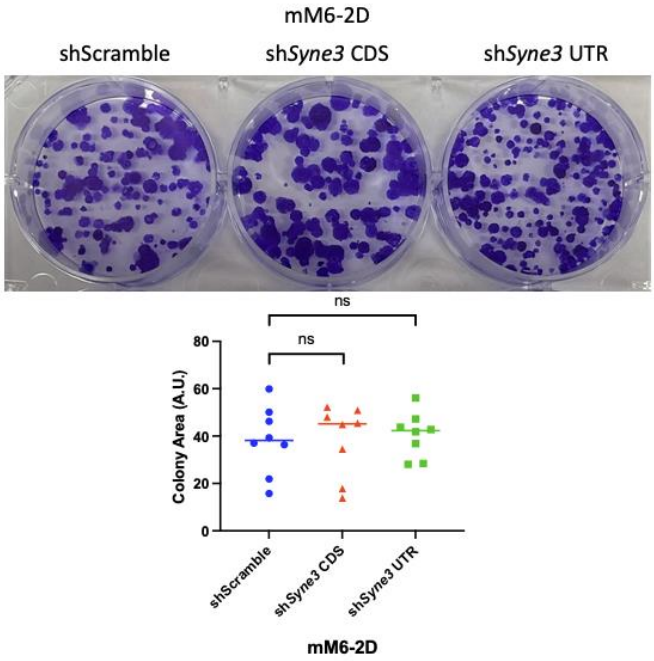


**Figure 53.** mM6-2D cells with shScr, shSyne3 CDS, and shSyne3 UTR were subject to colony formation assay for 14 days, and the colonies were stained by crystal violet (top) and quantified (down) by percentage growth area. n=9, mean ± SD.

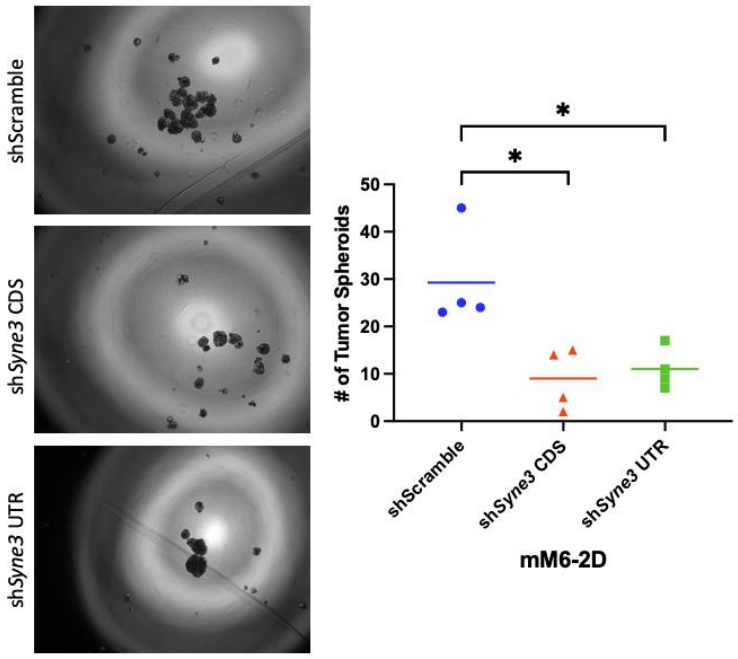


**Figure 54.** mM6-2D cells with shScr, shSyne3 CDS, and shSyne3 UTR were subject for anchorage-independent tumor spheroid formation assay for 14 days, and the numbers of spheroids were monitored (right) and quantified (left). n=3, mean ± SD. * $p < 0.01$, student t-test.

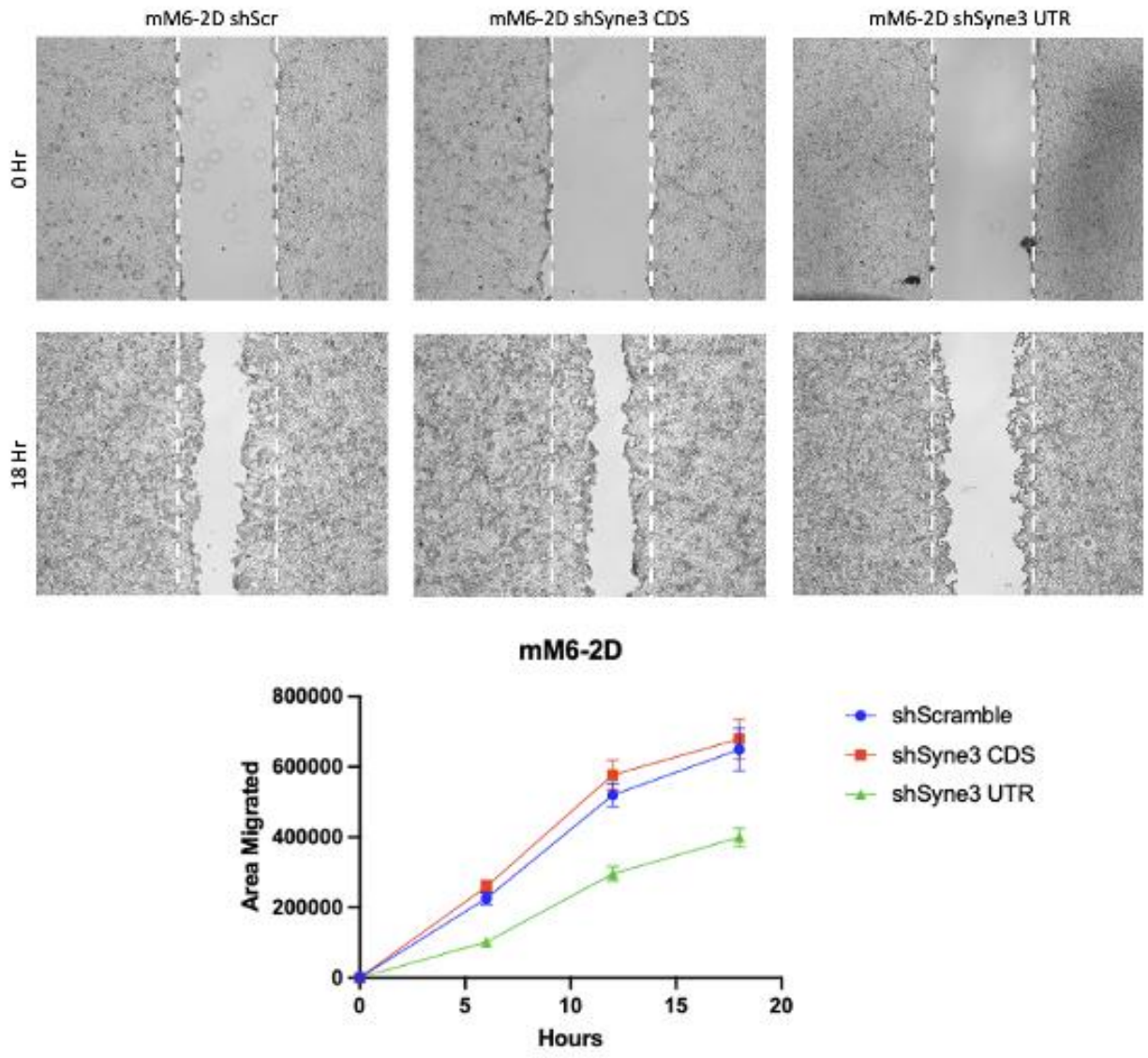


**Figure 55.** mM6-2D cells with shScr, shSyne3 CDS, and shSyne3 UTR were subjected to wound-healing assay, and the percentage of wound closure was monitored (right) and quantified (left) at 0-, 6-, 12-, and 18-hour post-scratching. n=3, mean ± SD.

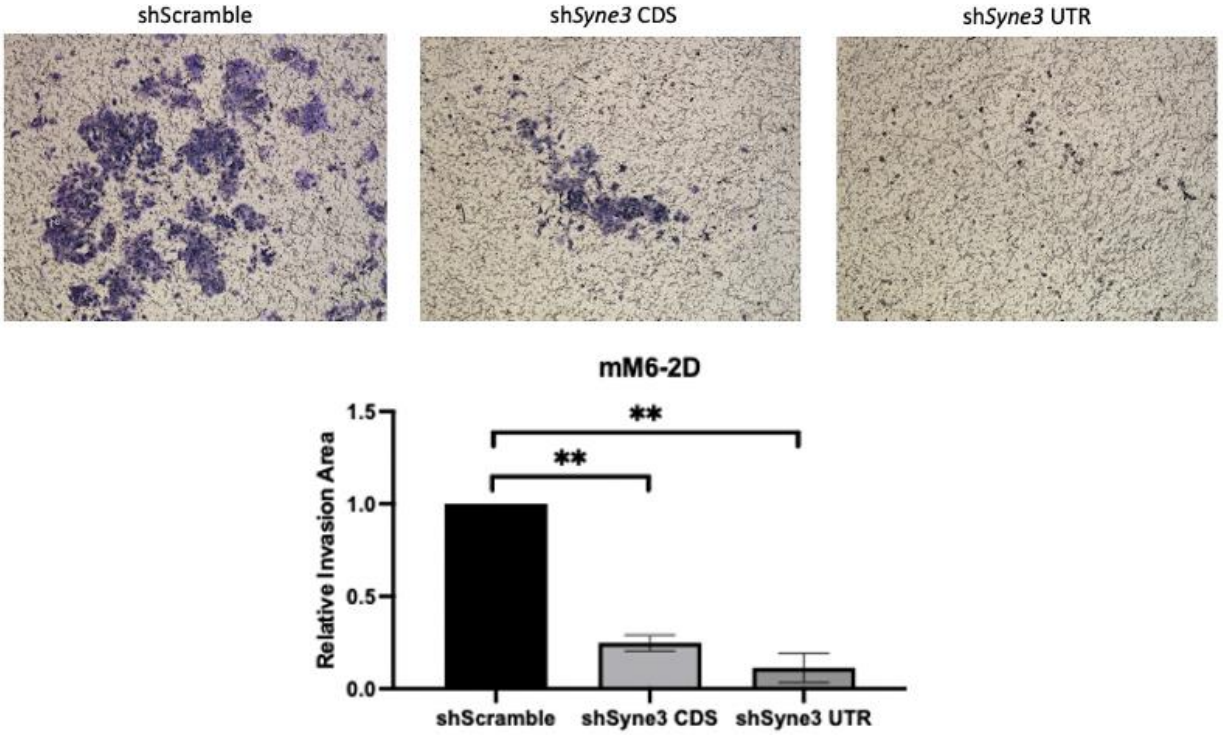


**Figure 56.** mM6-2D cells with shScr, shSyne3 CDS, and shSyne3 UTR were subjected to Boyden-chamber Matrigel invasion assay for 36 hours, and the cells migrating across the transwell were fixed with methanol, stained by Giemza (top), and quantified per 4x image field (bottom). n=3, mean ± SD. $^{**}p < 0.001$, student t-test.

Finally, to determine if Nesprin-3 regulates the nucleoplasmic macromolecular crowing, we ectopically introduced nucGEM into mM6-2D cells expressing shScr, shSyne3 CDS, and shSyne3 UTR constructs and tracked the nucGEM particle motion. The depletion of nesprin-3 from mM6-derived 2D cells decreased the level of nucleoplasmic macromolecular crowding observed in the scramble control (Figure 57), suggesting Nesprin-3 could regulate nucleoplasmic particle diffusion at the mesoscale.

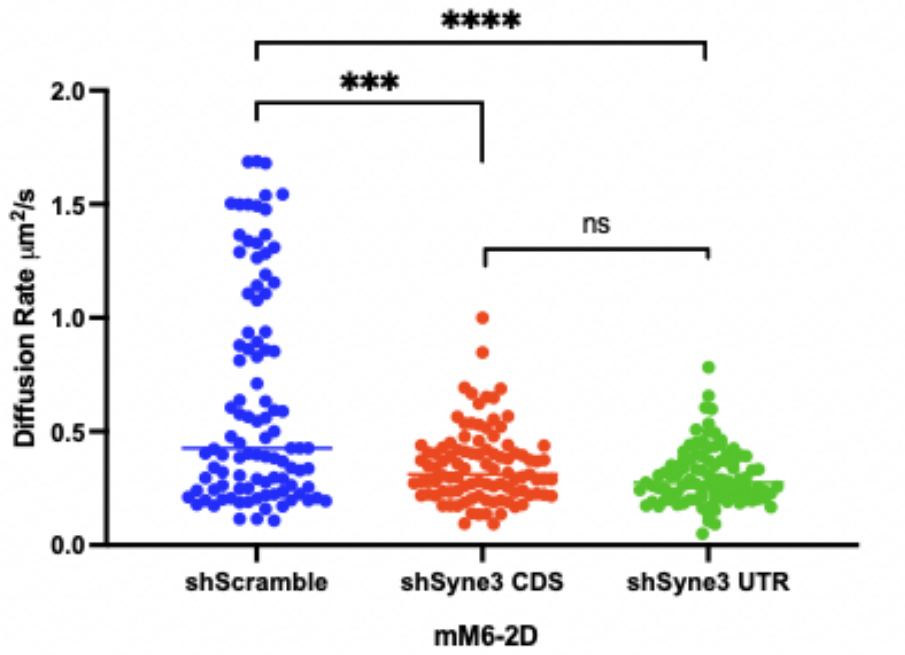


**Figure 57.** Nucleoplasmic macromolecular crowding in mM6-2D cells expressing scramble shRNA, shSyne3 CDS, and shSyne3 UTR. Each data point represents the average effective diffusion of nucGEMs in a single nucleus from the indicated organoids. N = 99 for each cell line. *** $p < 0.001$, **** $p < 0.0001$, one-way ANOVA.

## Discussion

The alteration of nucleoplasmic macromolecular crowding during PDA progression remains an unexplored area of research. Previous studies have shown that highly invasive cells exhibit distinct physical properties, such as increased cell deformability and traction forces, compared with less invasive cancer cells[5]. Our preliminary data from paired mT and mM organoids indicate that mM organoids exhibit higher nucGEMs effective diffusion compared to mT organoids. Furthermore, we observed that Nesprin-3/SYNE3 is a key regulator of metastatic PDA cell nucleoplasmic macromolecular crowding, anchorage-independent cell growth, cell migration, and invasion. Overall, these results provided novel insights into how physical properties of the nucleus are tightly associated with molecular and cellular processes in metastatic PDA cells, which could potentially lead to the identification of new targets for metastatic pancreatic cancer.

Macromolecular crowding is implicated in various biological and cellular processes, including chromatin compaction, epigenetic regulation, and gene expression regulation[6]. Nuclei, constituting 20-40% of the cellular volume, are densely packed with biological macromolecules such as proteins and nucleic acids[7]. A balanced concentration of these crowding agents energetically favors intermolecular interactions, thereby accelerating reaction rates. Alterations in macromolecular crowding can significantly impact biological functions within nuclei, including RNA synthesis[8], chromatin interaction and compaction[9], and the transcription rate of certain genes[7]. Consequently, macromolecular crowding

impacts cell differentiation[10] and nuclear volume[11], a hallmark of cancer. The specific mechanisms of how macromolecular crowding impacts chromatin organization, transcriptional regulations, and subsequent metastasis remain elusive. In a simulation model and an artificial cellular nanosystem, increased nucleoplasmic macromolecular crowding, to a certain degree, can promote transcriptional bursting by limiting macromolecular crowding and decreasing the kinetics between transcription factor and promoter interactions[35,36]. At the nuclear architecture level, an interesting model was proposed in which nuclear crowding promotes chromatin fiber to form 10-nm fiber instead of 30-nm fiber[37]. Nevertheless, the relationship between nuclear crowding and epigenetic regulations could be further assessed by altering the concentration of the crowding agents inside the nuclei and analyzing heterochromatin/euchromatin, chromosomal A/B compartments, and transcriptional profiling using ATAC-sequencing, chromosome conformation capture experiments, and RNA-sequencing analysis; furthermore, the metastatic phenotype can be assessed upon perturbing the nuclear macromolecular crowding to establish the relationship between nuclear crowding and cancer metastasis.

In this study, we compared the nuclear macromolecular crowding between organoids and organoid-derived 2D cell lines. We found a significant increase in nuclear diffusion in 2D cells with a wide range of diffusion rates. Furthermore, when the 2D cells reformed into organoids, the nuclear diffusion remained constant, indicating the alteration of the diffusion was due to cell-intrinsic properties. Indeed, the 2D cell lines and the parental 3D organoid displayed distinct molecular and in vivo phenotypic differences. It was found that comparing

orthotopic transplantations of PDA 3D organoid vs. 2D cell lines, the organoids transplantation led to the formation of desmoplasia, resembling the autochthonous KPC pancreatic cancer mouse model[15]. In contrast, 2D cell transplants lacked desmoplasia[38], suggesting that 3D organoid and 2D cell lines have distinct cellular phenotypes. At the molecular level, it was found that KPC metastasis organoid and organoid-derived tumor and metastasis 2D cell lines exhibit *Trp53* loss of heterozygosity and aneuploidy[15,39], while the tumor organoid did not exhibit Trp53 loss of heterozygosity and aneuploidy[15]. Furthermore, when the pancreatic normal, PanIN, tumor, and metastasis were transplanted into the mouse pancreas, they formed the normal ductal structure, preinvasive PanIN, and tumor, respectively, while the metastasis transplant rapidly formed invasive PDA within one month[15]. These observations indicated that the organoid model preserved the biological characteristics of PDA tumors in vitro compared to in vivo and that the adaptation of a 2D plastic petri dish is a selective process that only isolates a subset of PDA cells. Therefore, the nuclear diffusion rates must also be determined in the organoids with SYNE3 overexpression or knockdown to recapitulate the in vivo biological characteristics.

From RNA-seq analysis, we identified the overexpression of vimentin and plectin in metastatic PDA organoids. It is known that Plectin-1, a cytoskeletal crosslinker protein, is a biomarker for pancreatic cancer[40]. Interestingly, Nesprin-3 interacts with plectin, which anchors intermediate filament vimentin[41,34]. Furthermore, a Plectin-1-based chimeric antigen receptor (CAR) T-cell has been developed to improve the pancreatic cancer therapeutic regimen[42]. However, the functional significance of Plectin-1 in PDA has never

been discovered. Given the observation of impaired cell migration and invasion upon SYNE3 knockdown, it is reasonable to hypothesize that the nucleus, the nuclear positioning, and the physical connections of the nucleus to the cytoskeleton are important for cell migration, invasion, and cancer progression. Therefore, further mechanistic experiments should be conducted to elucidate the significance of the Syne3-Plec-Vim axis during PDA progression and metastasis to develop a more robust therapeutic regimen. Furthermore, several other LINC genes were also dysregulated in PDA metastasis, including *Tor1a/1b* and *Sun1/2*. Therefore, it would be beneficial also to investigate the role of these proteins on nucleoplasmic macromolecular crowding and PDA metastasis.

The mechanical properties of the cancer cells, such as softness vs. stiffness and deformability, represent an important characteristic of their ability to adapt and survive throughout the metastasis cascade[43–45]. Furthermore, it was demonstrated that intracellular viscosity can be used to distinguish the efficiency of metastatic cancer cells in extravasating into the blood vessel[46]. Interestingly, it has been shown that different composition of lamin isoforms interacts with LINC complexes distinctively to modulate cytoplasmic stiffness[47]. For example, loss of lamin A can lead to an increase in the nuclear volume[47]. In our RNA-seq data, we found lamin A expression was significantly upregulated, and lamin B expression was significantly downregulated in the metastatic PDA organoid. Therefore, it's possible that lamin-LINC interaction is an important factor in regulating PDA metastasis. Cell volume, density, and viscosity can also regulate macromolecular diffusion[6,14,48]. Moreover, it was theorized that increasing nuclear volume while remaining constant in macromolecule

concentrations would reduce nuclear stiffness and promote cellular invasion through tight junctions[49]. Therefore, to conclude that PDA metastasis nuclei are less crowded and that SYNE3 regulates nuclear macromolecular crowding, one must measure the size and volume of the nuclei from PDA tumor, metastasis, and cells upon SYNE3 overexpression or knockdown.

Several experiments and questions must be addressed in order to make definitive conclusions about the regulatory roles of Nesprin-3 and nucleoplasmic macromolecular crowding in PDA metastasis. First, we must conduct in vitro functional genetic perturbation experiments using biological replications to ensure scientific reproducibility, including using mT3-2D and mM10-2D for SYNE3 overexpression experiments and mM1-2D and mM10-2D for SYNE3 knockdown experiments. In addition, rescue experiments in sh*Syne3* 3'UTR by overexpressing SYNE3 should be performed to ensure the target specificity of the shRNAs. Furthermore, nucGEM should be ectopically expressed in these biological replications and rescue experiments. In particular, since *Syne3* knockdown resulted in a decreased effective diffusion rate, one would expect an increase in nucleoplasmic diffusion upon SYNE3 overexpression in the sh*Syne3* 3'UTR cell lines to properly establish the correlative relations between SYNE3 and nucleoplasmic macromolecular crowding.

From a cancer biology perspective, SYNE3 expressions during PDA tumor progression in vivo and patient relevance must be established. For example, orthotopic transplantation of murine metastatic PDA cell lines/organoids with SYNE3 knockdown or knockout (loss-of-

function) and murine tumor PDA cell lines/organoids with SYNE3 overexpression (gain-of-function) should be performed to demonstrate the in vivo relevance of SYNE3 during PDA progression and metastasis. In addition, SYNE3 expressions should be assessed using PDA patient samples, such as performing immunohistochemistry staining of SYNE3 in PDA tissue microarray containing both tumor and metastasis samples or performing RNA-seq analysis probing SYNE3 expressions, and patient survival should be stratified based on SYNE3 expression levels. Furthermore, nucGEM should be introduced to human normal, tumor, and/or metastasis PDA organoids to recapitulate the findings from the murine organoid models. These experiments would be sufficient to establish the in vivo and human relevance of SYNE3 in PDA progression. From the molecular crowding perspective, perturbation of the nuclear diffusion rate and assessment of cancer aggressiveness should be conducted. For example, performing a titration of nucGEM lentivirus experiment to alter the nuclear density followed by in vitro functional assays would lead to a robust conclusion as to whether macromolecular crowding inside the nuclei regulates PDA progression and metastasis. Furthermore, determining the nucleoplasmic macromolecular crowding using murine normal and PanIN organoids would provide a comprehensive relationship of molecular crowding during pancreatic carcinogenesis and disease progression.

**Reference**

1. Siegel, R. L., Giaquinto, A. N. & Jemal, A. Cancer statistics, 2024. *CA. Cancer J. Clin.* **74**, 12–49 (2024).

2. SEER*Explorer Application. https://seer.cancer.gov/statistics-network/explorer/application.html?site=40&data_type=1&graph_type=2&compareBy=sex&chk_sex_3=3&chk_sex_2=2&rate_type=2&race=1&age_range=1&stage=101&advopt_precision=1&advopt_show_ci=on&hdn_view=0&advopt_show_apc=on&advopt_display=2#resultsRegion0.

3. Maitra, A. & Hruban, R. H. Pancreatic Cancer. *Annu. Rev. Pathol. Mech. Dis.* **3**, 157–188 (2008).

4. Yachida, S. *et al.* Distant metastasis occurs late during the genetic evolution of pancreatic cancer. *Nature* **467**, 1114–1117 (2010).

5. Denais, C. & Lammerding, J. Nuclear Mechanics in Cancer. in *Cancer Biology and the Nuclear Envelope: Recent Advances May Elucidate Past Paradoxes* (eds. Schirmer, E. C. & de las Heras, J. I.) 435–470 (Springer, New York, NY, 2014). doi:10.1007/978-1-4899-8032-8_20.

6. Zhou, H.-X., Rivas, G. & Minton, A. P. Macromolecular Crowding and Confinement: Biochemical, Biophysical, and Potential Physiological Consequences. *Annu. Rev. Biophys.* **37**, 375–397 (2008).

7. Shim, A. R. *et al.* Dynamic Crowding Regulates Transcription. *Biophys. J.* **118**, 2117–2129 (2020).

8. Pederson, T. & Robbins, E. RNA SYNTHESIS IN HELA CELLS : Pattern in Hypertonic Medium and Its Similarity to Synthesis during G2-Prophase. *J. Cell Biol.* **47**, 734–744 (1970).

9. Bancaud, A. *et al.* Molecular crowding affects diffusion and binding of nuclear proteins in heterochromatin and reveals the fractal organization of chromatin. *EMBO J.* **28**, 3785–3798 (2009).

10. Cell volume change through water efflux impacts cell stiffness and stem cell fate | PNAS. https://www.pnas.org/doi/10.1073/pnas.1705179114?url_ver=Z39.88-2003&rfr_id=ori%3Arid%3Acrossref.org&rfr_dat=cr_pub++0pubmed.

11. Jevtić, P., Edens, L. J., Vuković, L. D. & Levy, D. L. Sizing and shaping the nucleus: mechanisms and significance. *Curr. Opin. Cell Biol.* **28**, 16–27 (2014).

12. Grabocka, E. & Bar-Sagi, D. Mutant KRAS Enhances Tumor Cell Fitness by Upregulating Stress Granules. *Cell* **167**, 1803-1813.e12 (2016).

13. Szórádi, T. *et al.* nucGEMs probe the biophysical properties of the nucleoplasm. 2021.11.18.469159 Preprint at https://doi.org/10.1101/2021.11.18.469159 (2021).

14. Delarue, M. *et al.* mTORC1 Controls Phase Separation and the Biophysical Properties of the Cytoplasm by Tuning Crowding. *Cell* **174**, 338-349.e20 (2018).

15. Boj, S. F. *et al.* Organoid Models of Human and Mouse Ductal Pancreatic Cancer. *Cell* **160**, 324–338 (2015).

16. Poulet, A. *et al.* The LINC complex contributes to heterochromatin organisation and transcriptional gene silencing in plants. *J. Cell Sci.* **130**, 590–601 (2017).

17. Bouzid, T. *et al.* The LINC complex, mechanotransduction, and mesenchymal stem cell function and fate. *J. Biol. Eng.* **13**, 68 (2019).

18. Lombardi, M. L. & Lammerding, J. Keeping the LINC: the importance of nucleo-cytoskeletal coupling in intracellular force transmission and cellular function. *Biochem. Soc. Trans.* **39**, 1729–1734 (2011).

19. Luxton, G. W. G., Gomes, E. R., Folker, E. S., Vintinner, E. & Gundersen, G. G. Linear Arrays of Nuclear Envelope Proteins Harness Retrograde Actin Flow for Nuclear Movement. *Science* **329**, 956–959 (2010).

20. Stewart-Hutchinson, P. J., Hale, C. M., Wirtz, D. & Hodzic, D. Structural requirements for the assembly of LINC complexes and their function in cellular mechanical stiffness. *Exp. Cell Res.* **314**, 1892–1905 (2008).

21. Ermis, M. *et al.* Chapter 15 - Hydrogels as a New Platform to Recapitulate the Tumor Microenvironment. in *Handbook of Nanomaterials for Cancer Theranostics* (ed. Conde, J.) 463–494 (Elsevier, 2018). doi:10.1016/B978-0-12-813339-2.00015-3.

22. Xu, J. *et al.* Engrailed-1 Promotes Pancreatic Cancer Metastasis. 2023.04.10.536259 Preprint at https://doi.org/10.1101/2023.04.10.536259 (2023).

23. Guzmán, C., Bagga, M., Kaur, A., Westermarck, J. & Abankwa, D. ColonyArea: An ImageJ Plugin to Automatically Quantify Colony Formation in Clonogenic Assays. *PLoS ONE* **9**, e92444 (2014).

24. High-Throughput Method for Automated Colony and Cell Counting by Digital Image Analysis Based on Edge Detection | PLOS ONE. https://journals.plos.org/plosone/article?id=10.1371/journal.pone.0148469.

25. Suarez-Arnedo, A. *et al.* An image J plugin for the high throughput image analysis of in vitro scratch wound healing assays. *PLoS ONE* **15**, e0232565 (2020).

26. Lee, E. *et al.* A new vulnerability to BET inhibition due to enhanced autophagy in BRCA2 deficient pancreatic cancer. *Cell Death Dis.* **14**, 1–11 (2023).

27. Oni, T. E. *et al.* SOAT1 promotes mevalonate pathway dependency in pancreatic cancer. *J. Exp. Med.* **217**, e20192389 (2020).

28. Kim, D., Paggi, J. M., Park, C., Bennett, C. & Salzberg, S. L. Graph-based genome alignment and genotyping with HISAT2 and HISAT-genotype. *Nat. Biotechnol.* **37**, 907–915 (2019).

29. featureCounts: an efficient general purpose program for assigning sequence reads to genomic features | Bioinformatics | Oxford Academic. https://academic.oup.com/bioinformatics/article/30/7/923/232889.

30. Moderated estimation of fold change and dispersion for RNA-seq data with DESeq2 | Genome Biology | Full Text. https://genomebiology.biomedcentral.com/articles/10.1186/s13059-014-0550-8.

31. Ge, H., Tian, M., Pei, Q., Tan, F. & Pei, H. Extracellular Matrix Stiffness: New Areas Affecting Cell Metabolism. *Front. Oncol.* **11**, 631991 (2021).

32. Deville, S. S. & Cordes, N. The Extracellular, Cellular, and Nuclear Stiffness, a Trinity in the Cancer Resistome—A Review. *Front. Oncol.* **9**, (2019).

33. Wilhelmsen, K. *et al.* Nesprin-3, a novel outer nuclear membrane protein, associates with the cytoskeletal linker protein plectin. *J. Cell Biol.* **171**, 799–810 (2005).

34. Petrie, R. J., Koo, H. & Yamada, K. M. Generation of compartmentalized pressure by a nuclear piston governs cell motility in a 3D matrix. *Science* **345**, 1062–1065 (2014).

35. Tan, C., Saurabh, S., Bruchez, M. P., Schwartz, R. & LeDuc, P. Molecular crowding shapes gene expression in synthetic cellular nanosystems. *Nat. Nanotechnol.* **8**, 602–608 (2013).

36. Golkaram, M., Hellander, S., Drawert, B. & Petzold, L. R. Macromolecular Crowding Regulates the Gene Expression Profile by Limiting Diffusion. *PLoS Comput. Biol.* **12**, e1005122 (2016).

37. Maeshima, K. *et al.* Nucleosomal arrays self-assemble into supramolecular globular structures lacking 30-nm fibers. *EMBO J.* **35**, 1115–1132 (2016).

38. Inhibition of Hedgehog signaling enhances delivery of chemotherapy in a mouse model of pancreatic cancer - PubMed. https://pubmed.ncbi.nlm.nih.gov/19460966/.

39. Hingorani, S. R. *et al.* Trp53R172H and KrasG12D cooperate to promote chromosomal instability and widely metastatic pancreatic ductal adenocarcinoma in mice. *Cancer Cell* **7**, 469–483 (2005).

40. Bausch, D. *et al.* Plectin-1 as a Novel Biomarker for Pancreatic Cancer. *Clin. Cancer Res.* **17**, 302–309 (2011).

41. Postel, R., Ketema, M., Kuikman, I., de Pereda, J. M. & Sonnenberg, A. Nesprin-3 augments peripheral nuclear localization of intermediate filaments in zebrafish. *J. Cell Sci.* **124**, 755–764 (2011).

42. Garcia-Robledo, J. E. *et al.* Novel Peptide-Based Plectin-1 CAR T-Cells Target Specifically Pancreatic Cancer Cells. *Blood* **142**, 6846 (2023).

43. Moose, D. L. *et al.* Cancer Cells Resist Mechanical Destruction in Circulation via RhoA/Actomyosin-Dependent Mechano-Adaptation. *Cell Rep.* **30**, 3864-3874.e6 (2020).

44. Oncogenic Signaling Alters Cell Shape and Mechanics to Facilitate Cell Division under Confinement: Developmental Cell. https://www.cell.com/developmental-cell/fulltext/S1534-5807(20)30005-8?_returnURL=https%3A%2F%2Flinkinghub.elsevier.com%2Fretrieve%2Fpii%2FS1534580720300058%3Fshowall%3Dtrue.

45. Gensbittel, V. *et al.* Mechanical Adaptability of Tumor Cells in Metastasis. *Dev. Cell* **56**, 164–179 (2021).

46. Gensbittel, V. *et al.* Cell viscosity influences hematogenous dissemination and metastatic extravasation of tumor cells. 2024.03.28.587171 Preprint at https://doi.org/10.1101/2024.03.28.587171 (2024).

47. Vahabikashi, A. *et al.* Nuclear lamin isoforms differentially contribute to LINC complex-dependent nucleocytoskeletal coupling and whole-cell mechanics. *Proc. Natl. Acad. Sci.* **119**, e2121816119 (2022).

48. Molines, A. T. *et al.* Physical properties of the cytoplasm modulate the rates of microtubule polymerization and depolymerization. *Dev. Cell* **57**, 466-479.e6 (2022).

49. Schirmer, E. C., Latonen, L. & Tollis, S. Nuclear size rectification: A potential new therapeutic approach to reduce metastasis in cancer. *Front. Cell Dev. Biol.* **10**, 1022723 (2022).

## Chapter Four—Organoid Technology and Pancreatic Cancer Research

### Summary

Given pancreatic cancer (PDA) organoids were used as the primary research model in Chapters Two and Three of the dissertation, it is imperative to provide a comprehensive overview of the current understanding of these organoids. Pancreatic epithelium organoid culture has revolutionized PDA research by faithfully recapitulating disease progression and therapeutic responses. Established through innovative techniques, these models preserve key physiological features and enable molecular characterization, unveiling transcriptional and epigenetic dynamics underlying PDA pathogenesis. Moreover, patient-derived organoids offer predictive biomarker identification and drug sensitivity testing, guiding precision medicine strategies. In addition, co-culture models reveal tumor microenvironment interactions, elucidating immune responses and therapeutic resistance mechanisms. Therefore, organoid culture represents a promising avenue for personalized PDA treatment development and warrants continued exploration for improved patient outcomes.

**History of Pancreatic Organoid Culture Development**

In 2015, the Tuveson and the Clevers laboratories reported an in vitro 3D tissue culturing method termed pancreatic organoid to model murine and human PDA progression and metastasis[1], which is widely adopted within the pancreatic cancer research community. A pancreatic organoid is defined by a group of adult pancreatic epithelial cells including progenitors organized into a 3D spheroid that can be expanded long-term ex vivo with defined cellular organizations, including basal-apical polarity and lumen formation[2]. Unlike the traditional 2D cell line or xenograft transplantation models, pancreatic organoids derived from a small quantity of both murine and human tissues accurately recapitulate the physiologically relevant characteristics of PDA progression in vitro, can be generated more efficiently in a relatively short time frame, and allow the PDA stage-specific comparisons at the genetic, epigenetic transcriptomic, and proteomic profiling[1,3,4], facilitating the discovery of novel biomarkers and therapeutic strategies. During the development of the pancreatic organoid culture, various culturing techniques, matrix composition, and media formulation were tested for the growth, expansion, and biological characteristics of the organoids.

The journey to developing effective pancreatic organoid culture began with the pioneering work of the Ruby lab in 1980, which marked the genesis of pancreatic 3D culture by achieving successful ex vivo culturing of the ductal epithelium from rat pancreas[5]. In 2012, the Bar-Sagi lab introduced a method enabling the passaging and expansion of murine primary ductal epithelial cells into spheroids[6]. This technique involved microdissection of murine

pancreatic ducts, enzymatic dissociation of the ducts into single cells or small clusters, and plating in an 80% Matrigel matrix, which formed spheroids within 48 hours[6]. However, these approaches were limited for research utilities in its capacity for cell expansion.

The Ku and Riggs laboratories introduced a method employing 1% methylcellulose and 5% Matrigel mix, facilitating the formation of "Ring" colonies characterized by hollow spheres with ductal epithelial identity[7]. Notably, this culture system selectively supported the proliferation of ductal cells while excluding cells with endocrine or acinar identities[7]. Furthermore, when the cells were placed into a laminin-based matrix, the cultured cells could differentiate into endocrine/acinar cell identities[7], not only indicating the bi-potency of the ductal epithelial cells but also highlighting the importance of culture conditions in establishing the appropriate research model for scientific inquiries. The Rustgi lab transitioned into growing spheroids not only from adult and embryonic mouse pancreas, but also from the genetically engineered mouse model harboring *Kras*$^{+/LSL\text{-}G12D}$; *Trp53*$^{+/LSL\text{-}R172H}$; *Pdx1-Cre* (KPC) alleles[8]. The lab developed a method utilizing *Dolichos biflorus* agglutinin lectin, a glycoprotein that specifically recognizes pancreatic ducts, to isolate the pancreatic ductal cells selectively[8]. Culturing these cells in type I collagen resulted in forming single-cell-layered spheroids with hollow cores within ten days[8].

The Clevers lab developed the first culturing method classified as organoid by embedding fragmented normal murine pancreatic ducts in a Matrigel matrix supplemented with roof plate-specific spondin 1 (RSPO1), a Wnt agonist[3]. This led to the formation of single-cell-

layered organoids containing adult pancreatic progenitor cells with hollow cores within 24-48 hours, capable of maintaining long-term expansion, passaging, and bi-potency without malignant transformation for over ten months. Intriguingly, upon orthotopic transplantation into the mouse pancreas, these organoids gave rise to ductal structures, indicating the preservation of the biological characteristics inherent to ductal nature within the organoid culture method. Taking a similar methodology, the Kuo lab pioneered an air-liquid interface organoid culture model, embedding minced pancreatic ductal tissues from wild-type or genetically engineered mice with *Kras*$^{+/LSL\text{-}G12D}$; *Trp53*$^{flox/flox}$ alleles in a collagen matrix exposed to both culture media and air[4]. These organoids comprised epithelial, endocrine, and stromal components and demonstrated oncogenic transformation potential in vitro upon the addition of adenovirus expressing Cre recombinase, enabling long-term expansion and passaging of oncogenic transformed organoids in contrast to limited passaging in contrast to the wild type or untransformed pancreatic ductal organoids.

Finally, the Clevers and Tuveson labs further refined Matrigel-embedded organoid culturing models to recapitulate different stages of pancreatic cancer, including normal, pancreatic intraepithelial neoplasia (PanIN), paired primary tumor, and metastases[1]. These refined culturing conditions facilitated the unlimited expansion of normal and PanIN epithelial cells[1], which, although does not fully represent the in vivo characteristics of the ductal epithelium, the organoid technology offered an invaluable platform for studying stepwise pancreatic cancer progression at the molecular and cellular levels.

Pancreatic organoids represent a significant advancement in the study of PDA, offering a more physiologically relevant and efficient model compared to traditional 2D cultures and xenograft models. By enabling detailed genetic and molecular analyses at various stages of disease progression, these organoids provide a powerful platform for identifying novel biomarkers and therapeutic targets. The evolution of 3D culturing techniques, as demonstrated by various pioneering laboratories, has greatly enhanced our ability to study pancreatic cancer, paving the way for more effective and targeted treatments in the future.

**Molecular and Cellular Characteristics of Pancreatic Organoid Culture**

Understanding the differences between 2D and 3D cultures is important for choosing proper preclinical models that align with our research questions. Although 2D cell culture plays a pivotal role in cancer research, it often fails to recapitulate the complexities of in vivo biology, leading to challenges in translating research findings to clinical applications[9]. Such a challenge is largely due to a lack of appropriate cellular organizations in 2D cell cultures, which affects downstream cell signaling and functions[10]. For example, when plating 2D-adapted PANC-1 cells in a methylcellulose-based matrix, it was observed an upregulation in the expression of key markers associated with hypoxia and anaerobic glycolysis, including glucose transporter 1, lactate dehydrogenase, and HIF-1a as the cells forming organoids, indicating hypoxia and aerobic glycolysis[11]. Moreover, analysis of the extracellular matrix showed an increased expression of E-cadherin, collagen I, and fibronectin I, along with chemoresistance-related genes, conferring gemcitabine resistance in vitro[11]. Furthermore, as Chapter Three described, macromolecular crowding inside of the nuclei is significantly increased in the 2D cells compared to the 3D parental organoid, rendering the possibility of cellular organization affect biophysical properties and the subsequent cell signaling and molecular profiling, including transcriptional, metabolomics, and proteomics landscapes.

In pancreatic 3D cultures, multiple studies reported that pancreatic epithelial cells were organized with proper basal-apical polarity and cytoskeletal establishment seen in vivo, evident by the localization of microvilli, transmembrane glycoprotein mucin 1 (MUC1), tight

junctions, and F-actin at the lumen-facing apical surface, and lamina and base membrane collagen localized the basal surface, respectively[5,7,8]. Moreover, organoids derived from PanIN also recapitulated the in vivo histopathology with enlarged pleomorphic nuclei and cribriform formations[4]. Overall, the pancreatic organoid model accurately recapitulates the tissue organization seen in vivo, demonstrating its reliability as a research model for studying pancreatic progression.

Organoid culture conditions, such as matrix compositions and media formulations, can significantly impact molecular and cellular profiling of the organoid, impacting research findings and therapeutic discovery. For instance, switching the Matrigel-based matrix to a laminin-based matrix promotes organoid differentiation from ductal lineage into endocrine/acinar lineages, evidenced by the expression of C-peptide, glucagon, amylase, and insulin[7]. The addition of RSPO1, for example, led to the exponential growth and expansion of the organoid but promoted the identity of the ductal cells to fetal progenitors identity, evidenced by the expression of Pdx1l Nkx6.1 and Ngn3[3]. In addition, growth factors and WNT/R-spondin-rich media conditions may skew the representation of the original tumor or alter the characteristics of the tumors, albeit this applies to every in vitro/ex vivo preclinical model. Despite of these potential shortcomings, pancreatic organoid models have proven valuable for recapitulating disease progression in vivo and patient settings. In the murine pancreatic organoids developed by the Clevers and Tuveson labs, a notable upregulation of Muc5ac, Muc6, and Tff1 was observed in mP organoids, indicative of preserved PanIN lesions[1]. These organoids exhibited the ability to form PanIN lesions

characterized by increased cell proliferation and stroma formation when orthotopically transplanted into the mouse pancreas. Both transplanted mT and mM organoids exhibited stroma formation and resembled autochthonous tumors from the KPC mouse model, in contrast to mT organoids, which required several months of progression to metastasis upon orthotopic transplantation, whereas mM organoids metastasize within one month. This discrepancy in metastatic potential highlights the importance of organoid models in studying cancer metastasis mechanisms. In the patient settings for clinical relevance, distinct morphological and molecular differences were observed in human normal (hN) and tumor (hT) (including human fine needle biopsy samples, hFNA) organoids. hN organoids displayed a cuboidal morphology, while hT organoids displayed a dysplastic tall columnar morphology. Furthermore, hT organoids were highly aneuploid and harbored mutations in KRAS, TP53, SMAD4, and CDKN2A, along with MYC amplification and loss of tumor suppressors TGFBR2 and DCC. Upon orthotopic transplantation into Nu/Nu mice, hN organoids formed normal ducts, while hT organoids rapidly progressed to form PanIN lesions within one month. Subsequently, they developed infiltrative carcinoma with a prominent desmoplastic reaction and distinct RNA signatures, including upregulation of AGR2, ACSM3, GCNT1, GCNT3, UGDH, and nucleoporin family genes, along with downregulation of PTPRD[1]. Pancreatic organoids can also behave differently under different oncogenic insults. For example, the oncogenic transduction of the organoid with $KRAS^{G12V}$ showed cystic organization with apical nuclei positioning and localization of SOX9 within the nuclei; in contrast, the oncogenic transduction of $TP53^{R175H}$ showed atypical organization of the nuclei

with filled lumens and localization of SOX9 in the cytoplasm, a marker for poor prognosis, offering insights into tumor behavior upon different oncogenic insults[12].

Together, pancreatic organoid culture offers a physiologically relevant platform for studying pancreatic cancer biology and exploring potential therapeutic strategies. By recapitulating key molecular and cellular characteristics of the disease, organoid models provide valuable insights into disease mechanisms and offer opportunities for personalized medicine approaches. Continued research in this area promises to enhance our understanding of pancreatic cancer further and improve patient outcomes.

**Organoid Modeling of Transcriptional and Epigenetic Dynamics**

Pancreatic carcinogenesis is mostly driven by gain-of-function mutations of the oncogene KRAS, which cooperate with loss-of-function mutations of tumor suppressor genes such as TP53, CDKN2A, and SMAD4[14]. However, recurrent genetic mutations that further drive cancer aggressiveness and metastatic capabilities remain largely unknown. Since metastatic PDA often maintains a similar mutation landscape to the primary tumor[15], it is essential to comprehend cell-autonomous factors, such as transcription factor (TF)-directed programming and epigenetic alterations, that can drive PDA progression and metastasis in order to develop effective cancer therapeutics. Patient-derived organoid models from tumor and metastasis tissues offer a promising platform that addresses many of these limitations[16]. These three-dimensional cultures maintain the epigenetic and transcriptional status of the original tumors[1,16,17], including basal-like and squamous characteristics, and allow for uniform culture conditions and longitudinal sampling. Unlike 2D cultures, which often lead to highly aggressive and metastatic phenotypes[18], organoids better preserve the heterogeneity and behavior of the original tumor cells[1], providing a more accurate representation of cancer cells. A significant advantage of organoid models is their ability to be derived from fine needle biopsy samples, enabling the expansion of organoids for various experimental approaches, including multi-omics studies[19,20]. This is particularly noteworthy given that most omics experiments with human PDA specimens have been performed on early-stage tumors from surgical resections[21]. Here, we comprehensively

review how PDA organoid models improve our understanding of how epigenetic alterations promote PDA progression and metastasis.

The PDA organoid model has provided unprecedented resolution of aberrant transcriptional regulation, underscoring the pivotal role of TFs in altering the epigenetic landscape to promote PDA progression and metastasis. Notably, Roe and colleagues identified metastasis-associated open chromatin and enhancer networks, revealing the role of TF Forhead Box A1 (FOXA1) in activating a subset of metastasis-associated enhancers and subsequent embryonic foregut endoderm transcriptional program, thereby promoting PDA metastasis[17]. This was elucidated using paired tumor- and metastasis-derived organoids from genetically engineered mouse models (GEMMs) of pancreatic cancer, which provided a robust platform for studying these epigenetic alterations. Similarly, we recently utilized the organoid model to compare PDA tumor and metastasis transcriptomics and epigenetic landscapes to identify the aberrant expressions of TF Engrailed-1 (EN1) in metastatic PDA. We discovered that EN1 deactivates promoter and/or enhancer activities of its target genes to initiate transcription repression, leading to downregulations of ERK1/2 antagonist, cell survival, and PDA metastasis[22].

Tonelli and colleagues discovered that the TF SAM Pointed Domain Containing ETS Transcription Factor (SPDEF) governs the progenitor subtype identity of PDA[23]. SPDEF regulates the mucus production program and supports tumor growth by regulating ER stress sensors AGR2, ERN2, and IRE1 beta for maintaining ER homeostasis[23], providing a

therapeutic avenue for targeting the progenitor subtype of PDA. Within a similar context, Kim and colleagues unveiled metastasis-associated super-enhancers driving the activation of embryonic development TF ecotropic viral integration site 1 (EVI1), leading to EVI1-directed chromatin accessibility alterations and subsequent activation WNT/beta-catenin/TCF signaling cascade to promote PDA malignancy[24]. Yoo and colleagues discovered the TEA domain transcription factor 2 (TEAD2) facilitates the transition of PDA cells to a basal-like subtype, characterized by enhanced angiogenesis and metastatic capability through the activation of endothelial-associated enhancers[25]. Together, these findings collectively illustrate how aberrantly expressed TFs can reprogram the epigenome, resulting in increased aggressiveness and metastatic potential in pancreatic cancer, offering new avenues for therapeutic interventions targeting these epigenetic changes.

Previous studies have delineated two major PDA subtypes: the progenitor subtype and the basal/squamous subtype, with the latter associated with poor clinical prognosis[26–28]. To better dissect cell-autonomous characteristics, such as PDA subtypes, Tiriac and colleagues pioneered a patient-derived organoid (PDO) culturing method using cells isolated from various PDA sources, including primary tumors (hT), metastases (hM), fine-needle biopsies (hF), and normal pancreatic ducts (hN)[16]. Molecular analysis of the organoids revealed that the PDOs not only mirrored the genetic hallmarks of PDA, including mutations in KRAS-related signaling pathways and common tumor suppressors, but also identified progenitor and basal/squamous transcriptomic subtypes that correlated with patient survival outcomes, providing a robust preclinical model for studying PDA

pathogenesis[16]. Moreover, pharmacotyping assessment of chemotherapeutic agents on the PDO showed a remarkable correlation between in vitro drug sensitivity and patient treatment response and survival[16], offering a potential platform for precision medicine.

Basal/squamous subtype of PDA, characterized by hypermethylation and concordant downregulation of genes that govern pancreatic endodermal cell-fate determination, including PDX1, MNX1, GATA6, and HNF1B, leading to a complete loss of endodermal identity[28]. This discovery underscores the critical role of DNA methylation in defining molecular subtypes of PDA and their respective prognoses. Building on these findings, Wang and colleagues compared to mouse and human PDA organoids and discovered that DNA could be differentially methylated based on PDA progression stage and subtypes[29]. Not only the hypermethylated DNA was associated with repressive enhancer/promoter markers, indicating the correlation between DNA methylation and gene expression, but it was discovered that genes associated with the progenitor subtypes were hypermethylated in the basal/squamous subtype samples, including HNF4A and GATA6[29], indicating the significance of epigenetic regulations and subtype maintenance in PDA. These findings reveal the significant impact of DNA methylation on PDA progression and molecular subtype differentiation. The ability to use organoids to study these epigenetic alterations not only enhances our understanding of PDA's molecular underpinnings but also offers the potential for developing diagnostic markers for molecular subtypes.

In conclusion, PDA organoid models have emerged as a transformative tool in pancreatic cancer research, enabling a more nuanced understanding of the disease's molecular and epigenetic alterations. These models offer distinct advantages over traditional preclinical models, preserving the complexity and heterogeneity of the original tumors. The ability to derive organoids from fine needle biopsy samples allows for the longitudinal study of tumor progression and metastasis, including advanced stages of PDA. This capability is crucial for investigating epigenetic alterations, such as DNA methylation and transcription factor-driven enhancer reprogramming, which play pivotal roles in PDA aggressiveness and metastasis. Research utilizing these organoids has highlighted the contributions of key transcription factors like FOXA1, EN1, EVI1, and TEAD2 in driving epigenetic changes that enhance tumor malignancy. Additionally, identifying subtype-specific DNA methylation patterns, particularly in the squamous subtype, underscores the potential of organoids in developing diagnostic markers and targeted therapies. As we continue to leverage the power of organoid technology, we anticipate significant advancements in our fundamental understanding of pancreatic cancer and the development of innovative clinical interventions to improve patient outcomes.

**Organoid Modeling of PDA Microenvironment**

The tumor microenvironment (TME) of PDA contains diverse cell populations, notably cancer-associated fibroblast (CAF), which profoundly influence tumor progression and therapeutic resistance. Desmoplasia, characterized by the deposition of a dense extracellular matrix (ECM) by activated CAFs, represents a prominent histopathological feature of PDA[30] and is a hallmark of PDA, presenting significant challenges in drug delivery[31]. As cancer progresses, CAF exhibits distinct functional phenotypes that can either facilitate or impede tumor growth, depending on contextual cues[32]. Various studies targeting CAFs in murine models, such as stromal depletion via the inhibition of Hedgehog signaling[31] or depletion of ECM component glycosaminoglycan hyaluronan[33], have shown promising results in enhancing chemotherapeutic delivery. However, clinical translation of CAF-targeting strategies has yet to yield significant improvements in PDA patient overall survival or progression-free survival[34,35]. A subsequent mechanistic study showed the inhibition of Hedgehog signaling-induced immunosuppressive TME by promoting CAF subtype differentiation[36], emphasizing the need for improved preclinical tools to decipher PDA stromal biology. In addition, PDA is often characterized as an immune “cold” tumor, largely resistant to immunotherapeutic interventions due to the minimal presence and/or dysfunctional effector immune cells within the tumor mass[37]. Recent development of co-culture models with organoids and various cell types, such as CAFs and immune cells, offer a promising platform and a comprehensive approach for examining and modeling the

dynamic interplay of PDA TME. Additionally, these models are invaluable for therapeutic discovery and testing new strategies to enhance drug delivery to combat PDA.

Tuveson laboratory laid a foundational understanding of the TME in PDA by developing co-culture models combining PDA organoids and pancreatic stellate cells (PSCs), the precursors of CAFs. The co-culture model demonstrated mutual benefits where both organoids and PSCs encouraged each other's growth, producing a dense stroma typical of PDA[38]. In-depth analysis of the co-culture model unveiled two distinct CAF subtypes: myofibroblast (myCAF) and inflammatory CAFs (iCAF)[39]. MyCAFs, marked by alpha-smooth muscle actin expression, localized proximally to cancer cells and secreted ECM organized into collagen fibrils. Conversely, interleukin 6 (IL-6)-positive iCAFs were positioned distantly from the cancer cells and secreted inflammatory cytokines, including IL-6 and IL-11[39]. Subsequent investigations by Biffi and colleagues elucidated the intricate signaling pathways governing CAF activation, revealing the dual role of TGF-beta/SMAD2/3 signaling pathways in myCAF activation and antagonism of IL1/JAK/STAT signaling required iCAF activation[40]. Importantly, these findings were corroborated by tissue staining and in vivo single-cell RNA-seq analysis of the KPC tumor[39,40], underscoring the physiological relevance of the co-culture model utilizing PDA organoids and PSCs. This nuanced understanding of CAF heterogeneity is essential for developing targeted therapies that more effectively address the complex stromal interactions in PDA.

Building on the foundation of CAF heterogeneity and the dynamic TME of PDA, PDO, and CAF co-culturing models have also been established, mirroring subtype differentiation observed in murine systems. These co-culturing conditions induced epithelial-to-mesenchymal transition gene signatures in PDA organoids and confer therapeutic resistance to chemotherapies, including gemcitabine, 5-FU, and paclitaxel[41,42].

In addition to CAF, T lymphocytes are also part of the PDA TME and play a significant role in PDA progression. The exploration of immunotherapy, particularly T-cell-based approaches, holds promise in PDA treatment. Yet, the patient response rates remain variable, providing the need for a deeper understanding of therapeutic resistance mechanisms[43]. D'Angelo and colleagues demonstrated increased T-cell activation, including increased granzyme B production and activation marker CD137, when co-culturing murine PDA organoids with peripheral blood mononuclear cells (PBMCs) isolated from healthy mice[44], highlighting the potential for preclinical modeling of immunotherapy responses. Zhou and colleagues further advanced this approach by incorporating additional TME components, such as endothelial cells, CAFs, and macrophages, into PDA organoid cultures[45]. Co-culturing with antigen-presented T-cells outside the Matrigel scaffold demonstrated T-cell infiltration into the PDA organoid, yielding a T-cell incorporated PDA organoid model that recapitulates the immunosuppressive TME[45]. Drug screening efforts within this model identified BET and HDAC inhibitors, ITF2357 and I-BET151, as potent enhancers of PDA antigen presentation and anti-tumor activity of the cytotoxic T-cells[45], offering a robust platform to discover immunotherapy vulnerability.

Further in-depth analysis by Knoblauch and colleagues revealed alterations in T-cell differentiation under co-culture conditions, characterized by decreased CD4+ memory T-cells and increased CD4+ regulatory T-cells[46], indicative of an immune suppressive environment. In short, the PDA organoid and immune cell co-culture models, particularly those developed by Zhou and colleagues, faithfully recapitulated immune TME in vivo, providing a reliable pre-clinical tool to elucidate underlying immunotherapy resistance mechanisms and develop effective therapeutic strategies, shifting from one-size-fits-all therapies to customized precision medicine.

Together, integrating organoid modeling with various cell types has significantly advanced our understanding of the complex interactions among different cells within the TME. Notably, the identification and functional characterization of CAF and their dynamic roles in tumor progression and therapeutic resistance underscore the importance of these stromal components in PDA. Furthermore, co-culture models with immune cells emphasized the need for tailored therapeutic strategies to overcome immune evasion and resistance. In conclusion, combining PDA organoids with various TME components such as CAFs, immune cells, and endothelial cells, have proven invaluable in mimicking the in vivo conditions and unraveling the intricate signaling pathways involved, offering a promising avenue for improving therapeutic discovery and precision medicine in PDA treatment.

**Organoid Modeling of Biomarker and Therapeutics Development**

PDA presents significant diagnostic challenges due to its late detection and rapid progression. Currently, the primary diagnostic biomarker for PDA is CA19-9[47]; however, its specificity is limited, as elevations in CA19-9 levels can also be observed in other gastrointestinal diseases and conditions such as pancreatitis[48,49]. A major constraint in advancing PDA diagnostics is the reliance on tissue samples obtained primarily through surgical resection, accessible in only about 20% of PDA cases due to the advanced stage of the disease at diagnosis[50]. This limitation significantly hinders the capacity to conduct extensive diagnostic and prognostic evaluations. Pancreatic cancer organoids have emerged as a revolutionary tool in oncology, enabling the expansion of patient-derived cells from minimal biopsy samples[1]. Moreover, organoids can be subjected to multi-omics analyses, thereby allowing a more thorough exploration of tumor heterogeneity, molecular characteristics, and novel biomarkers across different stages of cancer.

Using a humanized mouse-derived PDA organoid model, Engle and colleagues discovered the critical role of CA19-9 in promoting hyperactivation of EGFR signaling, evidenced by increased phosphorylation of EGFR and downstream effectors like FAK, AKT, and ERK1/2; additionally, fibulin-3 (FBLN3) is identified as a CA19-9-modified protein that acts as an EGFR ligand[51]. Blocking FBLN3 prevents EGFR phosphorylation, highlighting its crucial role in CA19-9-induced EGFR activation and underscoring the significance of CA19-9 in promoting pancreatic cancer[51], indicating therapeutic relevance. This model not only aids in

understanding the role of biomarkers in disease progression but also provides a platform for testing diagnostic and therapeutic strategies.

The urgent need for improved therapeutic strategies in PDA, coupled with the limited treatment options, poor prognosis, and observed chemorefractory diseases in patients[52], underscores the need for a preclinical model that can effectively model patient response to therapeutic regiments. By overcoming the limitations associated with the availability of patient-derived tissues and enhancing our understanding of tumor biology through models like humanized mice and the establishment of PDOs, organoids stand at the forefront of a paradigm shift in PDA diagnostics and therapeutics, providing a platform for rapid evaluation of treatment response and biomarkers[1,53]. Through deep molecular characterization, PDO drug sensitivity profiles can be generated within a clinically meaningful timeframe, reflecting patient response to therapy and predicting the acquisition of resistance[16,53]. Therefore, organoid models offer a promising platform for PDA therapeutic discovery by providing clinically relevant platforms for predictive biomarker identification and drug sensitivity testing.

Tiriac and colleagues provided important insights into the predictive power of organoids through the discovery of interpatient heterogeneity in chemotherapeutics using patient-derived organoids[16]. This study established that the therapeutic sensitivity of the PDOs correlates with the patient response to chemotherapeutic regimens, highlighting the clinical relevance of the model for guiding treatment strategies[16]. Additionally, organoid

pharmacotyping enabled the identification of alternative treatment strategies for chemorefractory tumors, such as broad-spectrum kinase inhibitors and other targeted agents[16], providing a platform for discovering patient-specific targeting agents to overcome chemoresistance.

One significant application of organoids in cancer therapeutics is identifying and evaluating drug resistance mechanisms and testing novel therapeutic combinations for synergistic treatment outcomes. Ponz-Sarvise and colleagues compared normal and tumor organoids to discover ERBB2/3 signaling activation during MEK and AKT inhibition, showing the advantage of dual inhibition using pan-ERBB and MEK/AKT inhibition in treating pancreatic cancer[54]. Moreover, Gulay and colleagues utilized PDOs to study the efficacy of $KRAS^{G12D}$ inhibitors in conjunction with pan-ERBB inhibitors[55]. This study not only demonstrated that targeting these $KRAS^{G12D}$ mutations alone can lead to the rapid development of drug resistance in PDA, but more importantly, the addition of pan-ERBB inhibitors circumvented the resistance phenotype[55], suggesting targeting synergistic interactions is more efficient and critical for clinical applications.

Hobbs and colleagues used PDA organoid to discover distinct molecular profiling between $Kras^{G12D}$ and $Kras^{G12R}$ mutations and found that $Kras^{G12R}$ PDA relies on PI3K$\gamma$ activity to support macropinocytosis therefore, the cells are sensitive to ERK and autophagy inhibition[56]. Similarly, Goodwin and colleagues used PDA organoids to identify synergistic inhibition of PDA using CDK4/6 and ERK-MAPK inhibitors[57]. Huang and colleagues also leveraged PDOs

to uncover the sensitivity of certain PDOs to epigenetic inhibitors, such as targeting EZH2, a histone modifier, suggesting EZH2-dependent epigenetic pathways can promote PDA progression and conferring therapeutic resistance[12].

In summary, the utilization of organoid models in pancreatic cancer marks a significant advancement in studies of cancer therapeutics and resistance mechanisms. These three-dimensional cultures offer an unprecedented opportunity to tailor and refine therapeutic strategies for individual patients. By mirroring patient-specific contexts, organoids may provide a more accurate prediction of drug efficacies and resistance patterns, facilitating the development of more effective combination therapies. Ultimately, aligning therapeutic interventions more closely with the unique characteristics of each tumor improves patient outcomes.

## Conclusion

The advancements in pancreatic organoid culture have revolutionized the field of cancer research, providing an invaluable tool for modeling the complex cellular and molecular dynamics of pancreatic cancer in a controlled environment. This model system has enabled the study of disease mechanisms, therapeutic responses, and the identification of biomarkers. By recapitulating the cellular architecture and signaling pathways of in vivo tumors, organoid cultures offer a robust platform for investigating cancer progression, metastasis, and drug resistance. These insights are crucial for developing personalized medicine approaches and improving patient outcomes. Despite certain limitations, such as the overactivation of specific signaling pathways and the lack of a precise tumor microenvironment in organoid cultures, continued refinement of organoid technology holds promise for enhancing our understanding of pancreatic cancer and translating research findings into clinical practice. Thus, pancreatic organoid models stand as an innovative and transformative approach, bridging the gap between basic research and therapeutic innovation in the fight against this formidable disease.

**Reference**

1. Boj, S. F. *et al.* Organoid Models of Human and Mouse Ductal Pancreatic Cancer. *Cell* **160**, 324–338 (2015).

2. Moreira, L. *et al.* Pancreas 3D Organoids: Current and Future Aspects as a Research Platform for Personalized Medicine in Pancreatic Cancer. *Cell. Mol. Gastroenterol. Hepatol.* **5**, 289–298 (2017).

3. Huch, M. *et al.* Unlimited in vitro expansion of adult bi-potent pancreas progenitors through the Lgr5/R-spondin axis. *EMBO J.* **32**, 2708–2721 (2013).

4. Li, X. *et al.* Oncogenic transformation of diverse gastrointestinal tissues in primary organoid culture. *Nat. Med.* **20**, 769–777 (2014).

5. Githens, S., Holmquist, D. R. G., Whelan, J. F. & Ruby, J. R. Ducts of the rat pancreas in agarose matrix culture. *In Vitro* **16**, 797–808 (1980).

6. Pylayeva-Gupta, Y., Lee, K. E. & Bar-Sagi, D. Microdissection and Culture of Murine Pancreatic Ductal Epithelial Cells. in *Pancreatic Cancer: Methods and Protocols* (ed. Su, G. H.) 267–279 (Humana Press, Totowa, NJ, 2013). doi:10.1007/978-1-62703-287-2_14.

7. Jin, L. *et al.* Colony-forming cells in the adult mouse pancreas are expandable in Matrigel and form endocrine/acinar colonies in laminin hydrogel. *Proc. Natl. Acad. Sci.* **110**, 3907–3912 (2013).

8. Reichert, M. *et al.* Isolation, culture and genetic manipulation of mouse pancreatic ductal cells. *Nat. Protoc.* **8**, 1354–1365 (2013).

9. Jensen, C. & Teng, Y. Is It Time to Start Transitioning From 2D to 3D Cell Culture? *Front. Mol. Biosci.* **7**, 33 (2020).

10. Piroli, M. E., Blanchette, J. O. & Jabbarzadeh, E. Polarity as a physiological modulator of cell function. *Front. Biosci. Landmark Ed.* **24**, 451–462 (2019).

11. Longati, P. *et al.* 3D pancreatic carcinoma spheroids induce a matrix-rich, chemoresistant phenotype offering a better model for drug testing. *BMC Cancer* **13**, 95 (2013).

12. Huang, L. *et al.* Ductal pancreatic cancer modeling and drug screening using human pluripotent stem cell– and patient-derived tumor organoids. *Nat. Med.* **21**, 1364–1371 (2015).

13. Fraunhoffer, N. A., Abuelafia, A. M., Dusetti, N. & Iovanna, J. Limitation and challenges in using pancreatic cancer-derived organoids as a preclinical tool. *Cancer Commun.* **42**, 1028–1031 (2022).

14. Maitra, A. & Hruban, R. H. Pancreatic Cancer. *Annu. Rev. Pathol. Mech. Dis.* **3**, 157–188 (2008).

15. Yachida, S. *et al.* Distant metastasis occurs late during the genetic evolution of pancreatic cancer. *Nature* **467**, 1114–1117 (2010).

16. Tiriac, H. *et al.* Organoid Profiling Identifies Common Responders to Chemotherapy in Pancreatic Cancer. *Cancer Discov.* **8**, 1112–1129 (2018).

17. Roe, J.-S. *et al.* Enhancer Reprogramming Promotes Pancreatic Cancer Metastasis. *Cell* **170**, 875-888.e20 (2017).

18. Hwang, C.-I., Boj, S. F., Clevers, H. & Tuveson, D. A. Pre-clinical Models of Pancreatic Ductal Adenocarcinoma. *J. Pathol.* **238**, 197–204 (2016).

19. Tiriac, H., Plenker, D., Baker, L. A. & Tuveson, D. A. Organoid Models for Translational Pancreatic Cancer Research. *Curr. Opin. Genet. Dev.* **54**, 7–11 (2019).

20. Shi, X. *et al.* Integrated profiling of human pancreatic cancer organoids reveals chromatin accessibility features associated with drug sensitivity. *Nat. Commun.* **13**, 2169 (2022).

21. Wang, S. *et al.* The molecular biology of pancreatic adenocarcinoma: translational challenges and clinical perspectives. *Signal Transduct. Target. Ther.* **6**, 1–23 (2021).

22. Xu, J. *et al.* Engrailed-1 Promotes Pancreatic Cancer Metastasis. 2023.04.10.536259 Preprint at https://doi.org/10.1101/2023.04.10.536259 (2023).

23. Tonelli, C. *et al.* A mucus production programme promotes classical pancreatic ductal adenocarcinoma. *Gut* (2024) doi:10.1136/gutjnl-2023-329839.

24. Kim, H.-R. *et al.* EVI1 activates tumor-promoting transcriptional enhancers in pancreatic cancer. *NAR Cancer* **3**, zcab023 (2021).

25. Yoo, H.-B. *et al.* A TEAD2-Driven Endothelial-Like Program Shapes Basal-Like Differentiation and Metastasis of Pancreatic Cancer. *Gastroenterology* **165**, 133-148.e17 (2023).

26. Collisson, E. A. *et al.* Subtypes of pancreatic ductal adenocarcinoma and their differing responses to therapy. *Nat. Med.* **17**, 500–503 (2011).

27. Moffitt, R. A. *et al.* Virtual microdissection identifies distinct tumor- and stroma-specific subtypes of pancreatic ductal adenocarcinoma. *Nat. Genet.* **47**, 1168–1178 (2015).

28. Bailey, P. *et al.* Genomic analyses identify molecular subtypes of pancreatic cancer. *Nature* **531**, 47–52 (2016).

29. Wang, S. S. *et al.* Whole-genome bisulfite sequencing identifies stage- and subtype-specific DNA methylation signatures in pancreatic cancer. *iScience* **27**, 109414 (2024).

30. Whatcott, C. J. *et al.* Desmoplasia in Primary Tumors and Metastatic Lesions of Pancreatic Cancer. *Clin. Cancer Res.* **21**, 3561–3568 (2015).

31. Olive, K. P. *et al.* Inhibition of Hedgehog Signaling Enhances Delivery of Chemotherapy in a Mouse Model of Pancreatic Cancer. *Science* **324**, 1457–1461 (2009).

32. Helms, E., Onate, M. K. & Sherman, M. H. Fibroblast Heterogeneity in the Pancreatic Tumor Microenvironment. *Cancer Discov.* **10**, 648–656 (2020).

33. Jacobetz, M. A. *et al.* Hyaluronan impairs vascular function and drug delivery in a mouse model of pancreatic cancer. *Gut* **62**, 112–120 (2013).

34. De Jesus-Acosta, A. *et al.* Phase 2 study of vismodegib, a hedgehog inhibitor, combined with gemcitabine and nab-paclitaxel in patients with untreated metastatic pancreatic adenocarcinoma. *Br. J. Cancer* **122**, 498–505 (2020).

35. Van Cutsem, E. *et al.* Randomized Phase III Trial of Pegvorhyaluronidase Alfa With Nab-Paclitaxel Plus Gemcitabine for Patients With Hyaluronan-High Metastatic Pancreatic Adenocarcinoma. *J. Clin. Oncol.* **38**, 3185–3194 (2020).

36. Steele, N. G. *et al.* Inhibition of Hedgehog Signaling Alters Fibroblast Composition in Pancreatic Cancer. *Clin. Cancer Res.* **27**, 2023–2037 (2021).

37. Ullman, N. A., Burchard, P. R., Dunne, R. F. & Linehan, D. C. Immunologic Strategies in Pancreatic Cancer: Making Cold Tumors Hot. *J. Clin. Oncol. Off. J. Am. Soc. Clin. Oncol.* **40**, 2789–2805 (2022).

38. Fibroblast heterogeneity in the cancer wound | Journal of Experimental Medicine | Rockefeller University Press. https://rupress.org/jem/article/211/8/1503/41747/Fibroblast-heterogeneity-in-the-cancer.

39. Öhlund, D. *et al.* Distinct populations of inflammatory fibroblasts and myofibroblasts in pancreatic cancer. *J. Exp. Med.* **214**, 579–596 (2017).

40. Biffi, G. *et al.* IL1-Induced JAK/STAT Signaling Is Antagonized by TGFβ to Shape CAF Heterogeneity in Pancreatic Ductal Adenocarcinoma. *Cancer Discov.* **9**, 282–301 (2019).

41. Go, Y.-H. *et al.* Modeling Pancreatic Cancer with Patient-Derived Organoids Integrating Cancer-Associated Fibroblasts. *Cancers* **14**, 2077 (2022).

42. Schuth, S. *et al.* Patient-specific modeling of stroma-mediated chemoresistance of pancreatic cancer using a three-dimensional organoid-fibroblast co-culture system. *J. Exp. Clin. Cancer Res.* **41**, 312 (2022).

43. Beatty, G. L., Eghbali, S. & Kim, R. Deploying Immunotherapy in Pancreatic Cancer: Defining Mechanisms of Response and Resistance. *Am. Soc. Clin. Oncol. Educ. Book* 267–278 (2017) doi:10.1200/EDBK_175232.

44. D'Angelo, A., Shibata, K., Tokunaga, M., Furutani-Seiki, M. & Bagby, S. Generation of murine tumour-reactive T cells by co-culturing murine pancreatic cancer organoids and peripheral blood lymphocytes. *Biochem. Biophys. Rep.* **32**, 101365 (2022).

45. Zhou, Z. *et al.* A T Cell-Engaging Tumor Organoid Platform for Pancreatic Cancer Immunotherapy. *Adv. Sci.* **10**, 2300548 (2023).

46. Knoblauch, M. *et al.* In-vitro model to mimic T cell subset change in human PDAC organoid co-culture. *J. Cancer Res. Clin. Oncol.* **149**, 13051–13064 (2023).

47. Ballehaninna, U. K. & Chamberlain, R. S. Serum CA 19-9 as a Biomarker for Pancreatic Cancer—A Comprehensive Review. *Indian J. Surg. Oncol.* **2**, 88–100 (2011).

48. Zhao, J.-Z. & Wu, B.-H. Clinical significance of CA19-9 in diagnosis of digestive tract tumors. *World J. Gastroenterol.* **3**, 253 (1997).

49. CA19-9 as a therapeutic target in pancreatitis - PMC. https://www.ncbi.nlm.nih.gov/pmc/articles/PMC6976502/.

50. Tamburrino, D. *et al.* Selection criteria in resectable pancreatic cancer: A biological and morphological approach. *World J. Gastroenterol. WJG* **20**, 11210–11215 (2014).

51. Engle, D. D. *et al.* The glycan CA19-9 promotes pancreatitis and pancreatic cancer in mice. *Science* **364**, 1156–1162 (2019).

52. Moriyama, T. *et al.* MicroRNA-21 modulates biological functions of pancreatic cancer cells including their proliferation, invasion, and chemoresistance. *Mol. Cancer Ther.* **8**, 1067–1074 (2009).

53. Tiriac, H. *et al.* Successful creation of pancreatic cancer organoids by means of EUS-guided fine-needle biopsy sampling for personalized cancer treatment. *Gastrointest. Endosc.* **87**, 1474–1480 (2018).

54. Ponz-Sarvise, M. *et al.* Identification of Resistance Pathways Specific to Malignancy Using Organoid Models of Pancreatic Cancer. *Clin. Cancer Res.* **25**, 6742–6755 (2019).

55. Gulay, K. C. M. *et al.* Dual Inhibition of KRASG12D and Pan-ERBB Is Synergistic in Pancreatic Ductal Adenocarcinoma. *Cancer Res.* **83**, 3001–3012 (2023).

56. Hobbs, G. A. *et al.* Atypical KRASG12R Mutant Is Impaired in PI3K Signaling and Macropinocytosis in Pancreatic Cancer. *Cancer Discov.* **10**, 104–123 (2020).

57. Goodwin, C. M. *et al.* Combination Therapies with CDK4/6 Inhibitors to Treat KRAS-Mutant Pancreatic Cancer. *Cancer Res.* **83**, 141–157 (2023).